Acceleration and Characterization of Protons and Ions from Nanometer-Scale Thin Polymer Foil

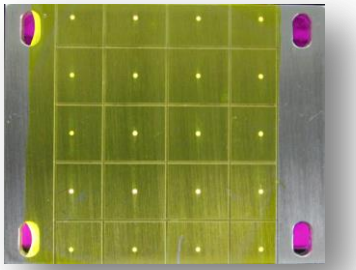

Il Woo Choi

Center for Relativistic Laser Science, Institute for Basic Science (IBS)

Advanced Photonics Research Institute, Gwangju Institute of Science and Technology (GIST)

Korea

Targetry for Laser-driven Proton (Ion) Accelerator Sources, Institute for Advanced Study, Garching, Germany, Oct. 9 2013.

Outline

1. PW laser and application facility at GIST
2. Contrast enhancement and laser beam focusing
3. Ultrathin free-standing polymer target
4. Ion acceleration using PW laser and ultrathin target
5. Conclusion

100 TW and PW Laser Systems, Interaction Target Chambers

100 TW laser-plasma laboratory

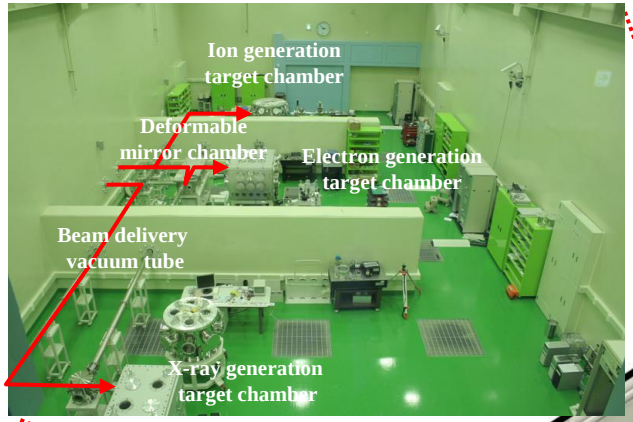

PW laser-plasma laboratory

Control room

Interaction of Ultrashort Ultraintense Laser with Matter

Interaction of laser and matter in relativistic regime

$$\text{Dimensionless laser amplitude}: \quad a_0 = \frac{eE}{m_0 \omega c} \approx 8.55 \times 10^{-10} I^{1/2}_{\mathrm{W/cm^2}} \lambda_{\mu m}$$

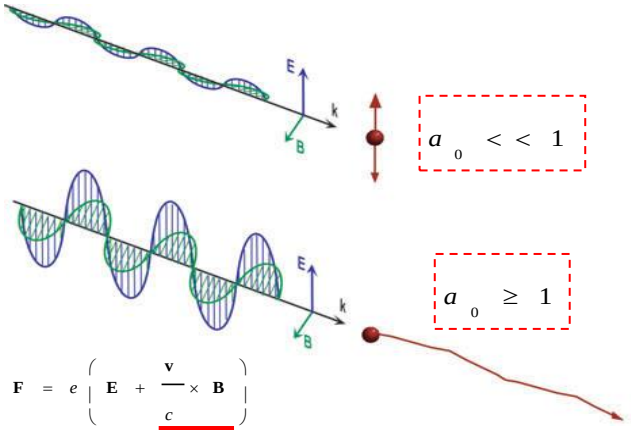

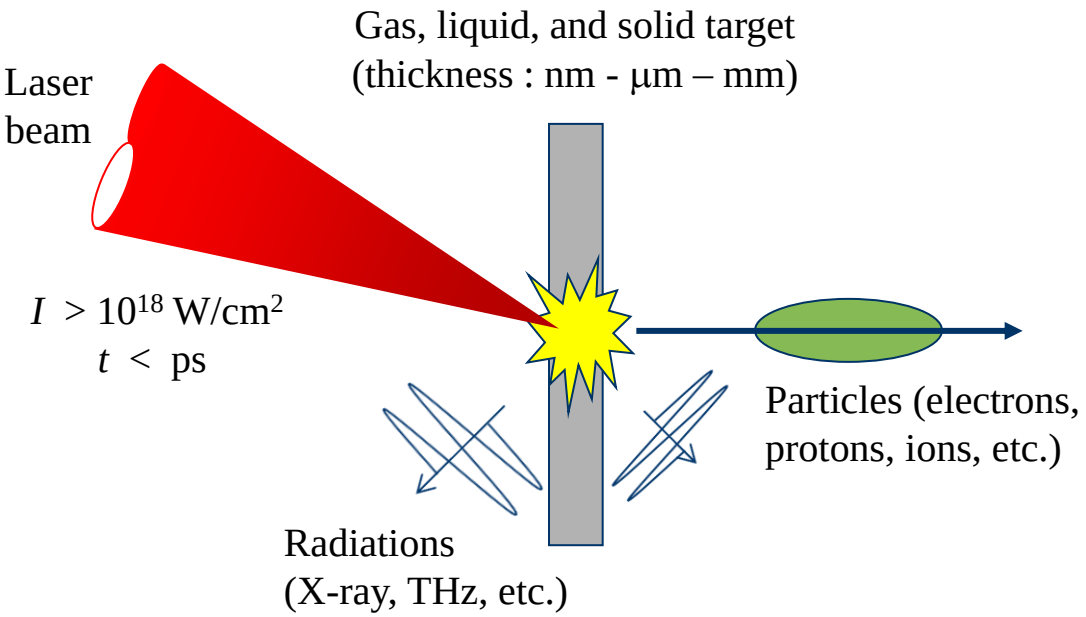

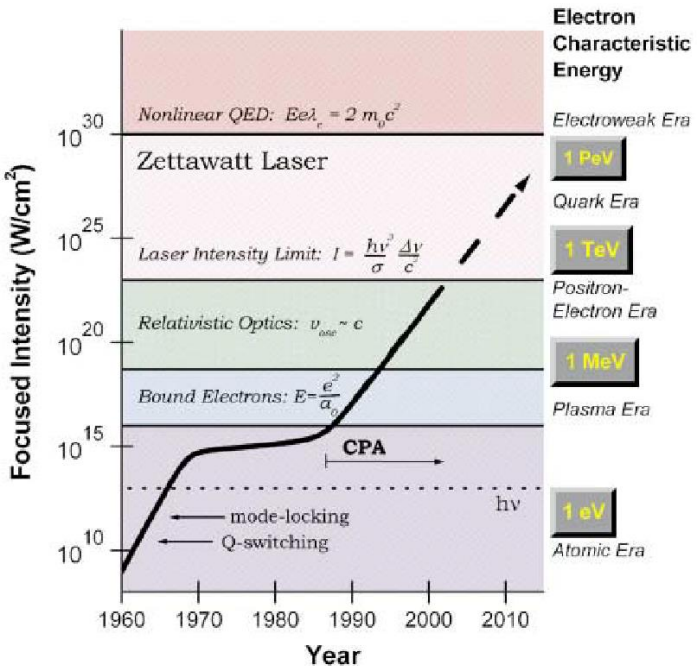

Opened up exotic research areas, such as the generation of ultrashort x-ray and particle sources, and the study on the high-field physics

T. Tajima and G. Mourou, PRST-AB **5**, 031301 (2002).

Target Normal Sheath Acceleration (TNSA) and Optimum Thickness

Hot electron propagation :
MeV energy, μC-mC charge

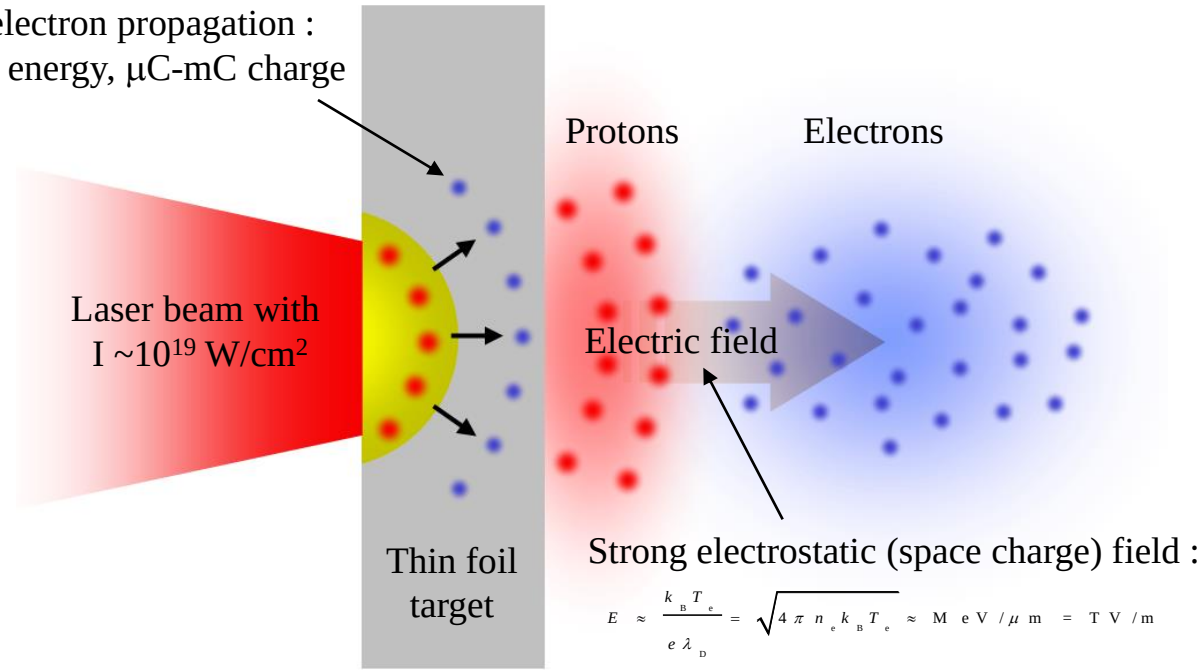

Strong electrostatic (space charge) field :

$$E \approx \frac{k_B T_e}{e \lambda_D} = \sqrt{4 \pi n_e k_B T_e} \approx \mathrm{MeV/\mu m} = \mathrm{TV/m}$$

- Transverse spreading
- Surface deformation and density gradient
- Recirculation and refluxing
- Absorption of laser energy in the target

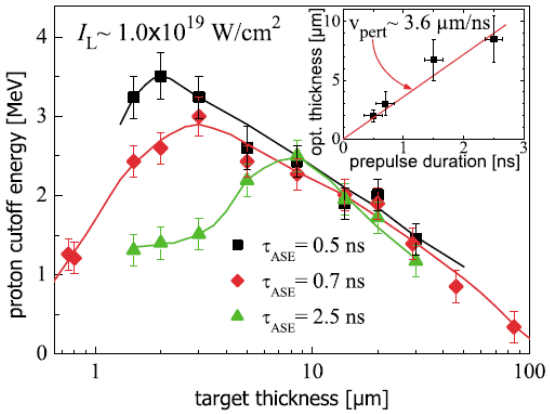

M. Kaluza, PRL **93**, 045003 (2004).

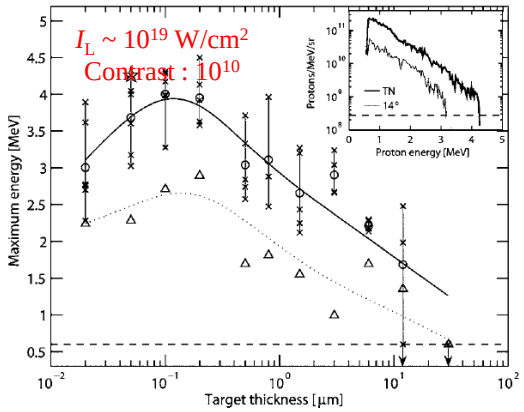

D. Neely, APL **89**, 021502(2006).

✓ Optimum thickness : several tens of nm - several μm, depending on the laser contrast, pulse duration, and intensity.

Radiation Pressure Acceleration (RPA) and Optimum Thickness

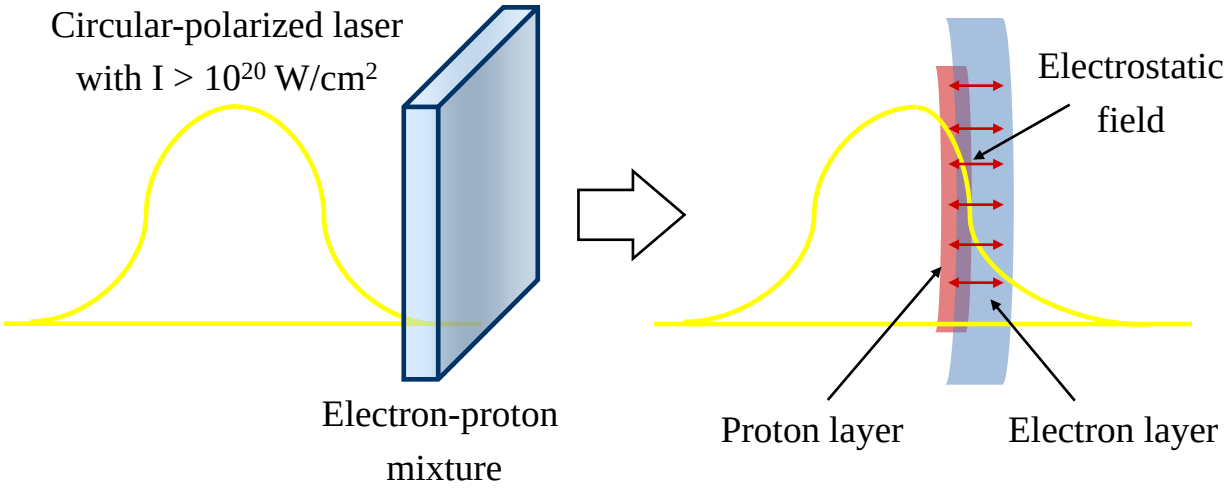

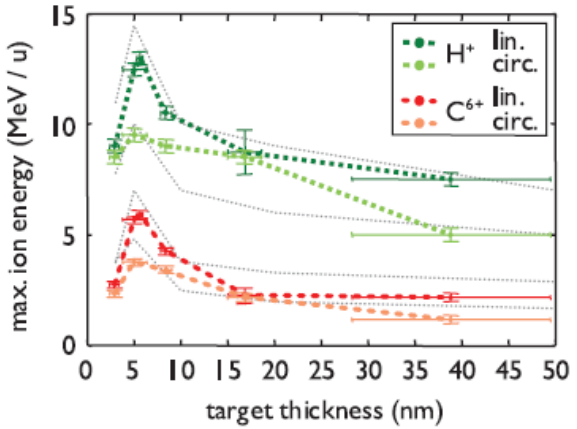

A. Henig, PRL **103**, 245003 (2009).

- ✓ Laser pulse pushes electrons forward and forms a high-density layer. A strong charge separation force accelerates ions as a thin layer.
- ✓ Ultrathin targets with nm-scale thickness are necessary to balance the radiation pressure with the restoring force given by the charge-separation field.

Normalized areal density : $\sigma = \frac{n_e d}{n_c \lambda}$

Optimal RPA condition : $a_0 \approx \pi \sigma$

$\lambda = 0.8\ \mu m$, $I = 5\times10^{20}\ W/cm^2$ ($a_0 = 10.8$ for c-pol. laser)

$n_e = 200\ n_c \rightarrow d = 14$ nm

Ti:Sapphire Laser Systems : LiFSA, PULSER

LiFSA (100 TW : Light source for Femto Science and Applications)

PULSER (1 PW : Petawatt Ultrashort Laser Source for Extreme science Research)

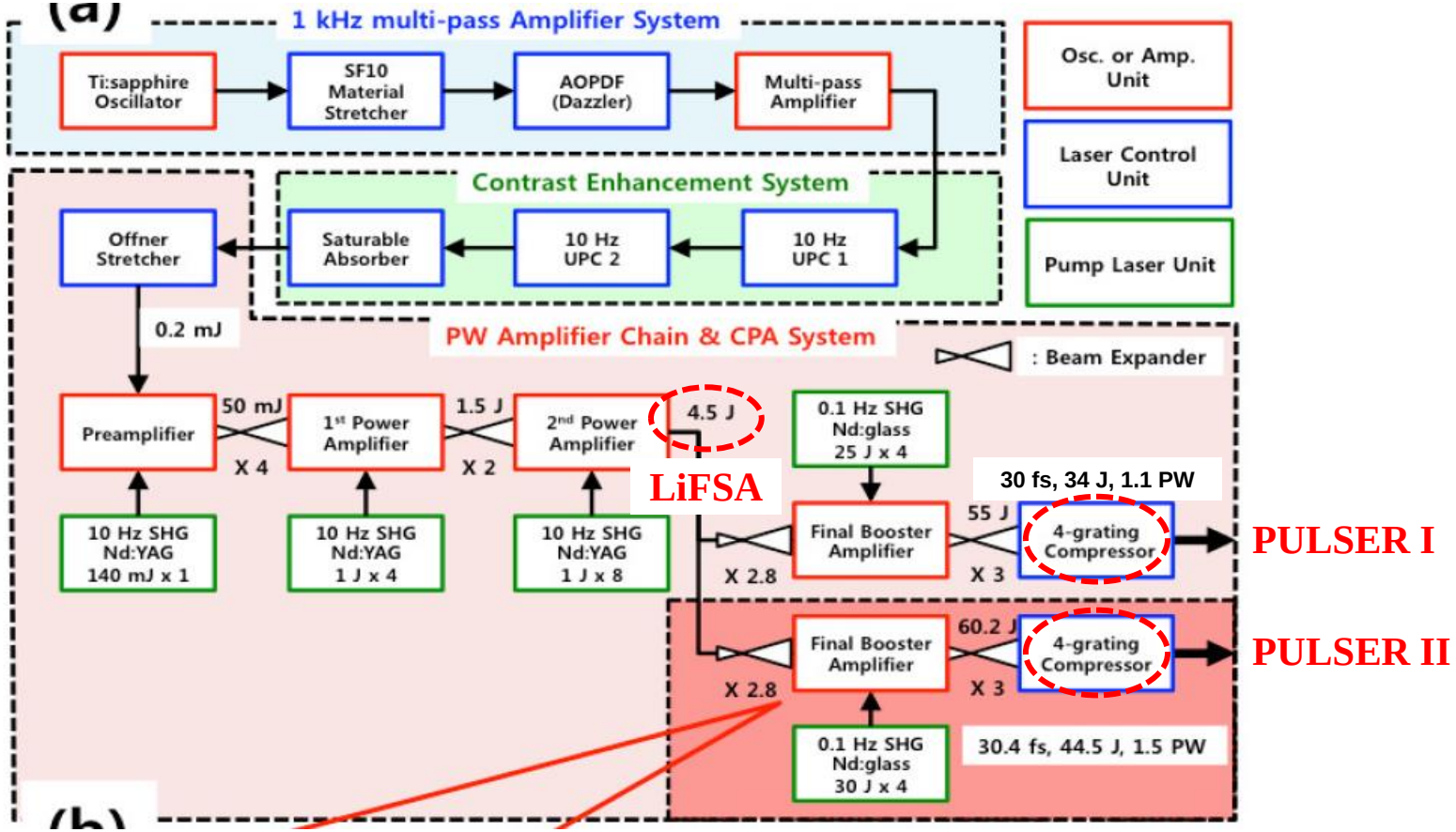

T. J. Yu *et al.*, Opt. Express **20**, 10807 (2012) ; J. H. Sung *et al.*, Opt. Lett. **35**, 3021 (2010).

Temporal Pulse Profile and Contrast Ratio of PULSER II

Spectral bandwidth : 46 nm (FWHM)

Pulse duration : 30.2 ± 1.8 fs for 30 pulses

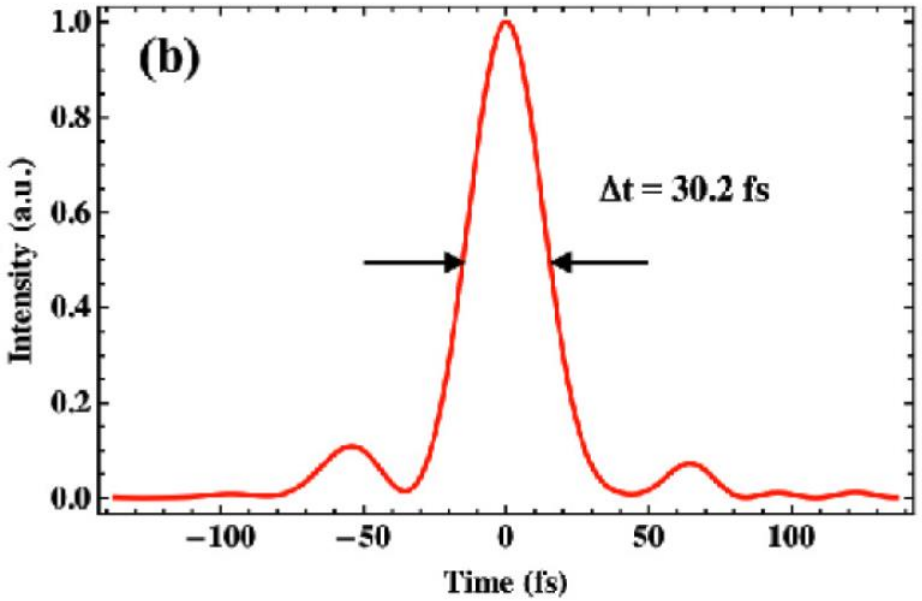

Pulse width after compressor

44.5 J, 30.2 fs → 1.5 PW

2.3×10^{-12} at -500 ps

4.8×10^{-10} at -50 ps

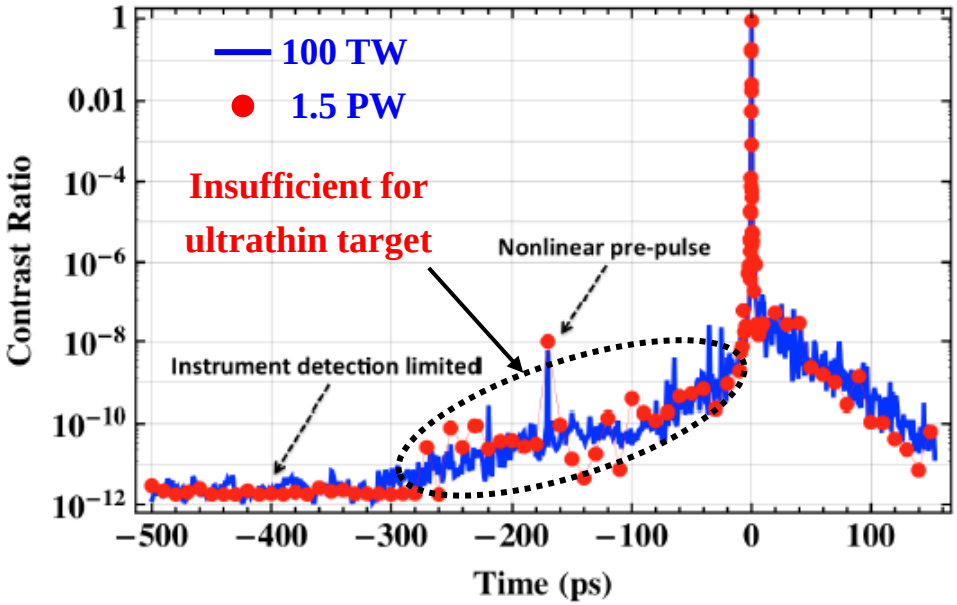

Contrast ratio of 1.5 PW and 100 TW laser pulses measured using a third-order autocorrelation

Contrast Enhancement Needed with Plasma Mirror

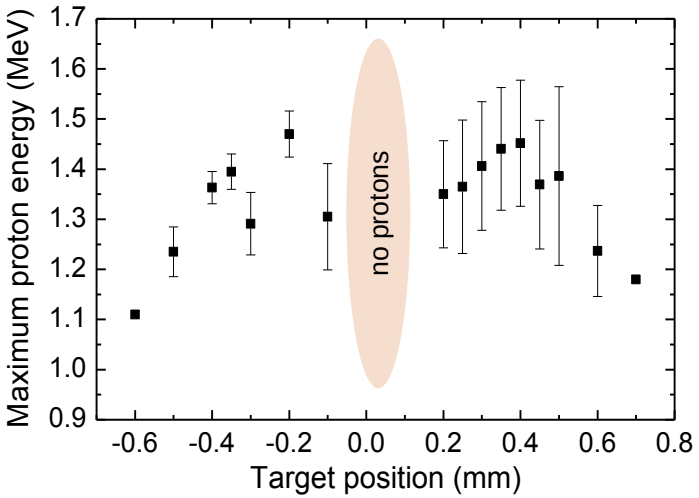

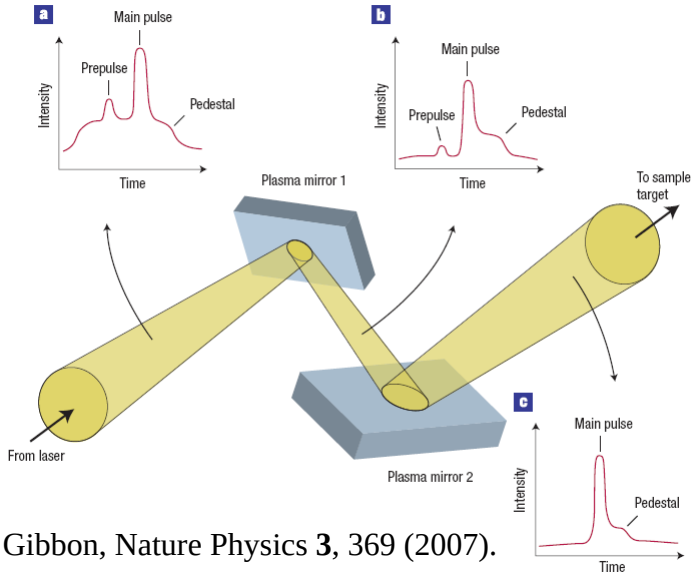

P. Gibbon, Nature Physics **3**, 369 (2007).

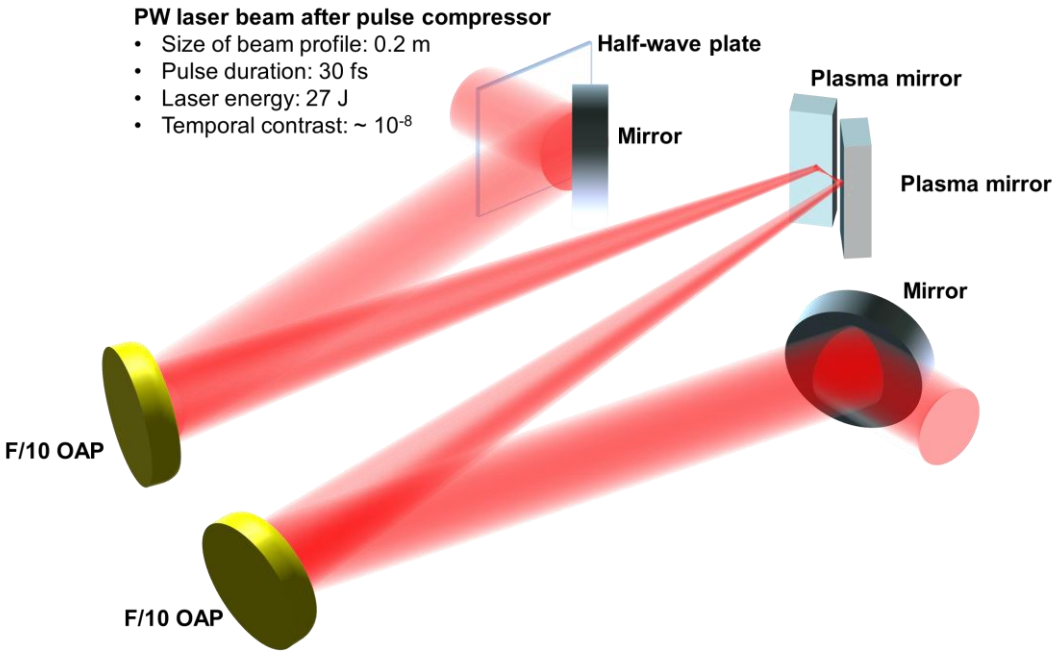

Contrast enhancement with one plasma mirror : ~100

Double plasma mirrors provide 10,000 times enhancement.

Double Plasma Mirror (DPM) System for 100 TW Laser Pulse

Large area DPM and precise pre-alignment allows repetitive operation.

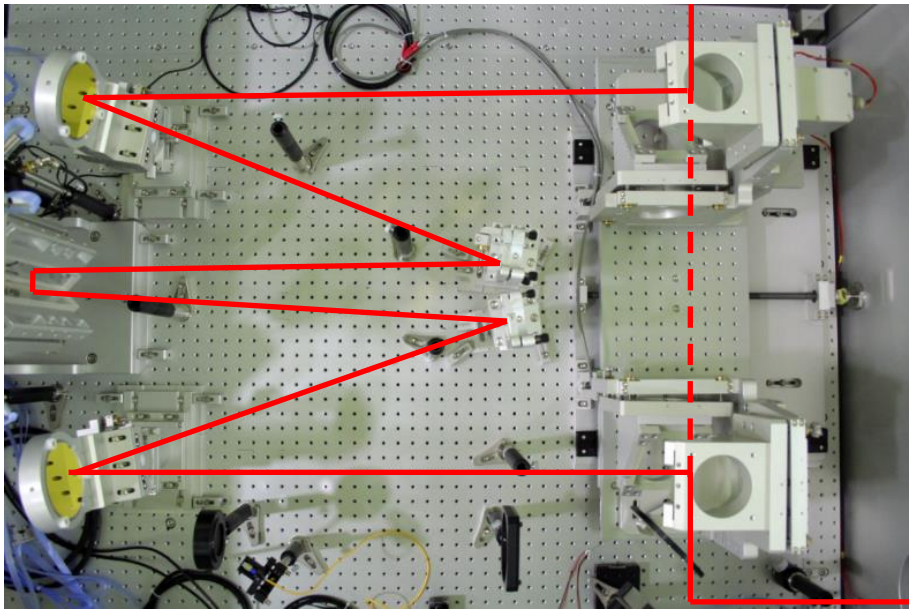

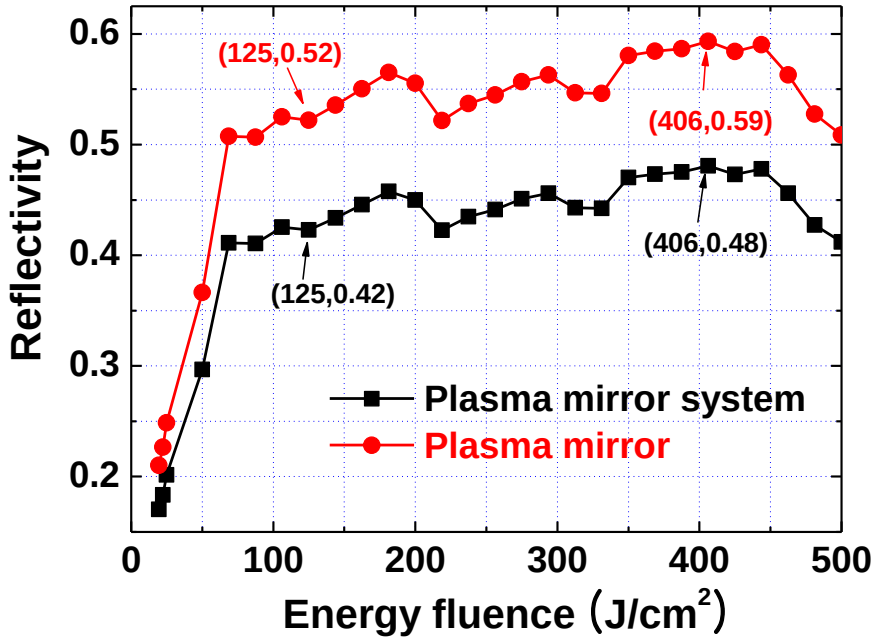

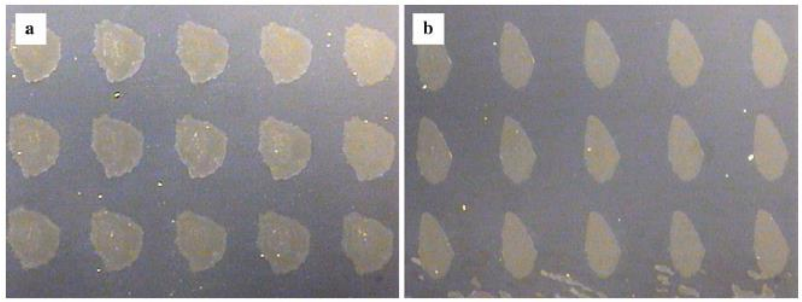

First PM at 90 J/cm^2 Second PM at 90 J/cm^2

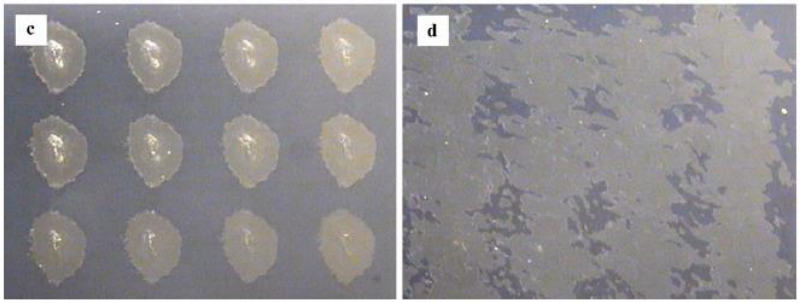

First PM at 290 J/cm^2 Second PM at 290 J/cm^2

Spatial Characteristics of Laser Beam Profile from DPM

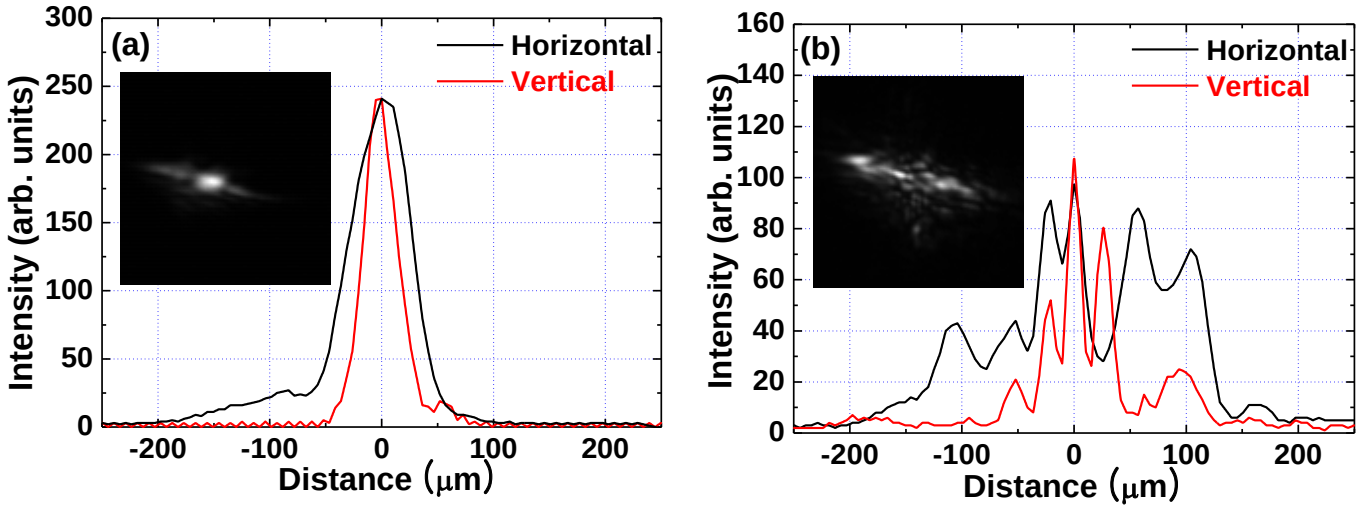

• **Spatial beam profile of the focused laser after DPM system for the energy fluence of (a) 90 J/cm^2 and (b) 290 J/cm^2. The insets show the focused image for these energy fluencies respectively**

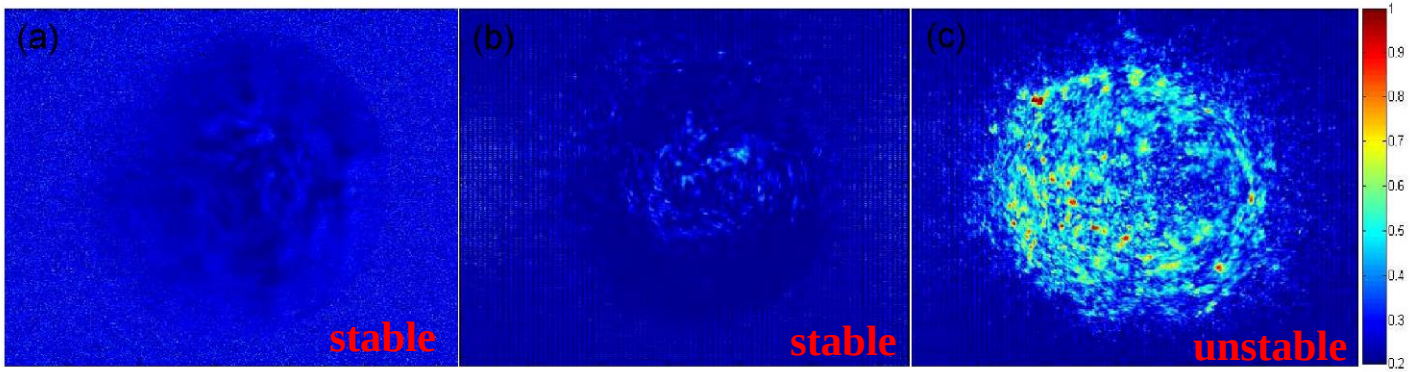

• **2-dimensional Normalized Standard Deviation distribution of near field for 15 laser shots with and without DPM. (a) without DPM, (b) for 90 J/cm^2 with DPM, (c) for 290 J/cm^2 with DPM.**

Double Plasma Mirror System for PW Laser Pulse

Repetitive operation is possible by large area DPM and precise pre-alignemnt.

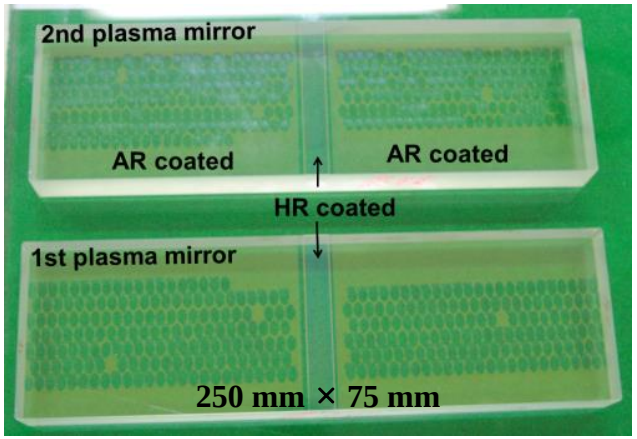

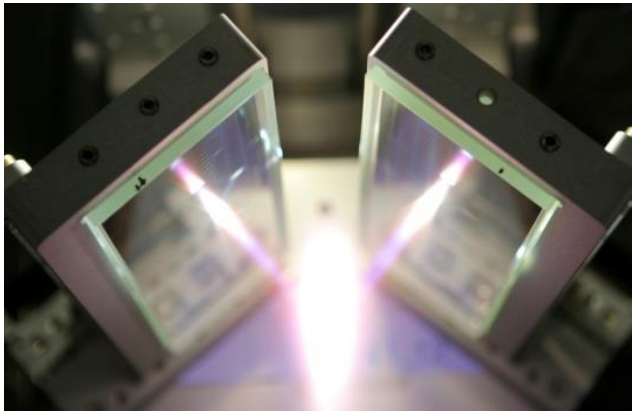

~350 shots available for ~100 J/cm^2

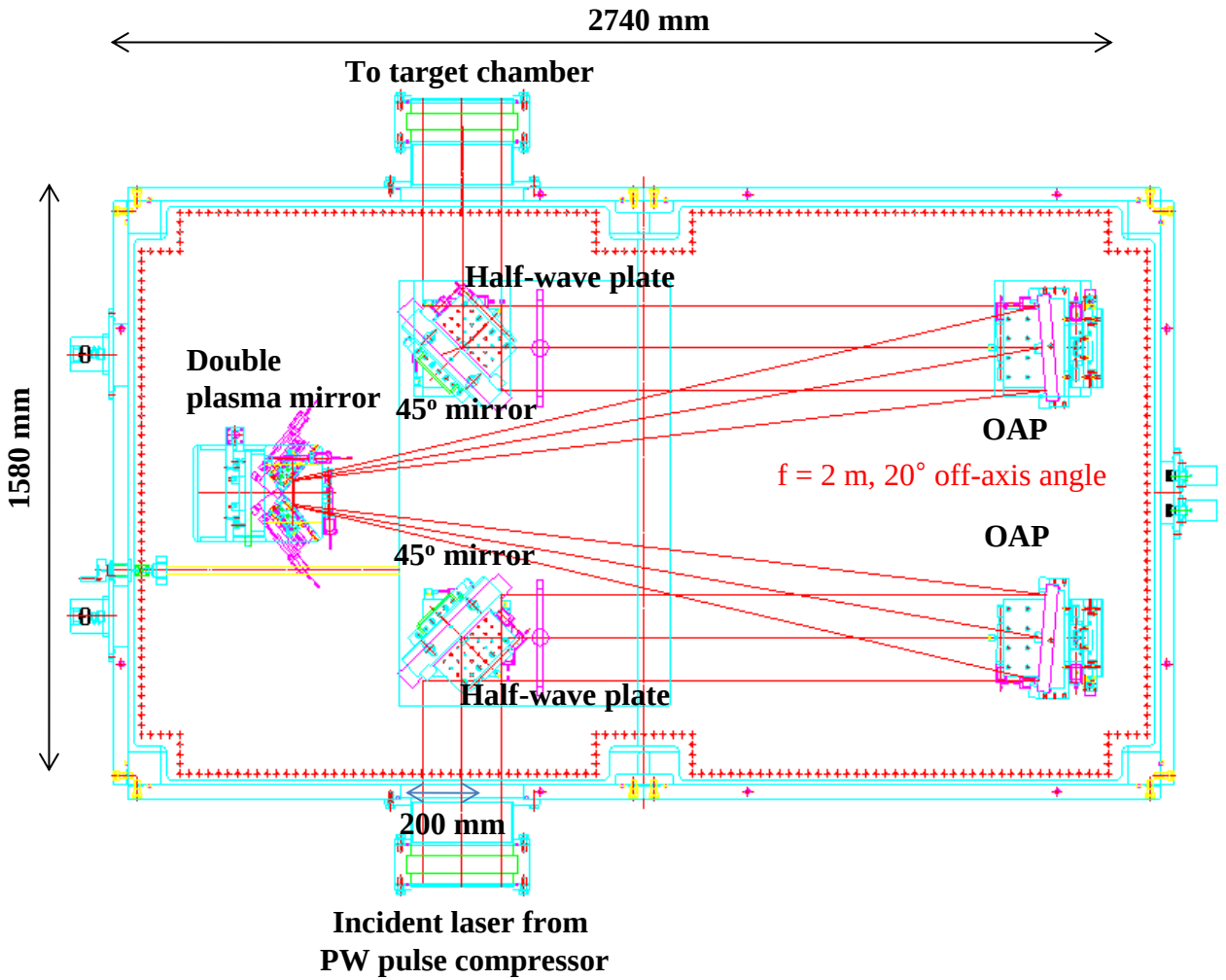

Temporal Contrast Ratio after PW Double Plasma Mirrors

100 TW DPM

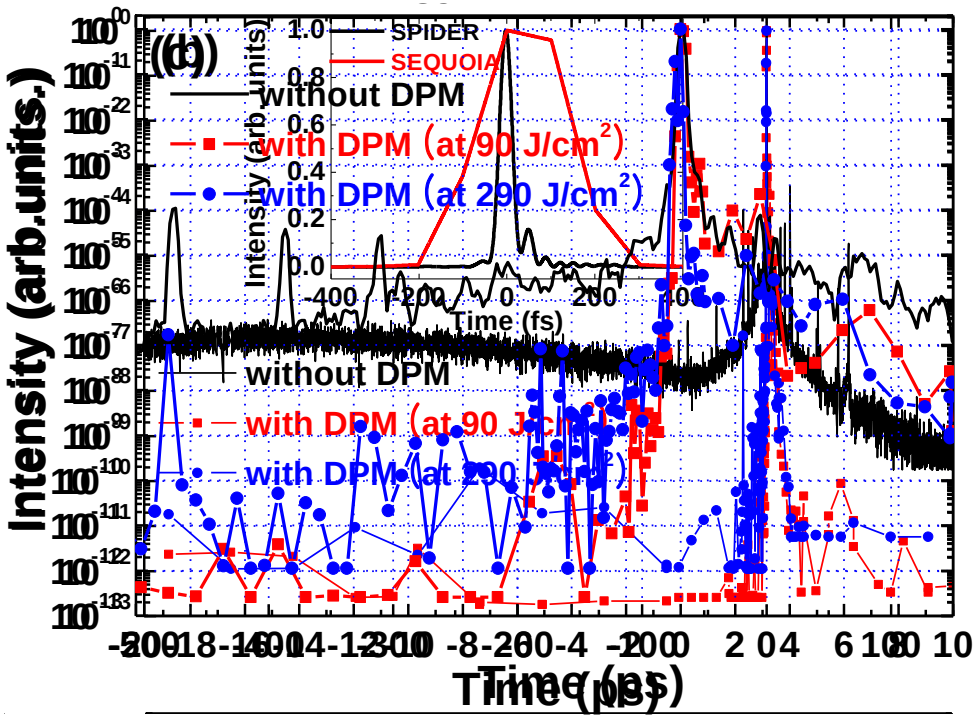

PW DPM

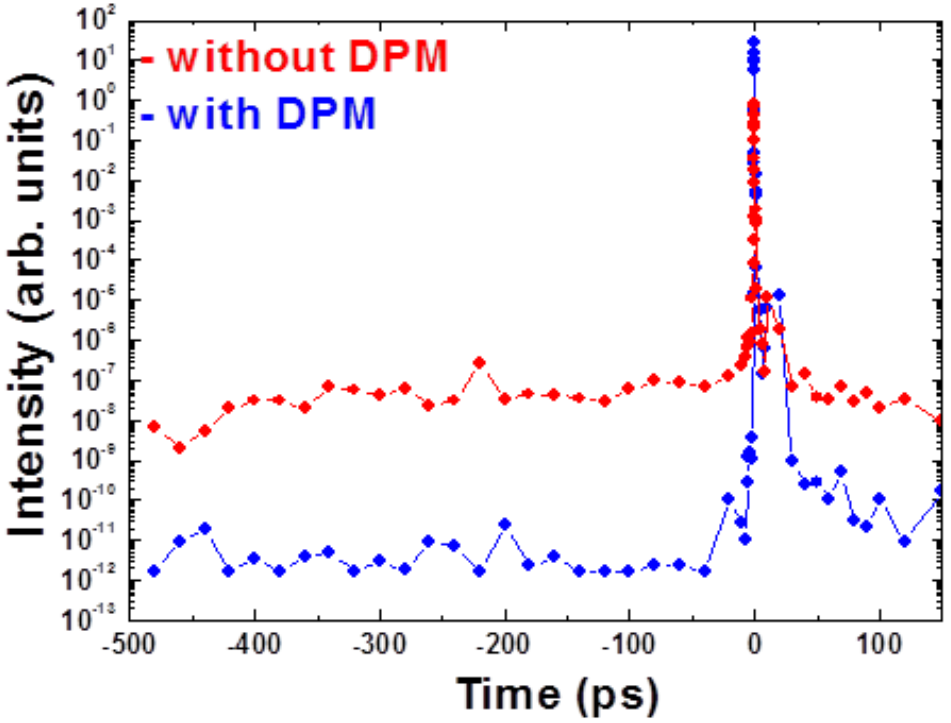

Advantages when using a plasma mirror

- Contrast enhancement : ~10^4
- < 3×10^{-11} up to 6 ps before the main pulse

But, the overall reflectivity is only about 40%.

100 TW Laser Beam Delivery and Target Chamber System

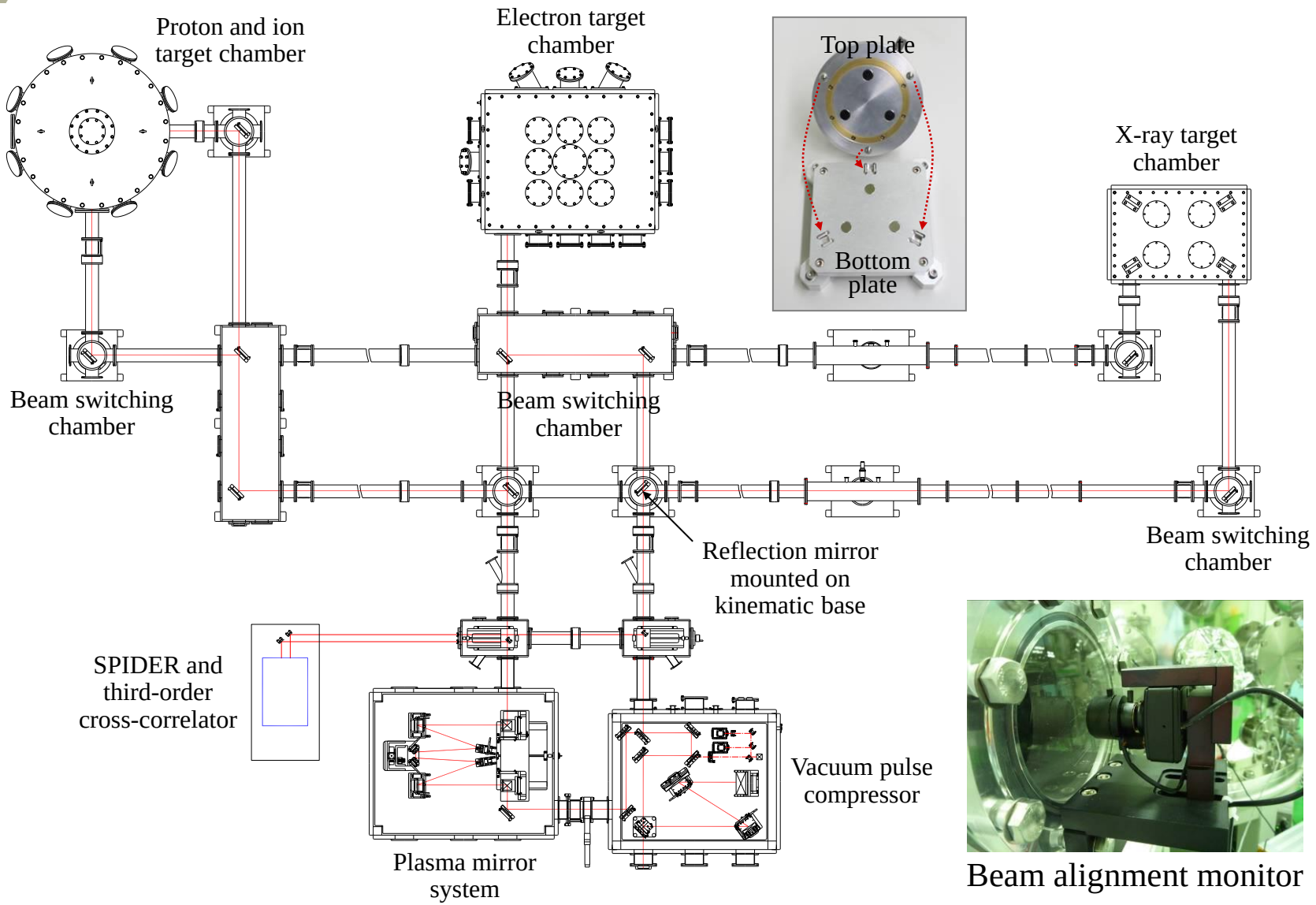

Beam alignment monitor

I. W. Choi *et al.*, J. Korean Phys. Soc. **55**, 517 (2009).

Three Interaction Target Chambers Operated for 100 TW Laser Application

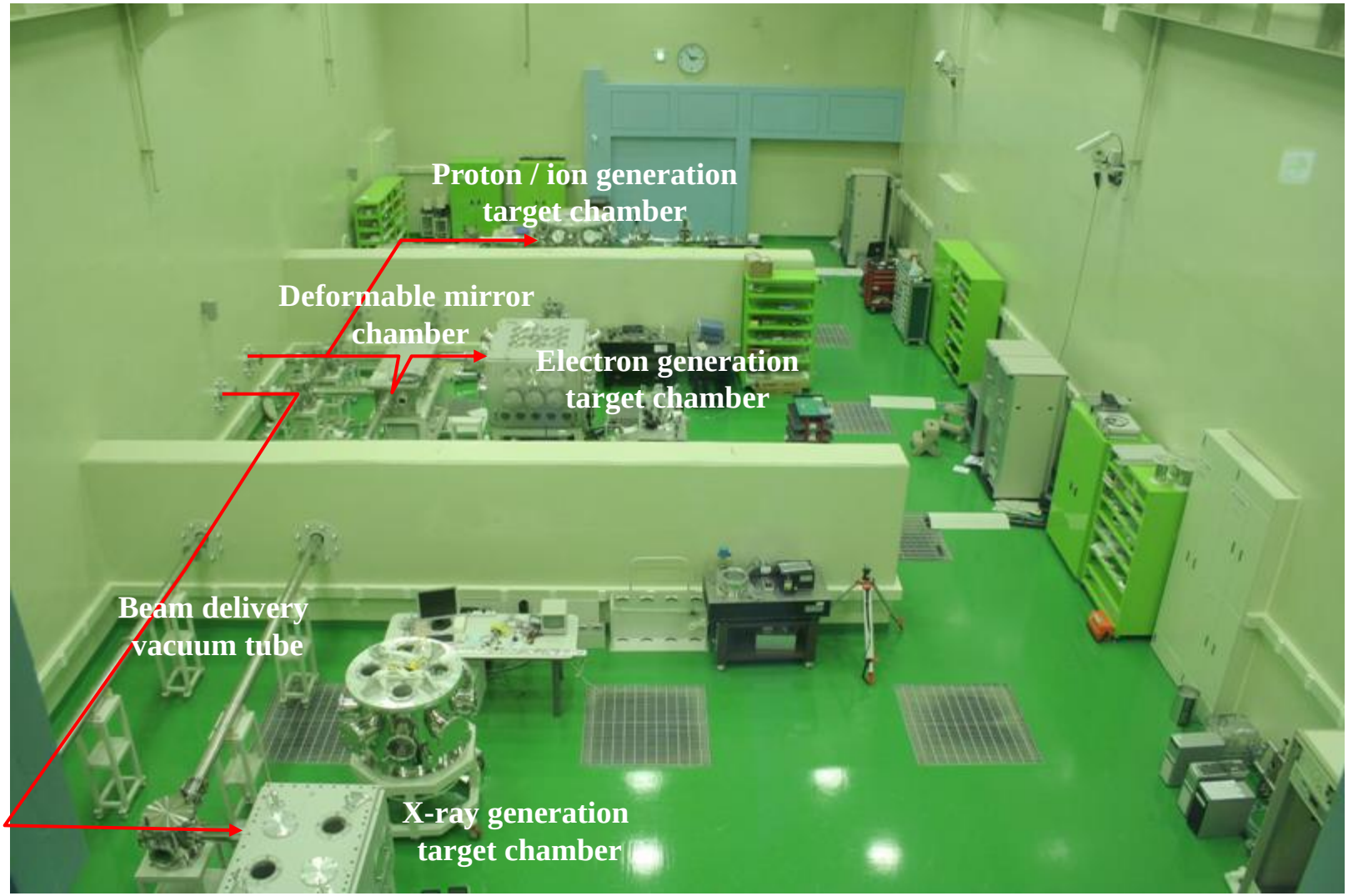

Two PW Target Chambers and Beam Delivery System

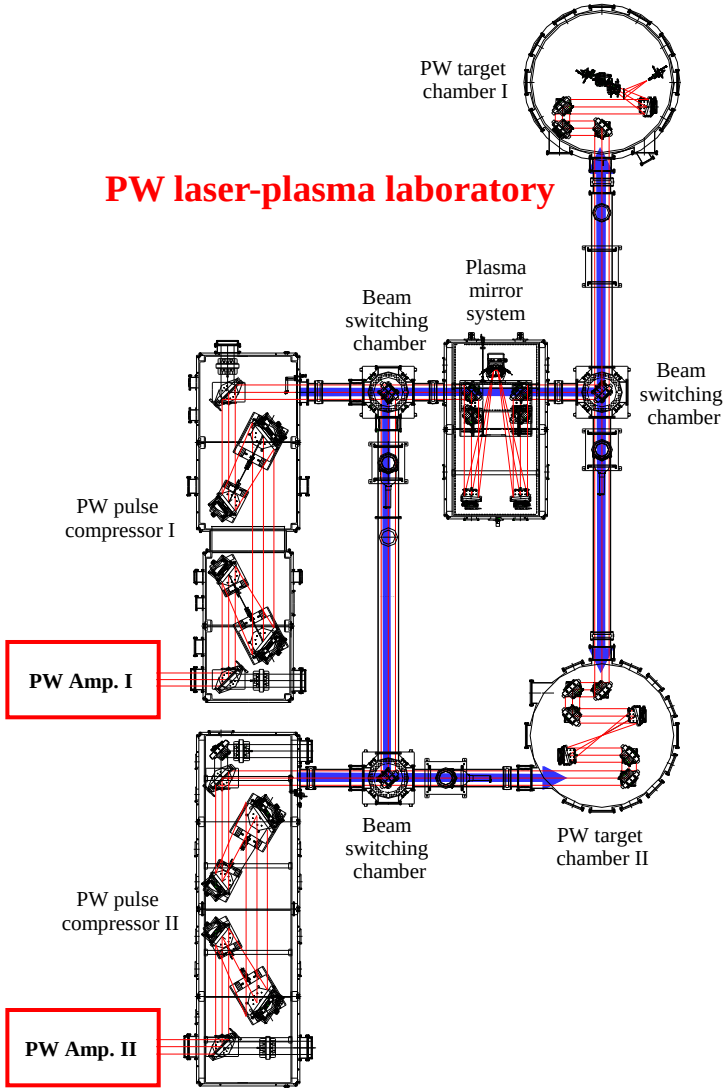

PW target chamber for solid target interaction

- Inner diameter : 2.2 m
- Depth : 1.07 m from bread board
- Volume : ~4 m^3
- Material : Stainless steel + Aluminum
- Height of laser beam : 1.4 m
- PW laser beam size : ~20 cm

Two Interaction Target Chambers Operated for PW Laser Application

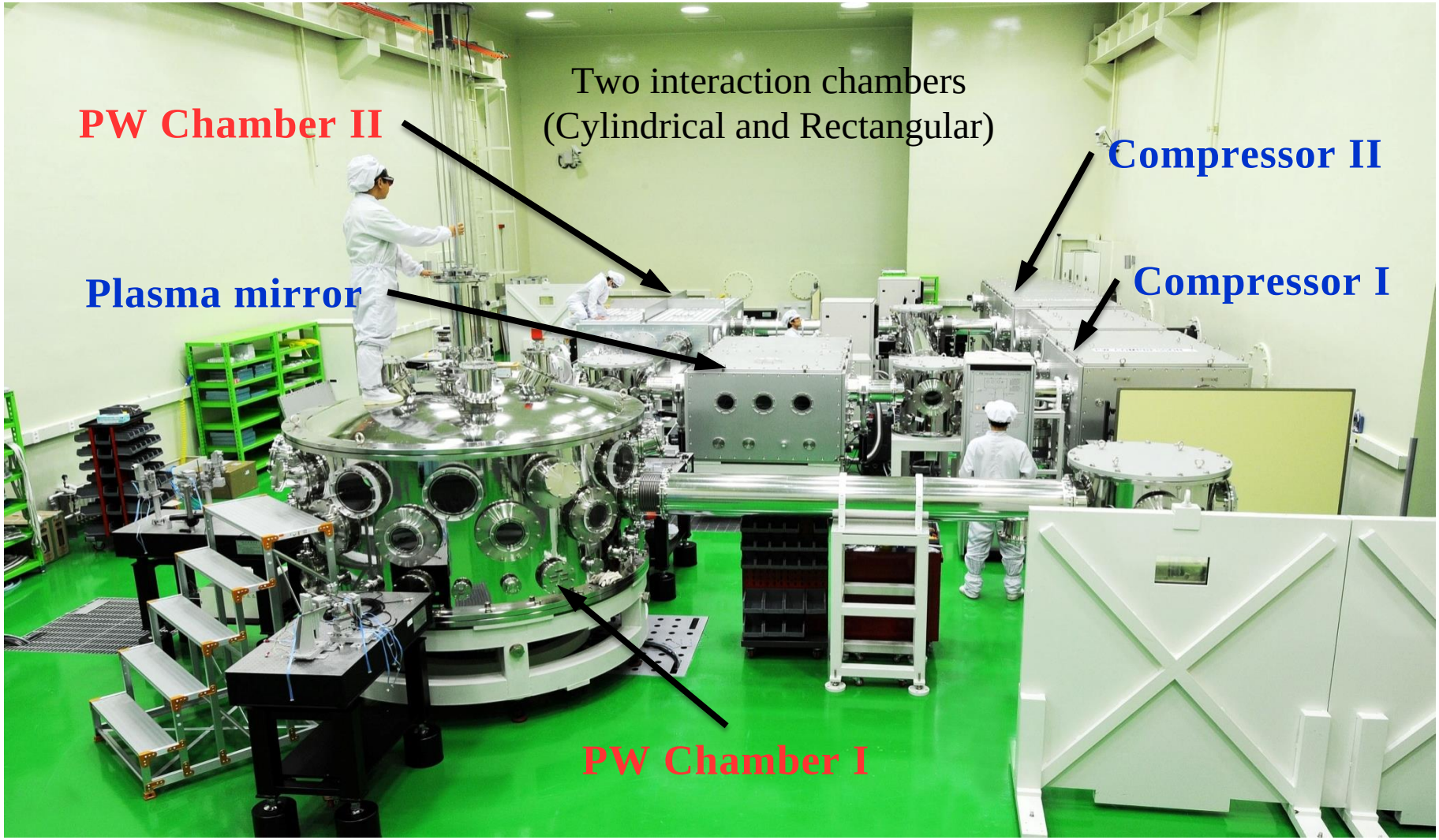

Alignment of Off-Axis Parabolic (OAP) Mirror and Target

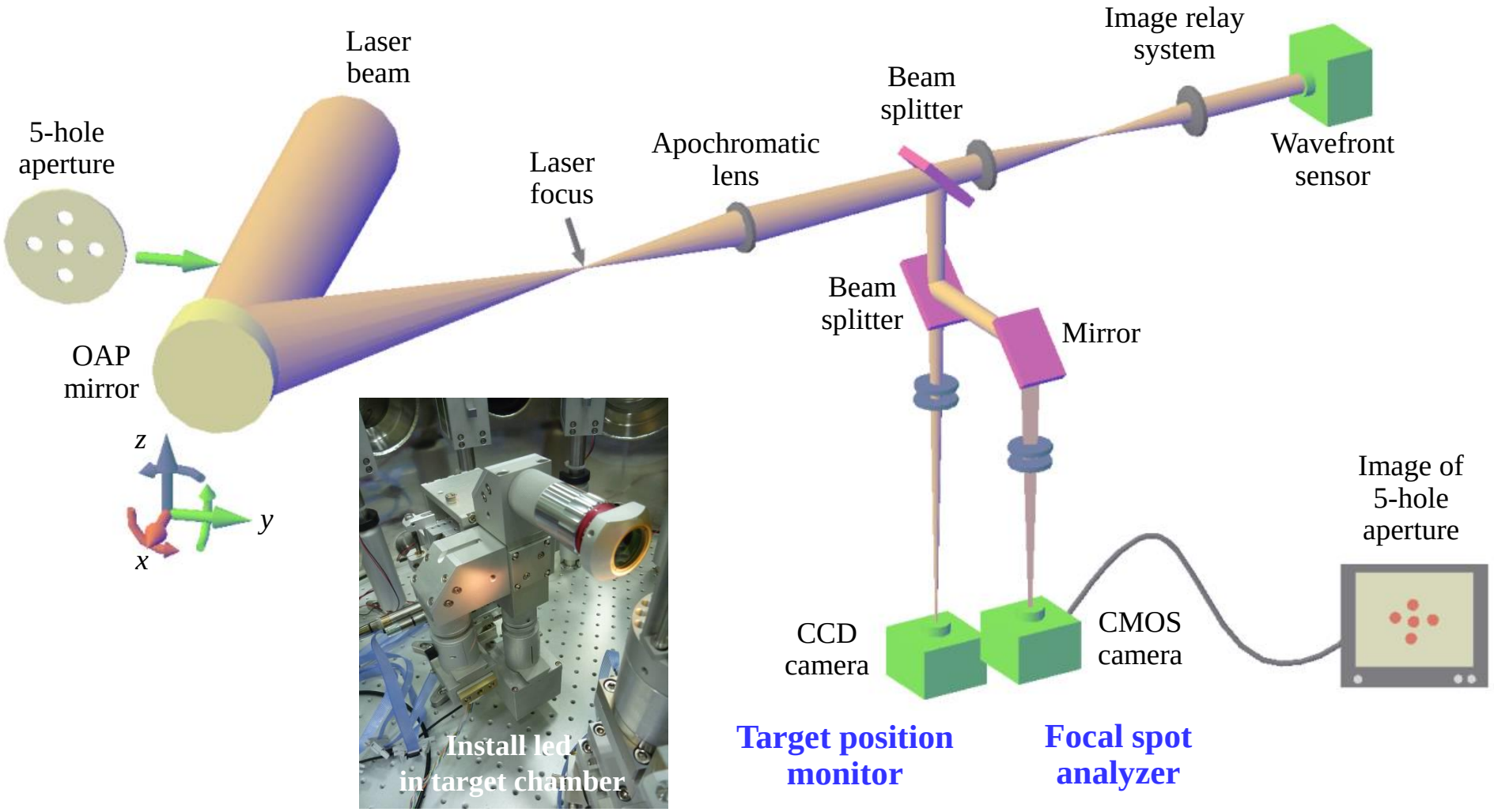

I. W. Choi *et al.*, J. Korean Phys. Soc. **55**, 517 (2009).

Focal Spot Characterization and Focusing Intensity

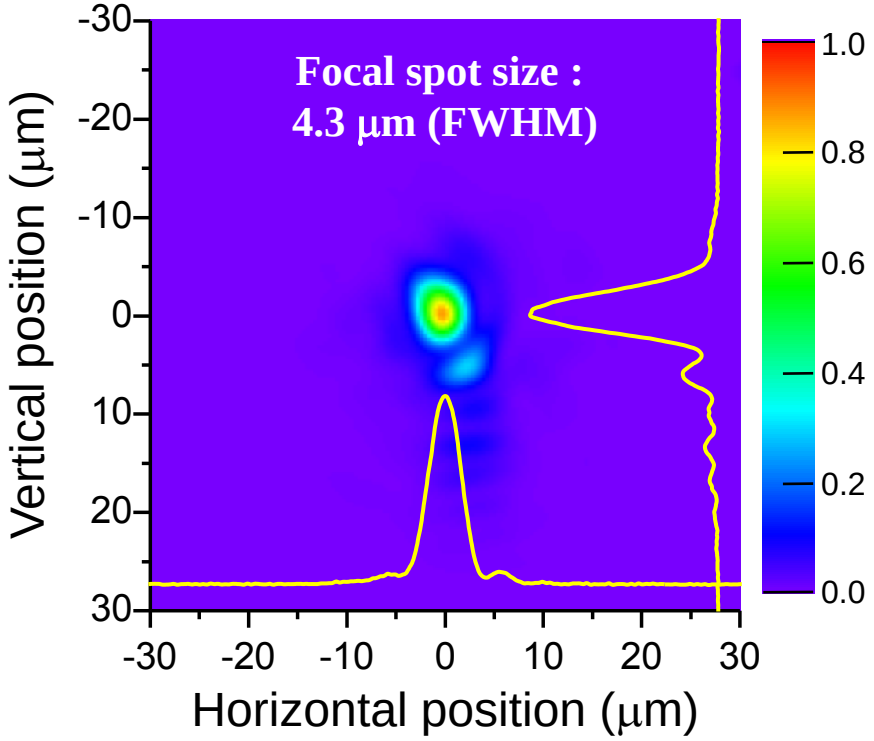

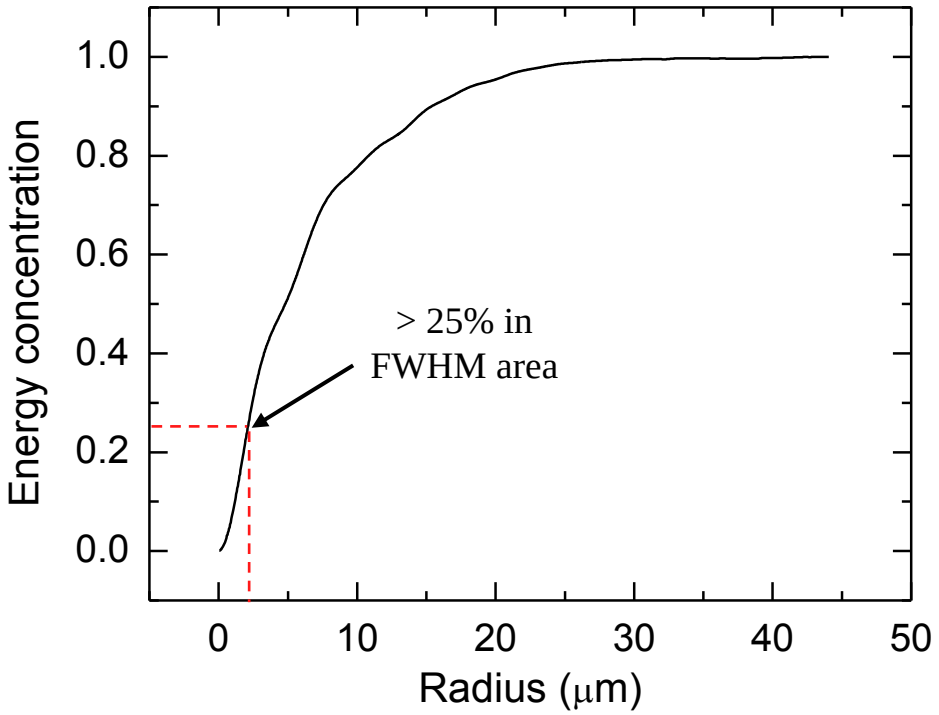

Laser energy and pulse width on target : 8.5 J, 30 fs

Focal spot size obtained with f/3 OAP : 4 μm

Energy concentration in FWHM area : > 25%

→ 7×10^{20} W/cm^2 for PW laser + DPM

Accurate Target Alignment

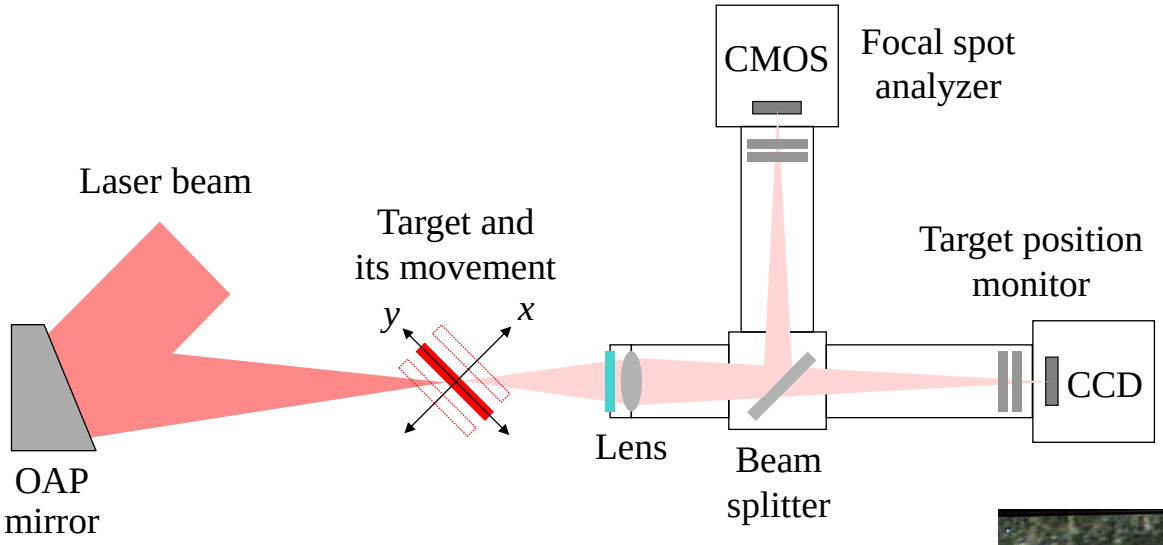

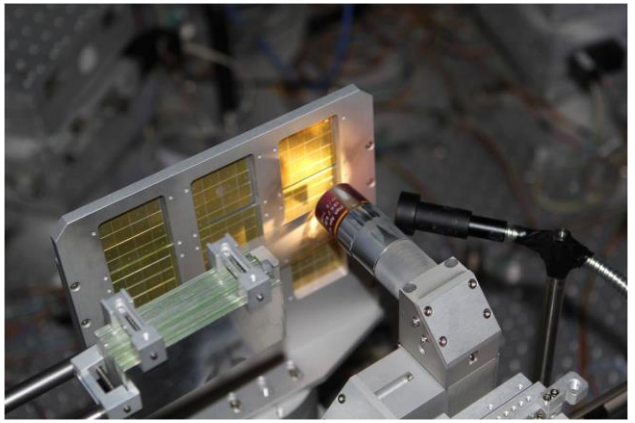

45° incidence

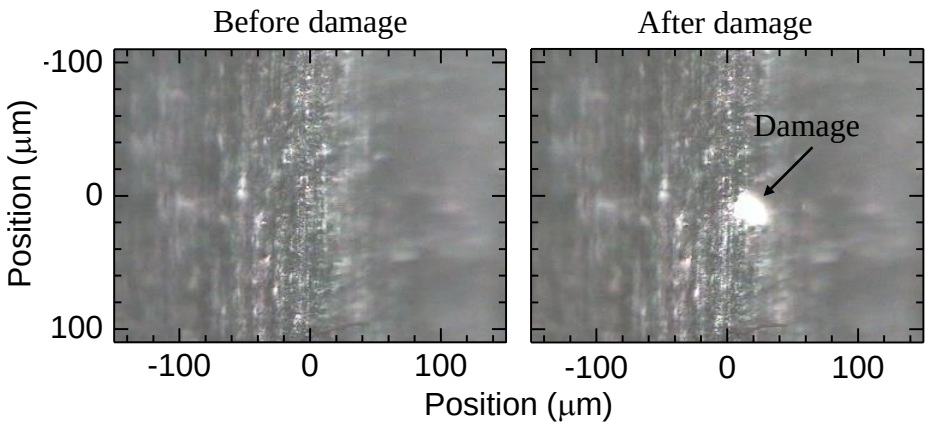

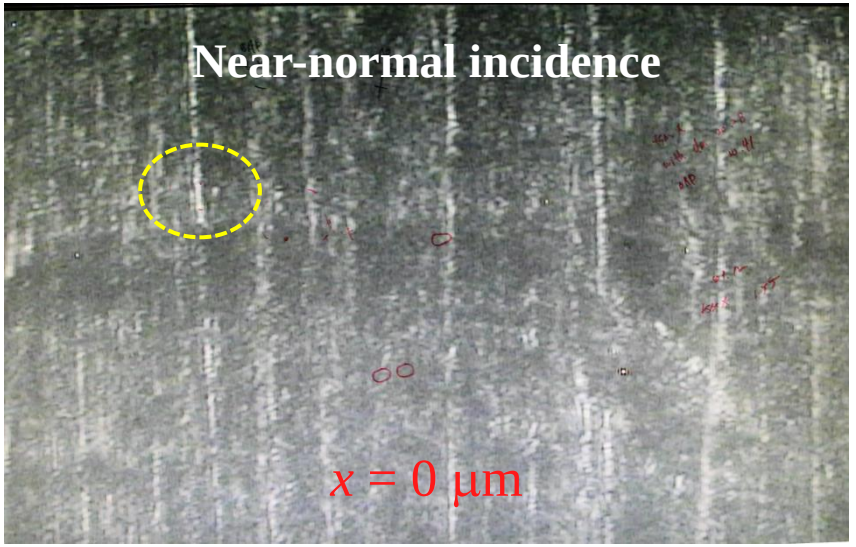

Much better accuracy than Rayleigh range ~50 μm

Ultrathin Free-standing Polymer Target : F8BT

1. Commonly used targets : Al, Mylar, Si_3N_4, Diamond-like carbon, etc.

2. Alternative ultrathin target proposed

- Conjugate polymer material : F8BT, poly(9,90-dioctylfluorene-co-benzothiadiazole)
- Polyfluorene derivative used for in polymer LED, organic solar cell and transistor
- Manufacture method : spin coating → floating on water → transferring to a target frame
- Available thickness : 5-500 nm
- Chemical formula : $(C_{35}H_{42}N_2S)_n$

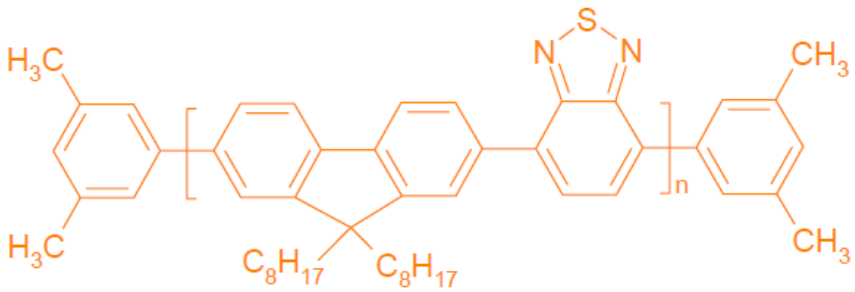

3. Advantages of the polymer target

- Easy manufacture, low material and production cost
- Low electron density of ~200 n_c for 800-nm wavelength laser

  → Realization of ultraintense laser-ultrathin target interaction using relatively low laser intensity, such as relativistic transparency, RPA, etc.

Ultrathin Free-standing Polymer Target

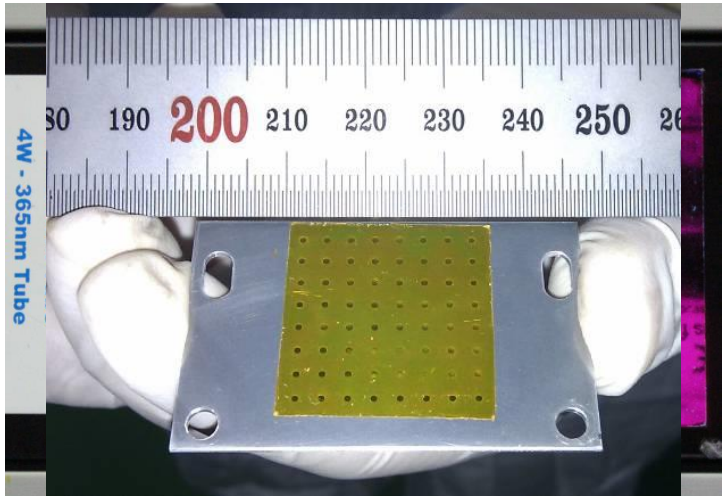

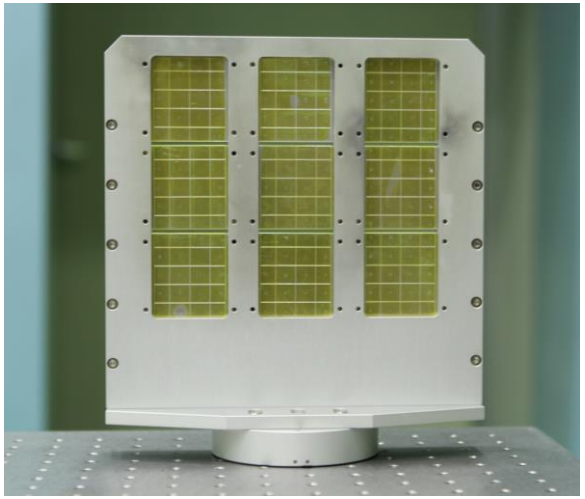

200-300 laser shots possible with one loading in target chamber

Free-standing polymer attached on target frame

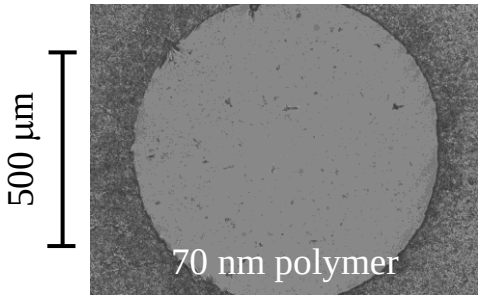

Flatness of 100-nm thick polymer

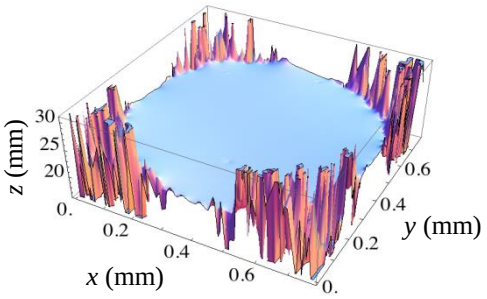

Roughness of 100-nm thick polymer

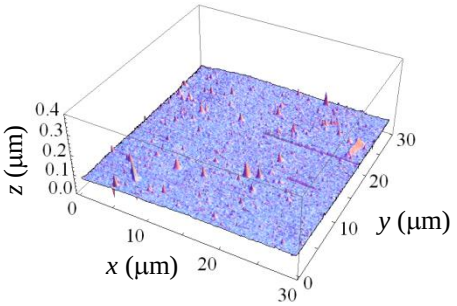

1.2-μm thick Al : r.m.s roughness ~1 μm

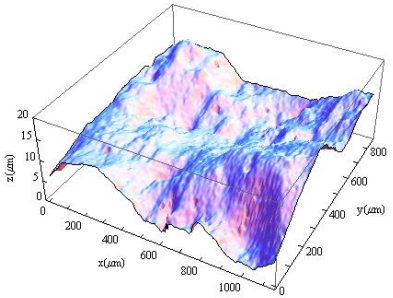

I. W. Choi *et al.*, Appl. Phys. Lett. **99**, 181501 (2011).

Characterization of Nanometer-Class Polymer Target

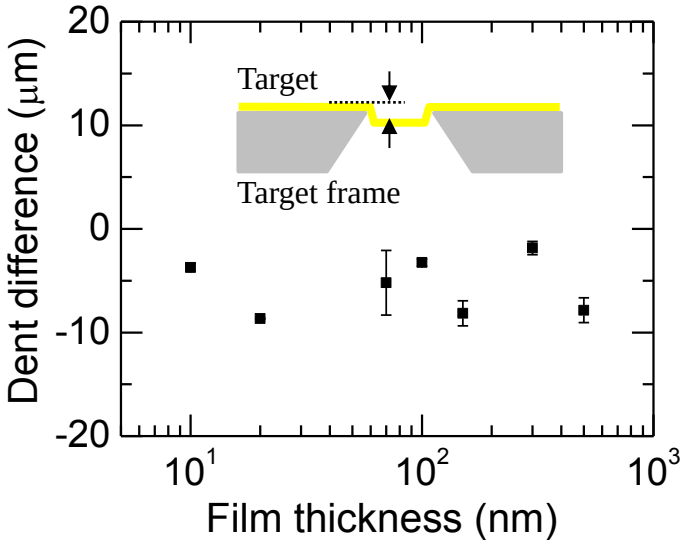

Raleigh range >>
dent distance

→ Frame surface alignment enough

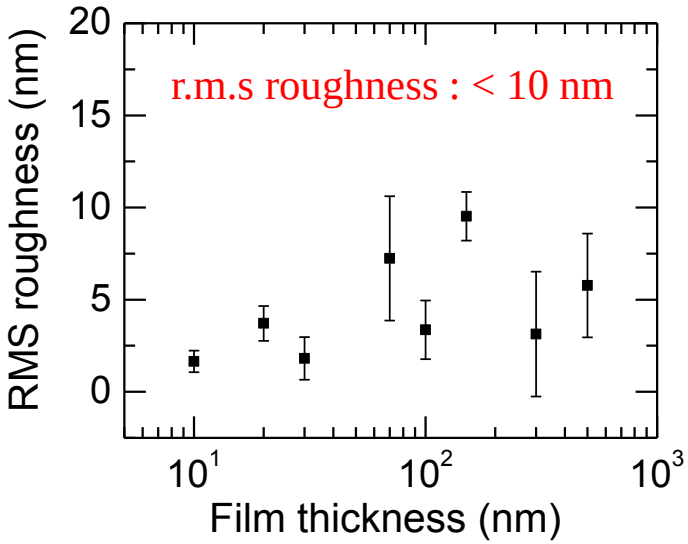

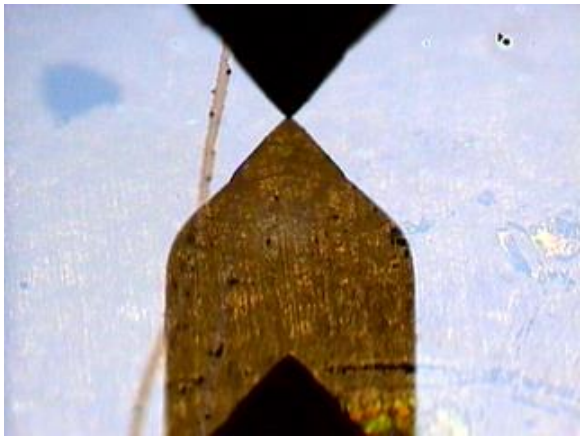

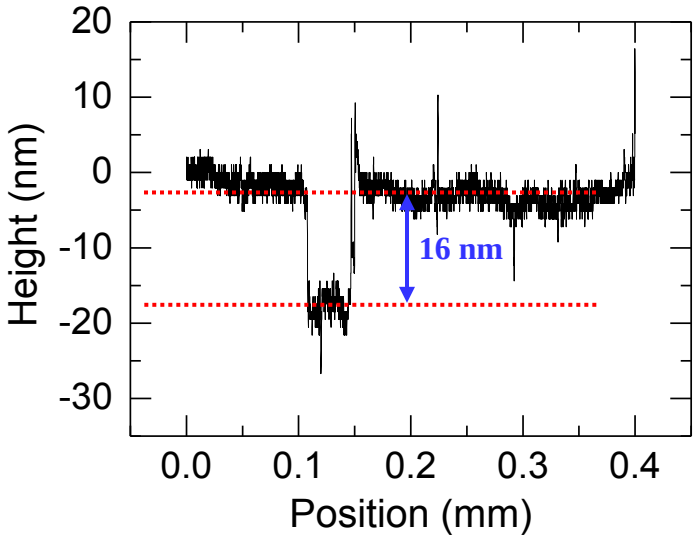

Alpha-step surface profiler
- Thickness measurement range : > ~20 nm

X-ray Reflectivity Measurement for Thickness and Density

X-ray reflectivity measurement

- Used for estimation of density, thickness, roughness

- Critical angle for total external reflection :

$$\cos\theta_c = \sqrt{1 - \omega_p^2 / \omega_0^2} \qquad \theta_c \approx \omega_p / \omega_0 = \sqrt{n_e / n_c}$$

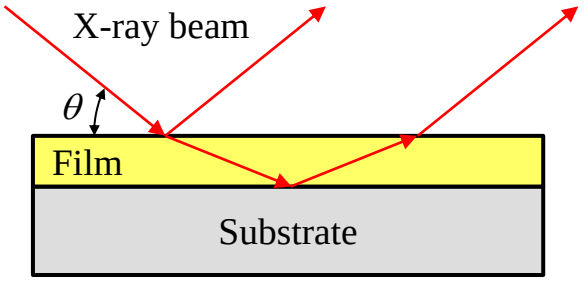

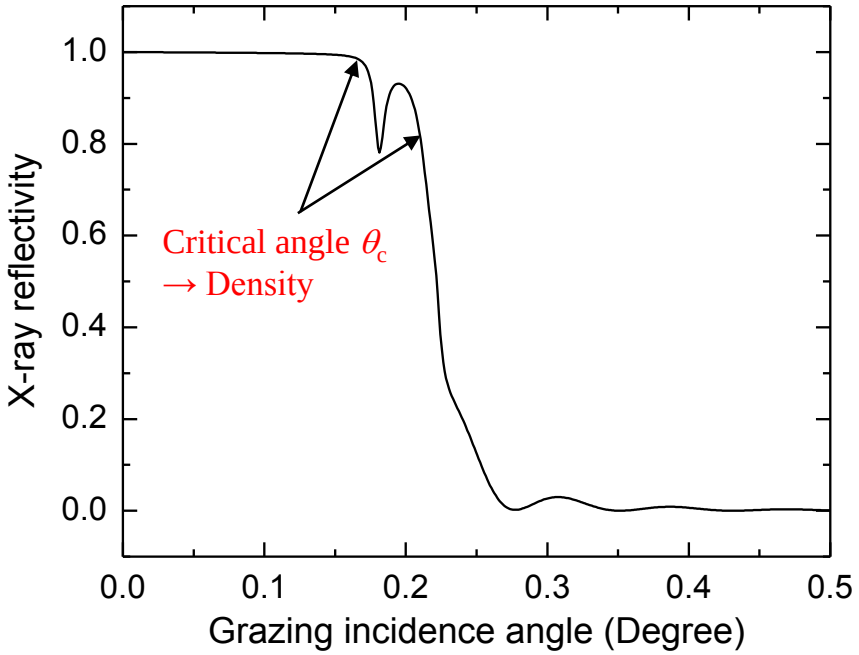

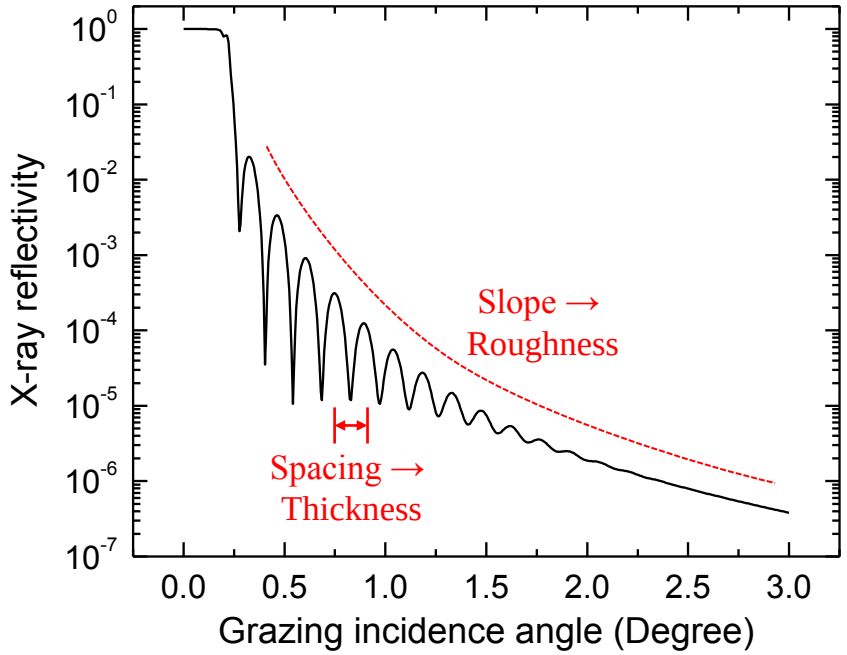

Thickness and Density of Nanometer-Class Polymer Target

X-ray reflectivity measurement

- Intensity maxima

$$2d\sqrt{\sin^2\theta_m - \sin^2\theta_c} = m\lambda$$

$$\sin^2\theta_m = \sin^2\theta_c + \left(\frac{\lambda}{2d}\right)^2 m^2$$

- Intercept with $m^2 = 0 \rightarrow$ critical angle θ_c
- Slope of the linear dependence $\rightarrow$ thickness d
- Thickness measurement range : > ~1 nm

X-ray photon energy : Cu Kα 8.05 keV

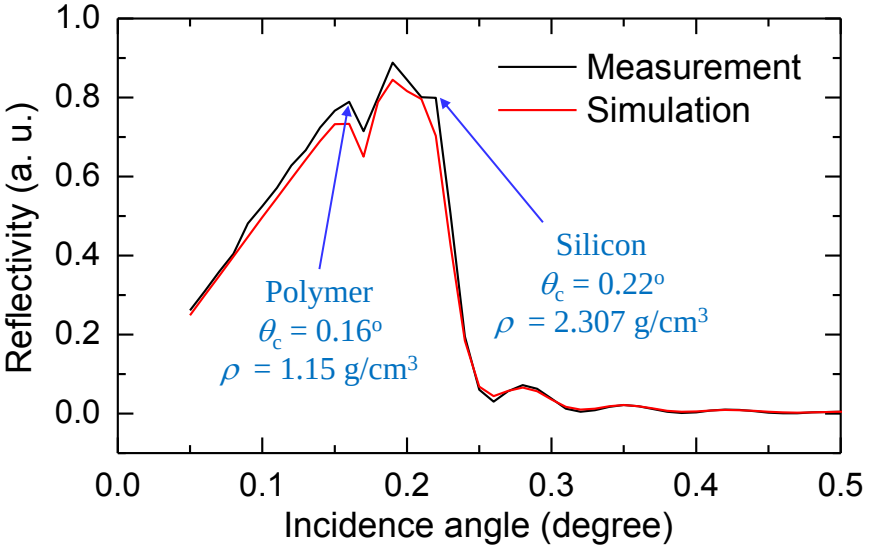

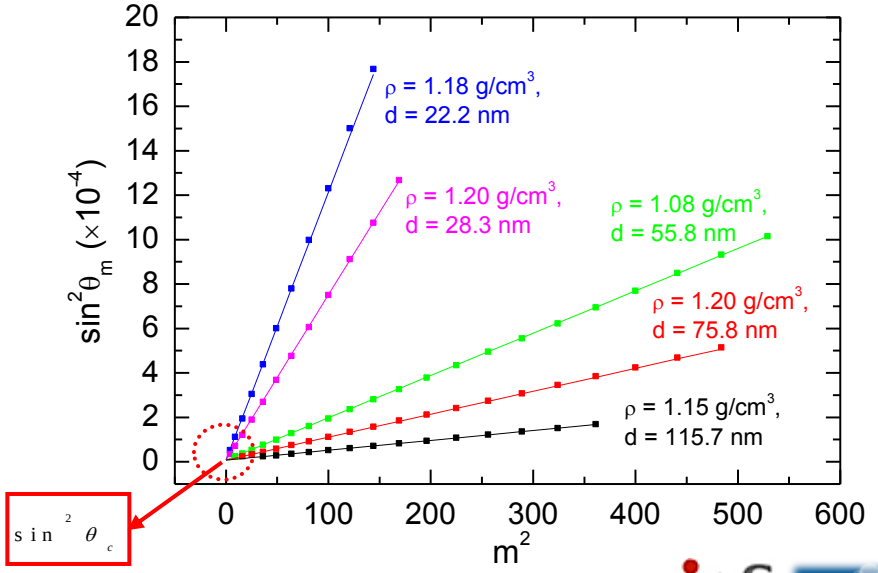

Conjugated polymer, F8BT

- Material density : 1.1-1.2 g/cm^2
- Electron density : 3.5-3.8×10^{23}/cm^3 for C^{6+}, H^+, N^{7+}, S^{10+}

→ **200-220 n_c for 800-nm laser wavelength**

Thickness Possible Down to ~4 nm

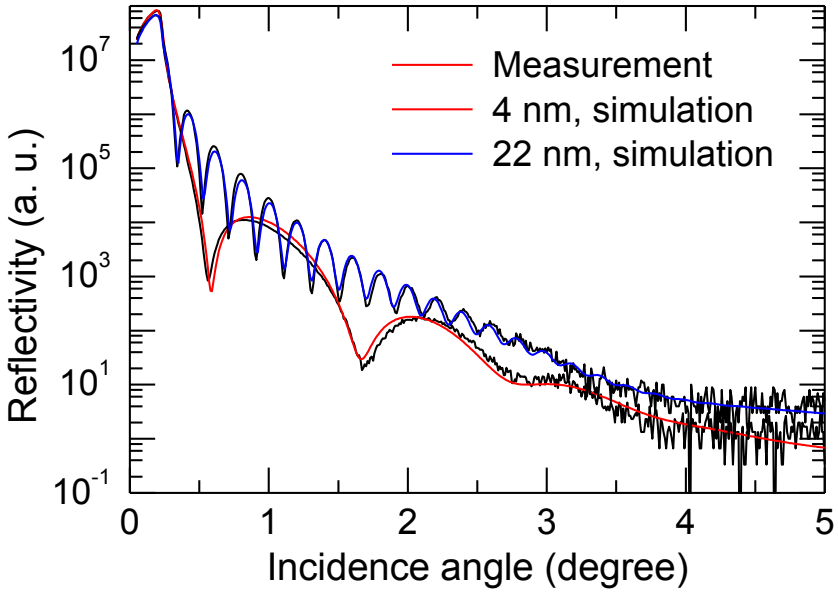

- Available thickness : < 5 nm
- Thickness reproducibility : ~90%
- Thickness uniformity over the surface : ~90%

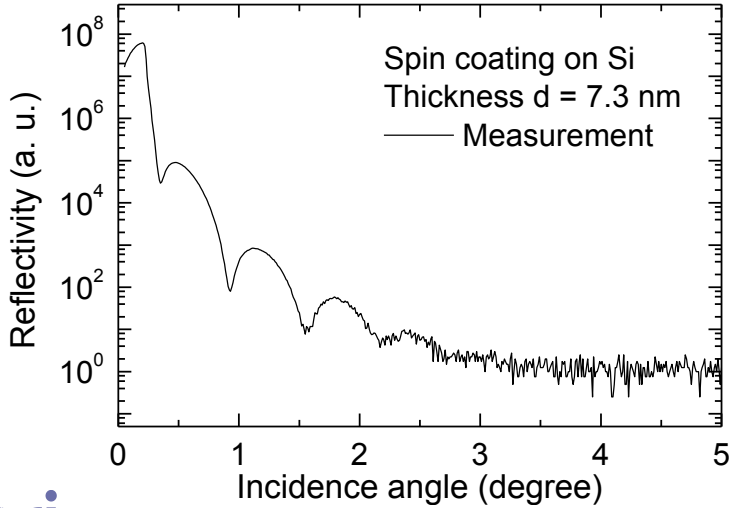

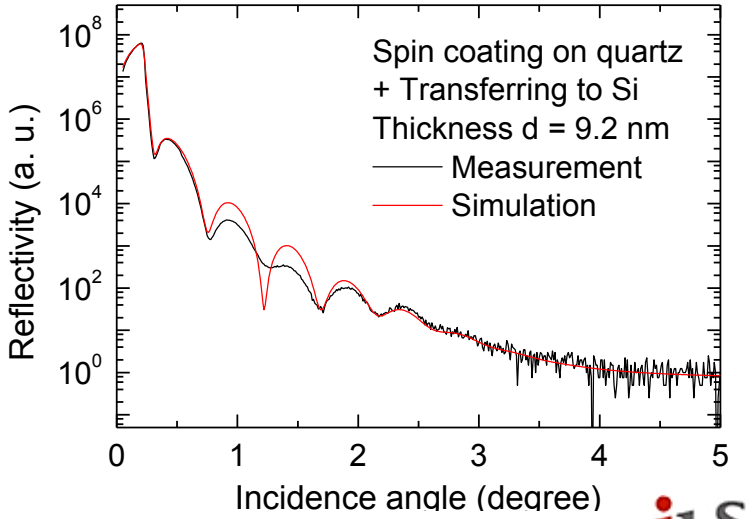

Thomson Parabola Spectrometer (TPS)

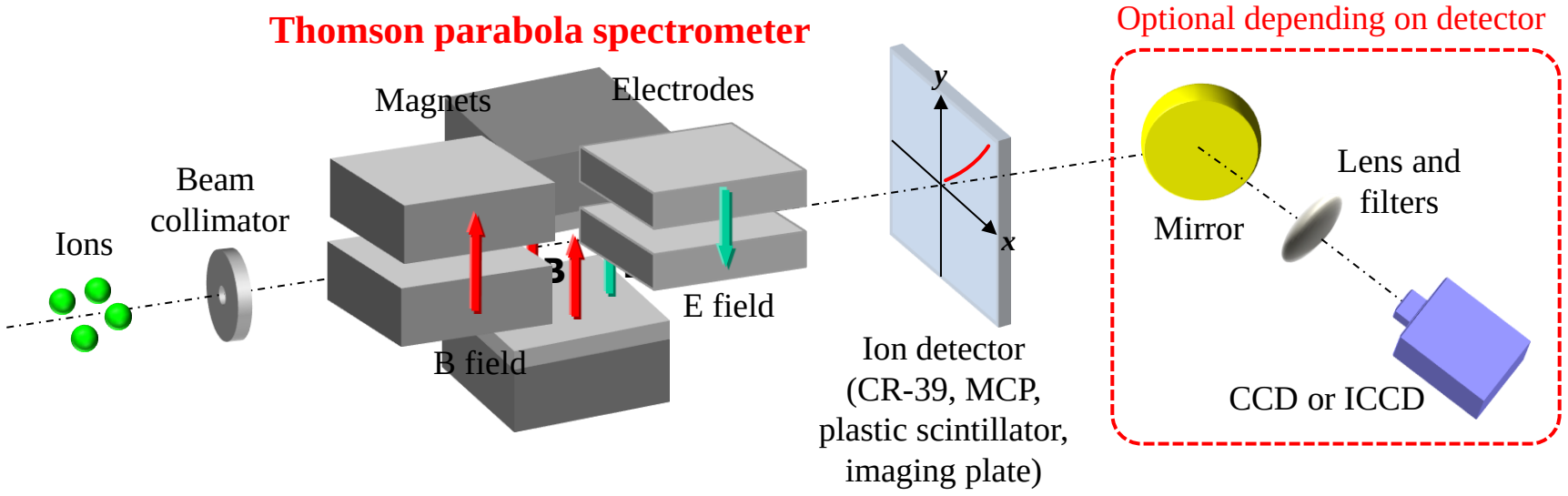

$$x = \frac{q B L_i}{m v}\left(\frac{L_i}{2} + L_f\right), \qquad y = \frac{q E L_i}{m v^2}\left(\frac{L_i}{2} + L_f\right)$$

$$y = \frac{m}{q} \frac{2E}{B^2 L_i (L_i + 2L_f)} x^2, \qquad y = \frac{E}{B} \frac{1}{v} x$$

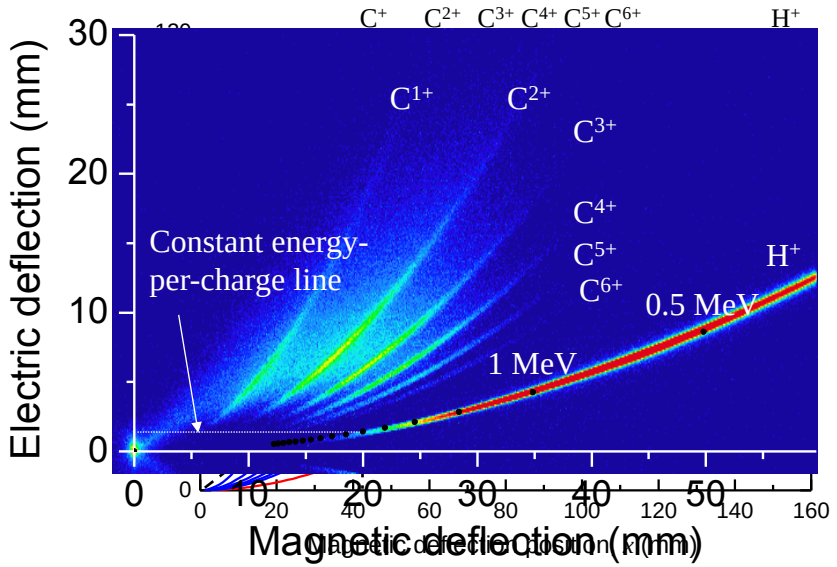

Time-Of-Flight (TOF) Spectrometer

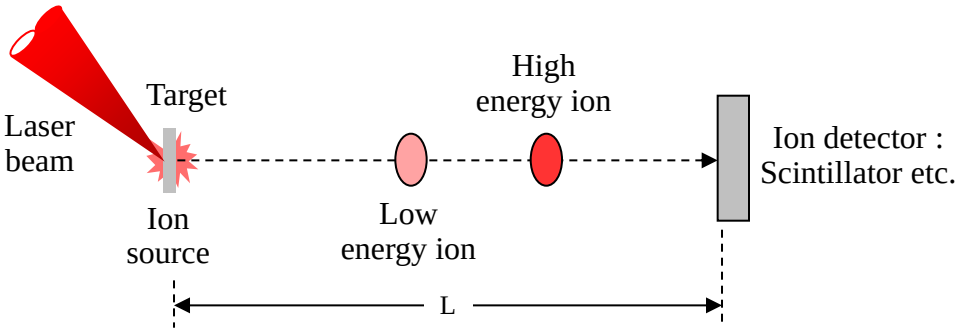

$$t = \frac{L}{c}\frac{1+\left(\frac{E}{m_i c^2}\right)}{\sqrt{\left(\frac{E}{m_i c^2}\right)^2+2\left(\frac{E}{m_i c^2}\right)}}, \qquad E = m_i c^2\left[\frac{1}{\sqrt{1-\frac{L^2}{(ct)^2}}}-1\right]$$

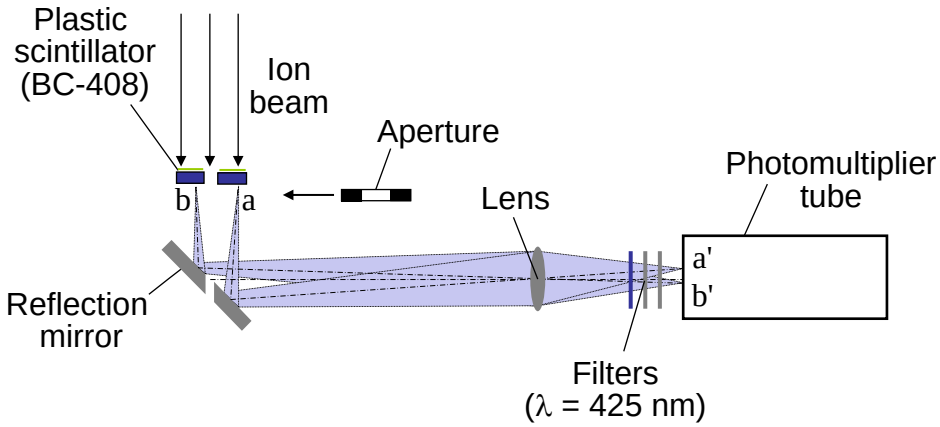

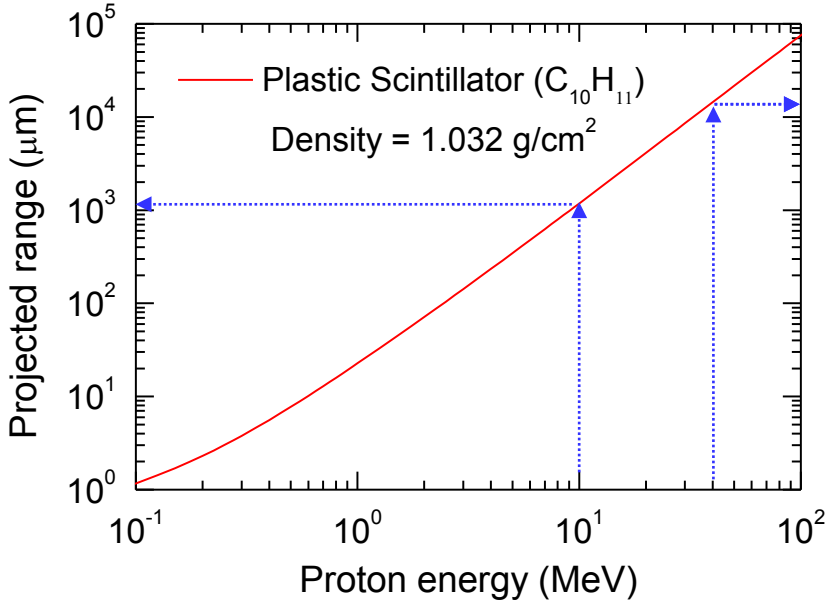

Selection of scintillator thickness

Ion Spectrometer Composed of TOF and TP Spectrometers

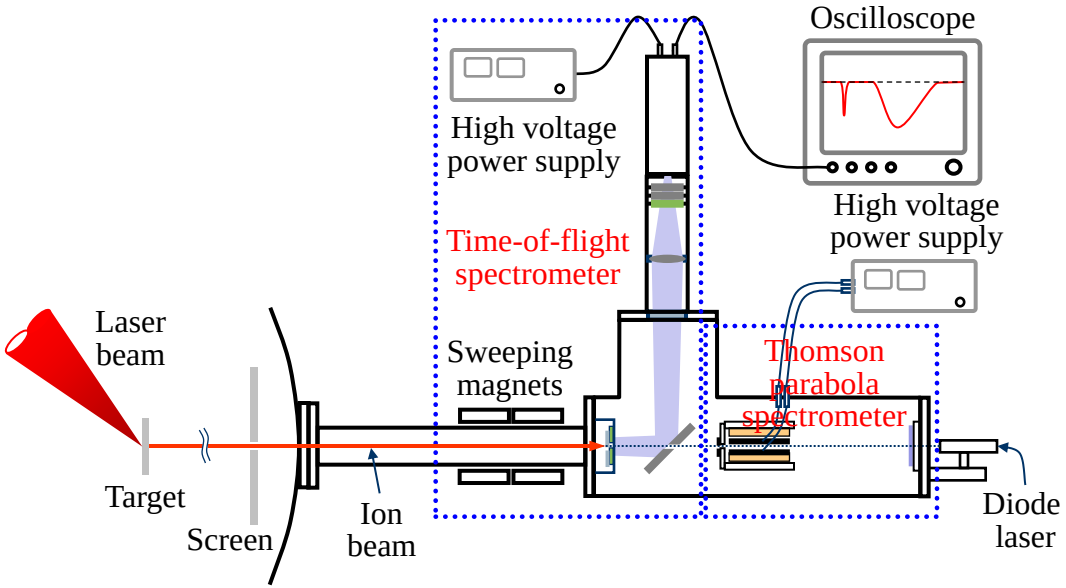

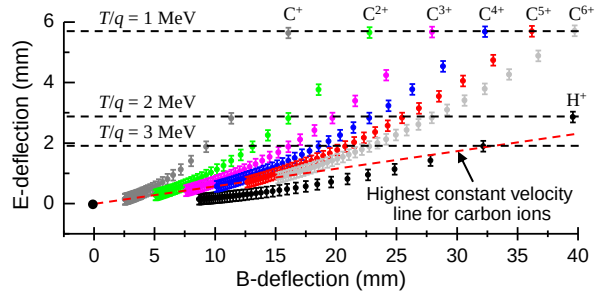

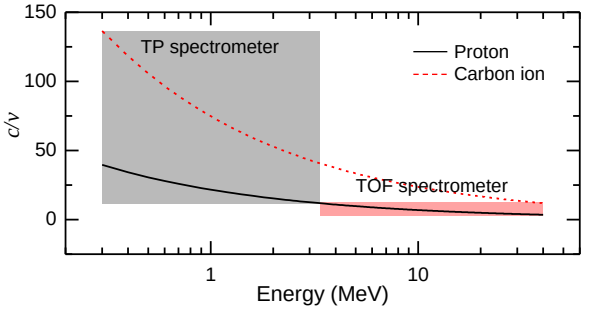

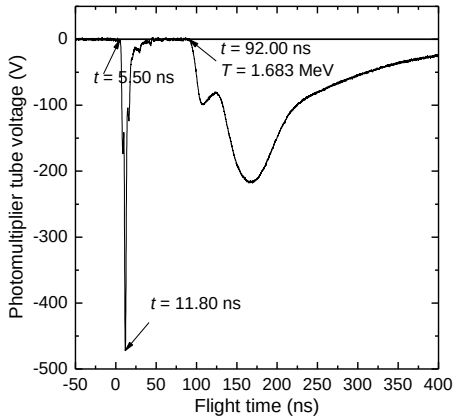

+

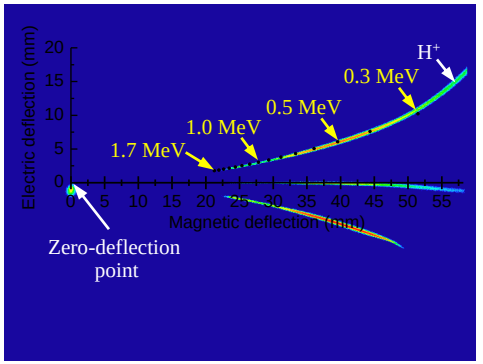

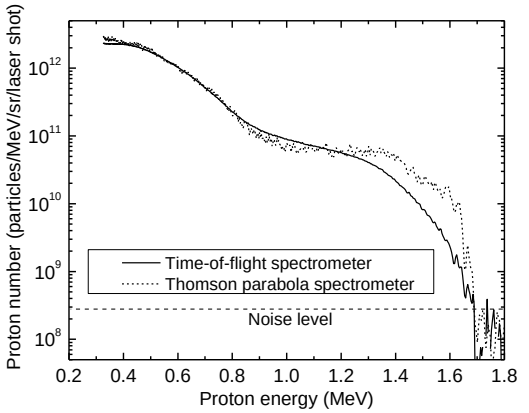

I. W. Choi *et al.*, Rev. Sci. Instrum. **80**, 053302 (2009).

Ion Detectors : MCP, Imaging Pate (Limited Thickness)

Microchannel plate (MCP)

Stopped energies in 1-mm glass : 13 MeV (Proton), 275 MeV (Carbon)

Response dependent on

- Ion energy and species
- Penetration depth of ions into the channel
- Channel bias angle
- Open area ratio
- Incident angle of the ions on channel

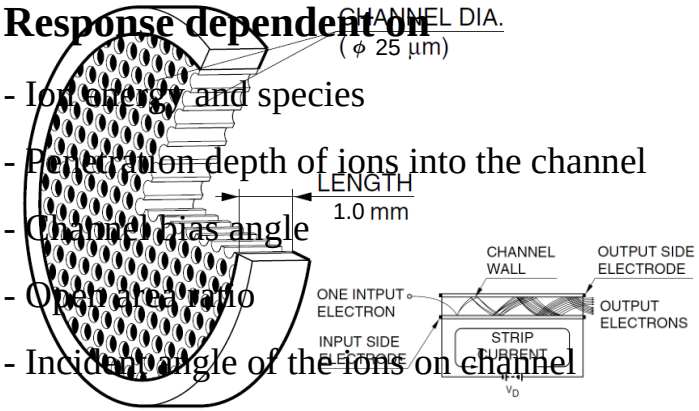

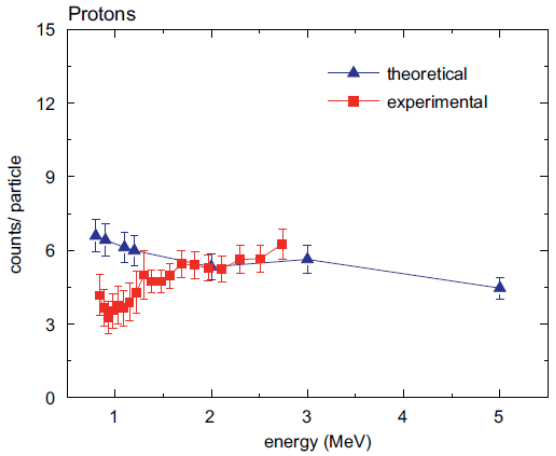

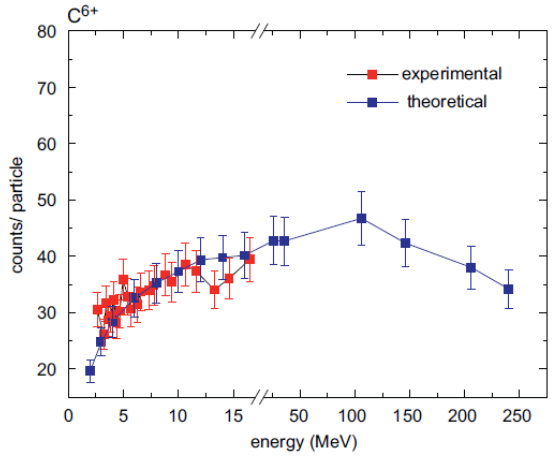

R. Prasad *et al.*, Nucl. Instrum. Methods Phys. Res. Sect. A. **623**, 712 (2010).

Imaging plate

IP type		Protective layer	Sensitive layer	Undercoat layer	Base film	Back layer
BAS-MS (white)	Area density (g/m^2)	14.9	380.3	16.5	266.7	443.7
	Thickness (μm)	9	115	12	190	160
BAS-SR (light blue)	Area density (g/m^2)	10.4	389.8	18.5	266.7	443.7
	Thickness (μm)	6	120	10	190	160
BAS-TR (intermediate blue)	Area density (g/m^2)	0	142.6	13.9	346.6	443.7
	Thickness (μm)	0	50	10	250	160
FDL-UR-V (deep blue, 25 μm)	Area density (g/m^2)	4.5	441.0	25.2	180.7	27.3
	Thickness (μm)	3	110	20	145	30

B. Hidding *et al.*, Rev. Sci. Instrum. **78**, 083301 (2007)

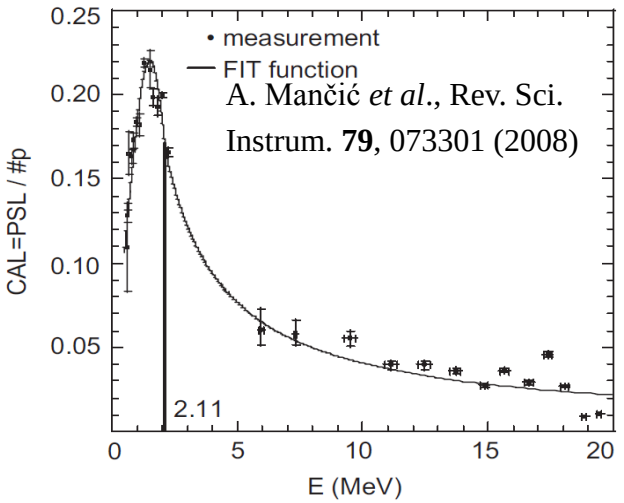

Ion Detectors : Plastic Scintillator

Plastic scintillator

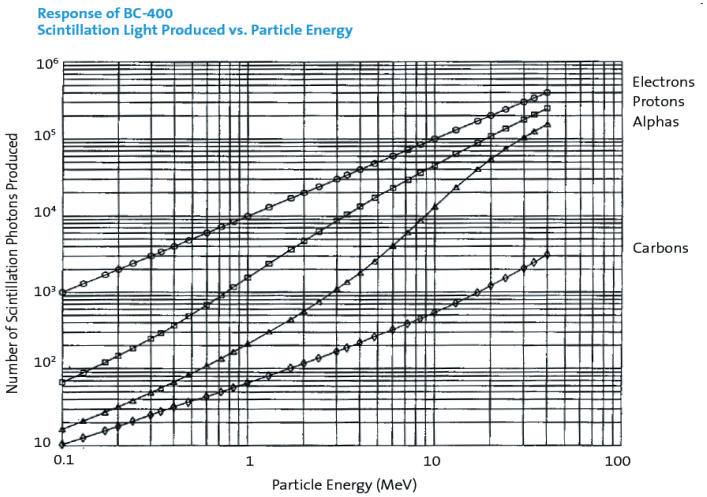

http://www.detectors.saint-gobain.com

Birks's Formula

$$\frac{dL}{dx} = \frac{S\left(\frac{dE}{dx}\right)}{1 + kB\left(\frac{dE}{dx}\right) + C\left(\frac{dE}{dx}\right)^2}$$

Quenching effect

dL/dx = Flourescence light

dE/dx = Energy loss

S = Scintillation efficiency

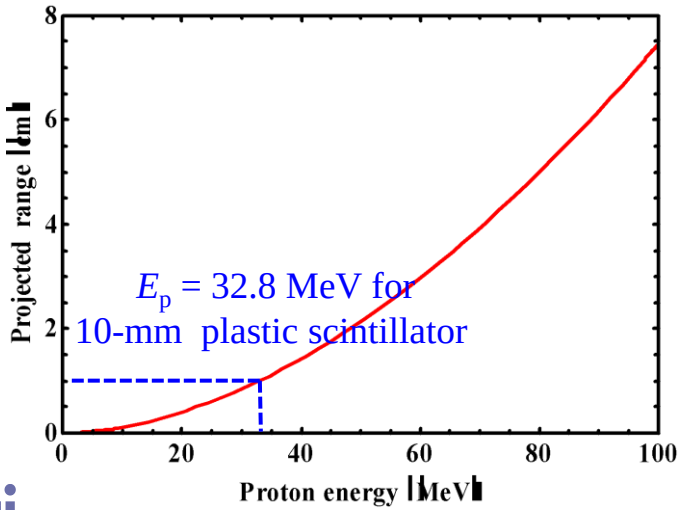

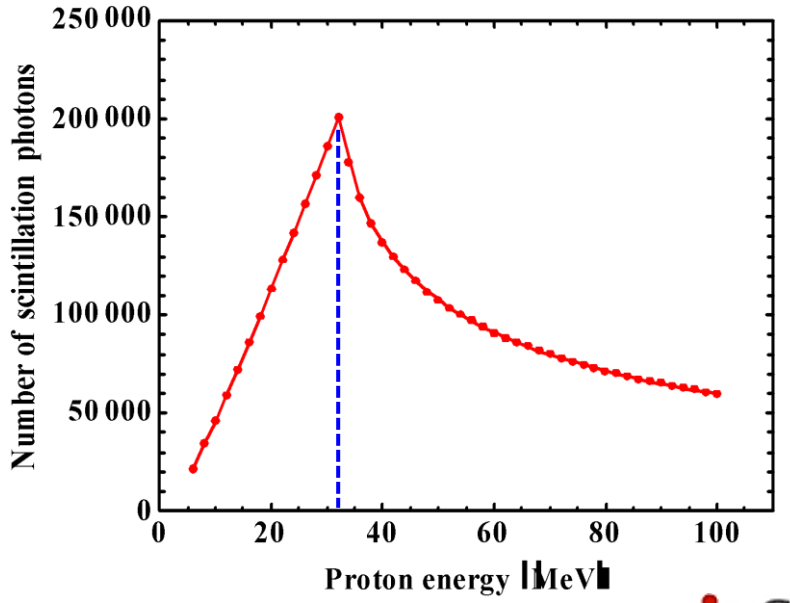

Energy and Beam Profile Measurement Using Stacked Detectors

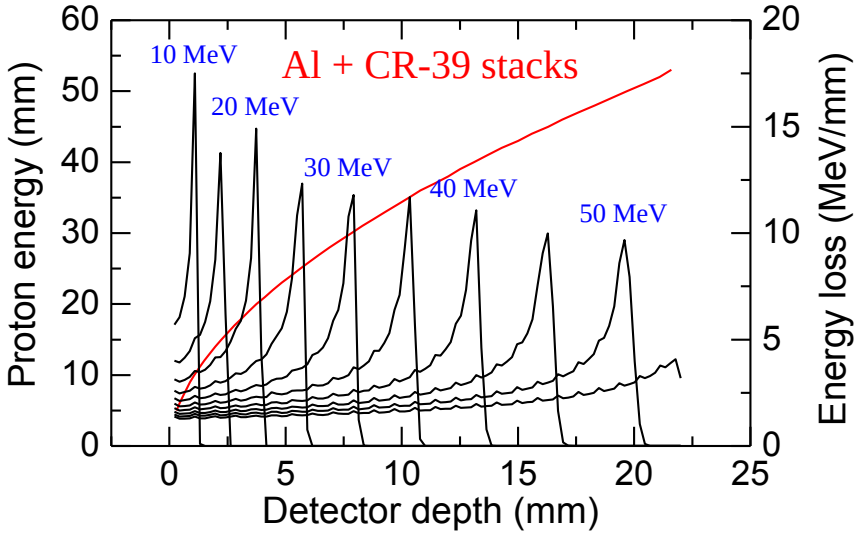

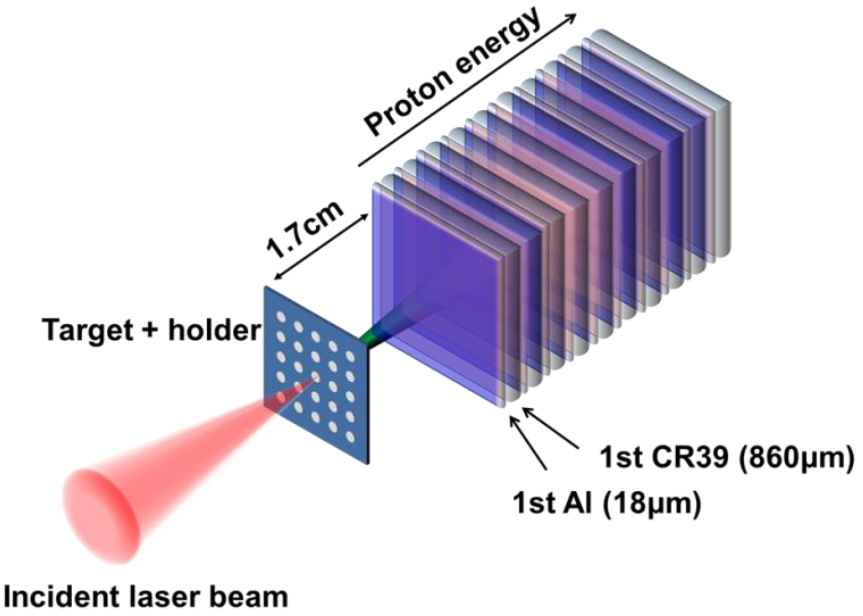

Al + CR-39 stacks

E_p = 40 MeV

Longitudinal range = 13.1 mm

Longitudinal straggle = 230 μm

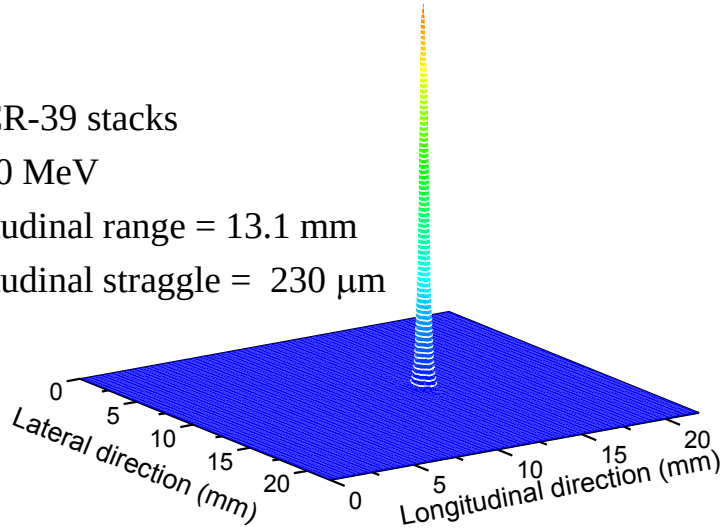

RCF stack : 19 films of HD-810 and 3films of MD-55

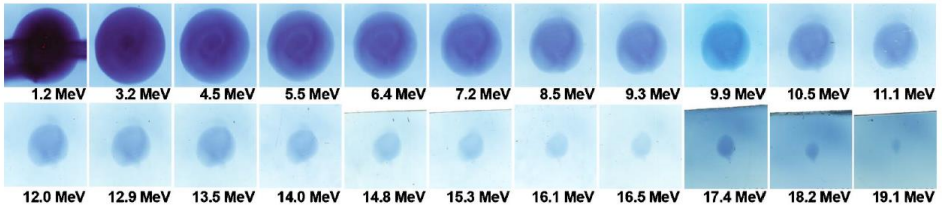

F. Nürnberg, Rev. Sci. Instrum. **80**, 033301 (2009)

Proton Acceleration Using PW Laser Pulses

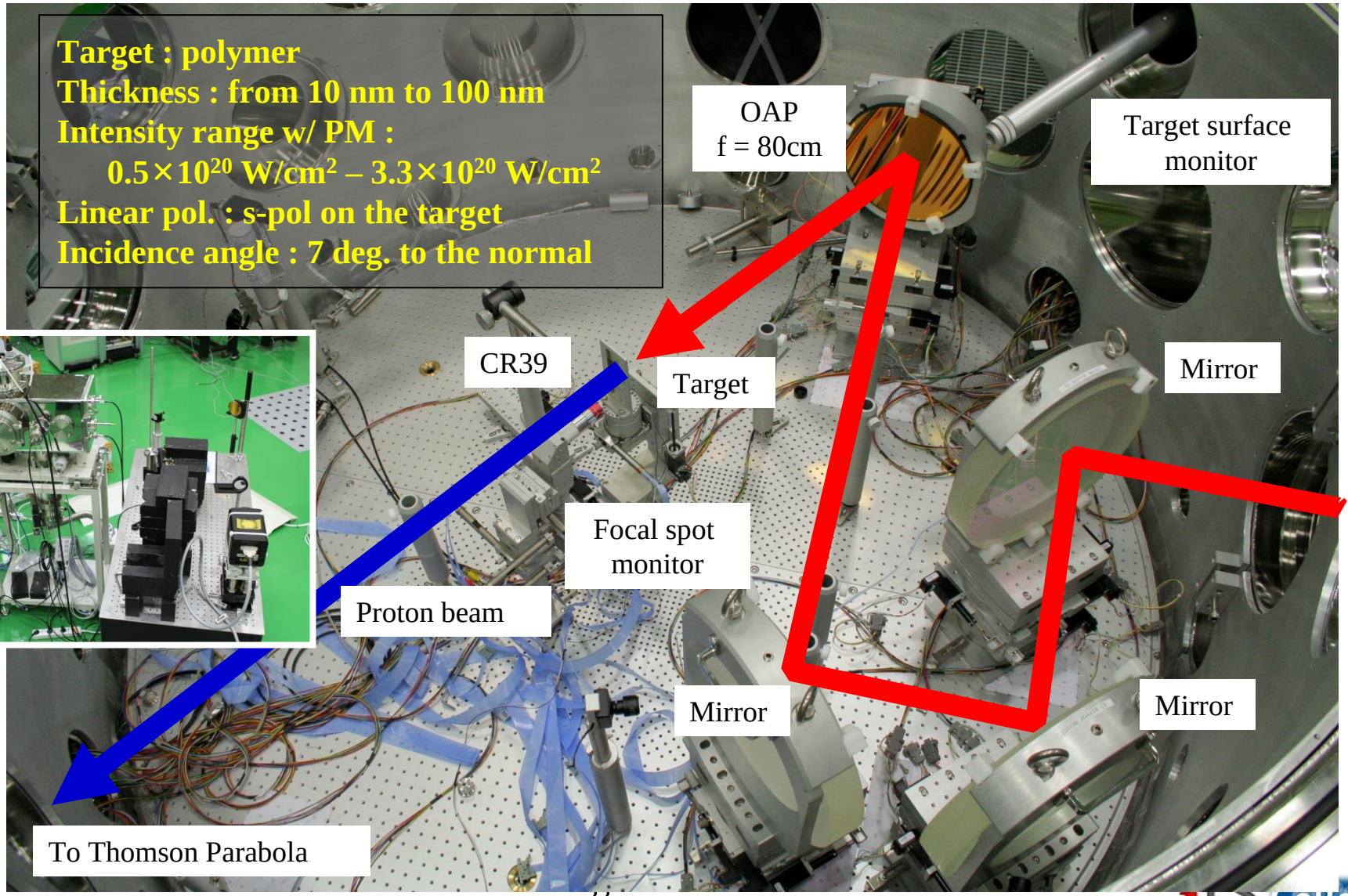

Good Agreement between TPS and CR-39 Measurement

- Target thickness : 30 nm
- Laser intensity : 3.3×10^{20} W/cm^2

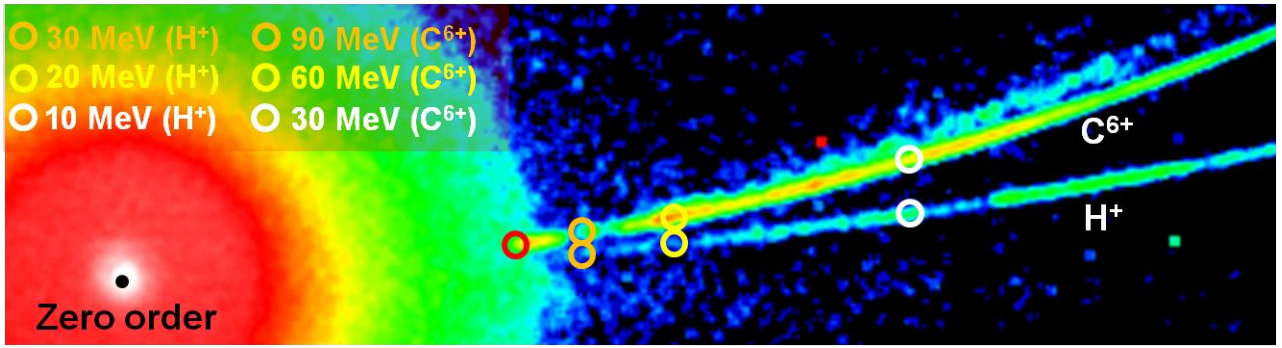

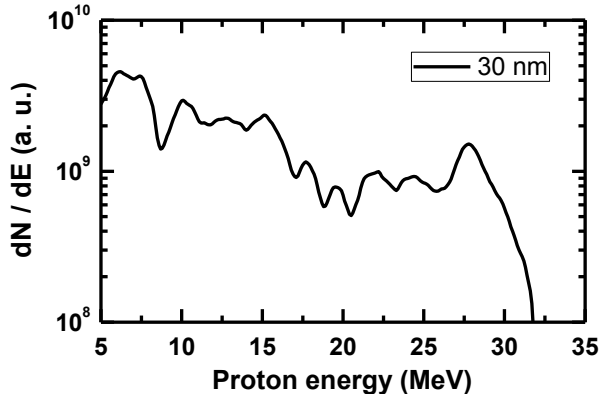

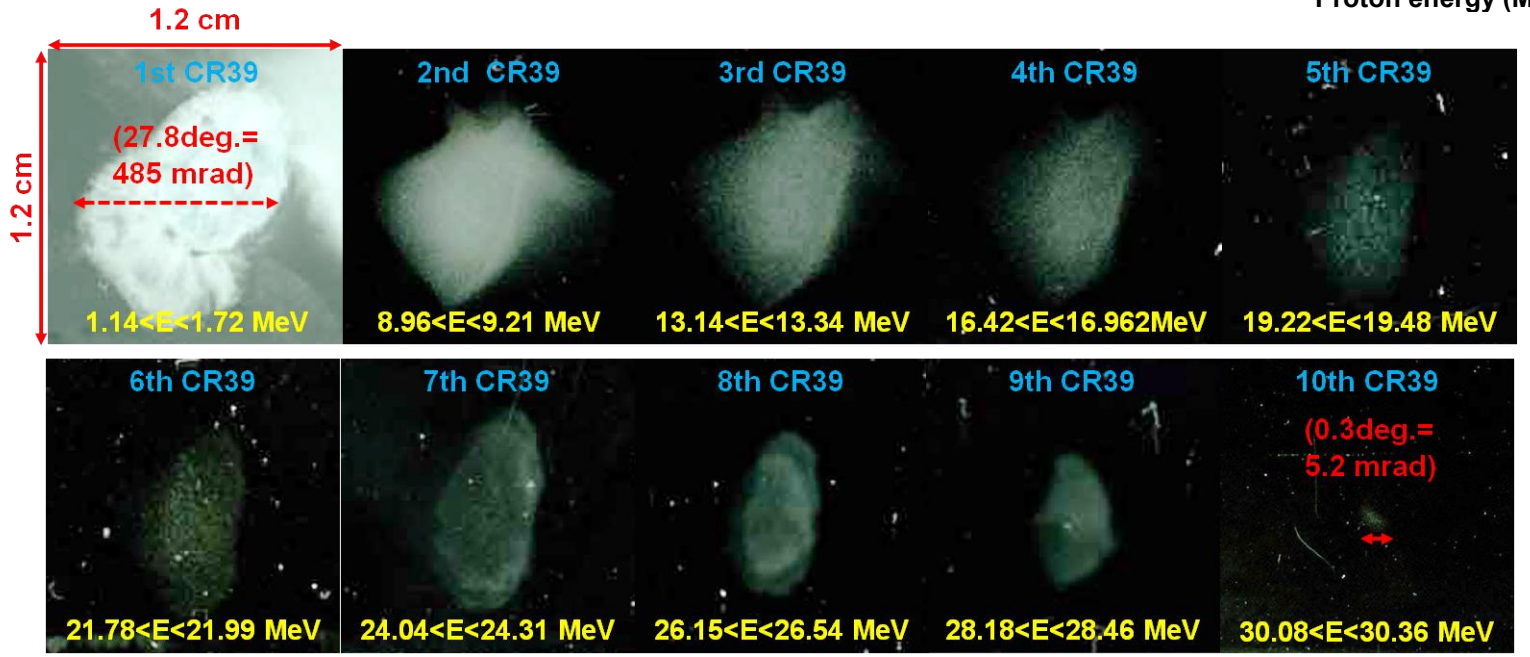

Good Agreement between TPS and CR-39 Measurement

- Target thickness : 70 nm - Laser intensity : 3.3×10^{20} W/cm^2

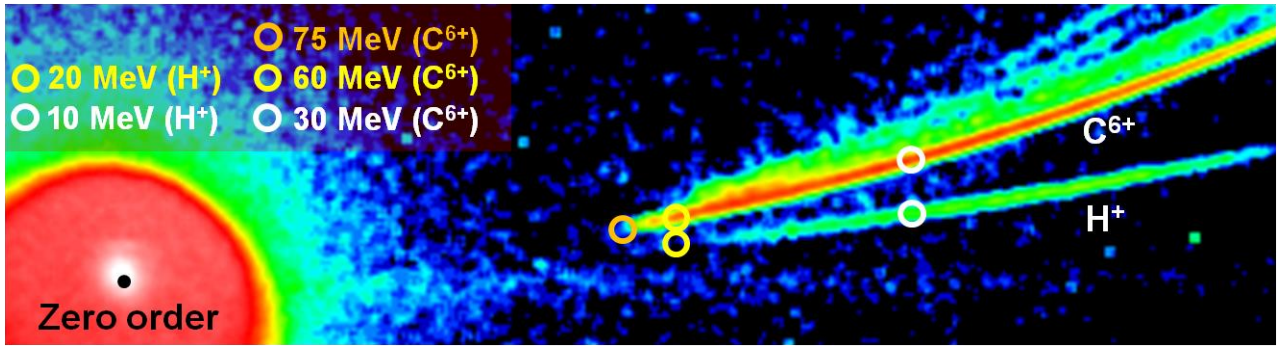

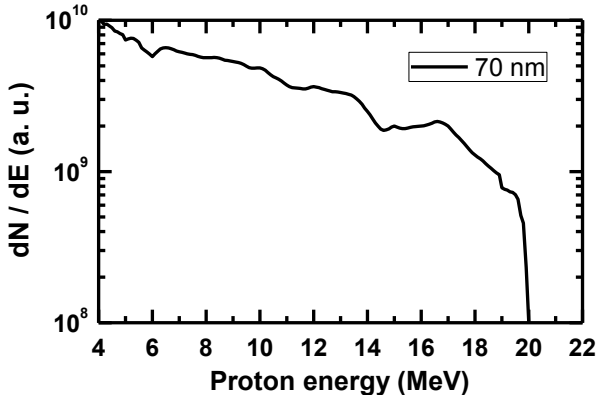

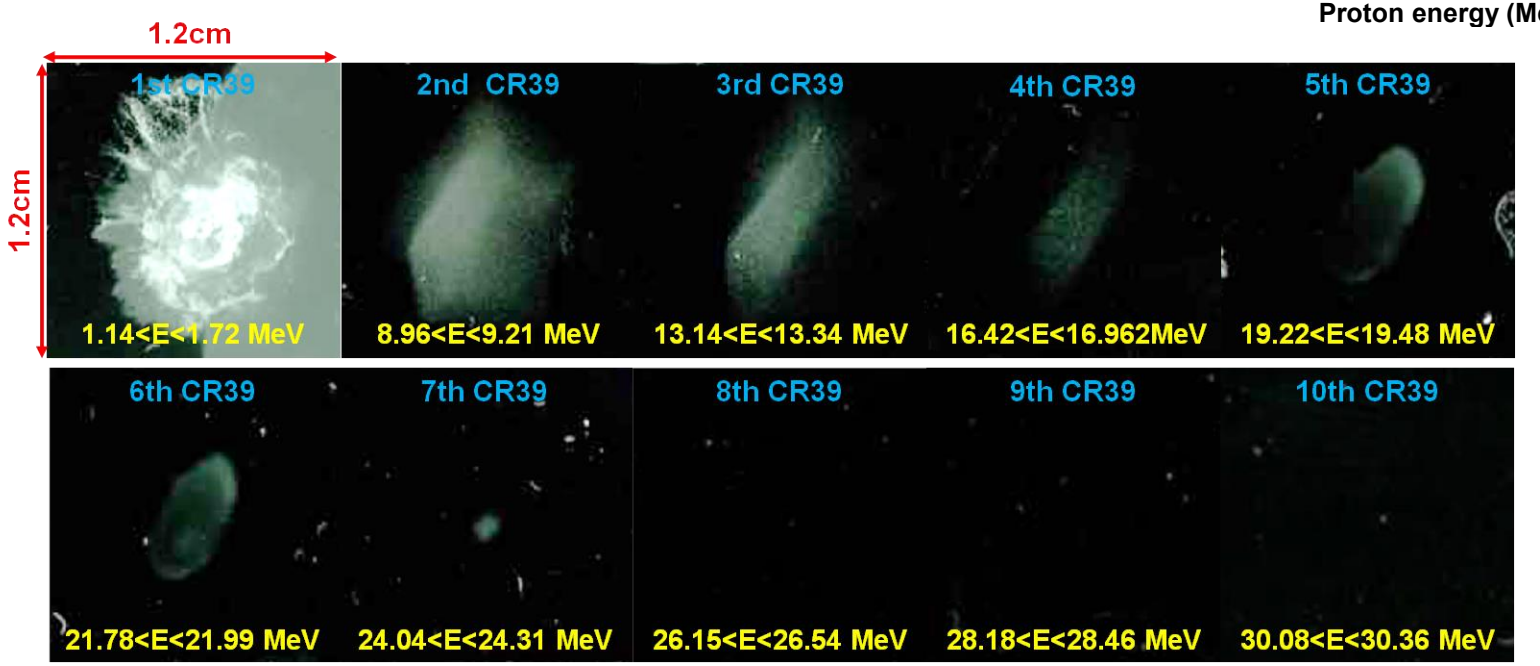

45 MeV Proton Energy Achieved with 10-nm Thick Polymer

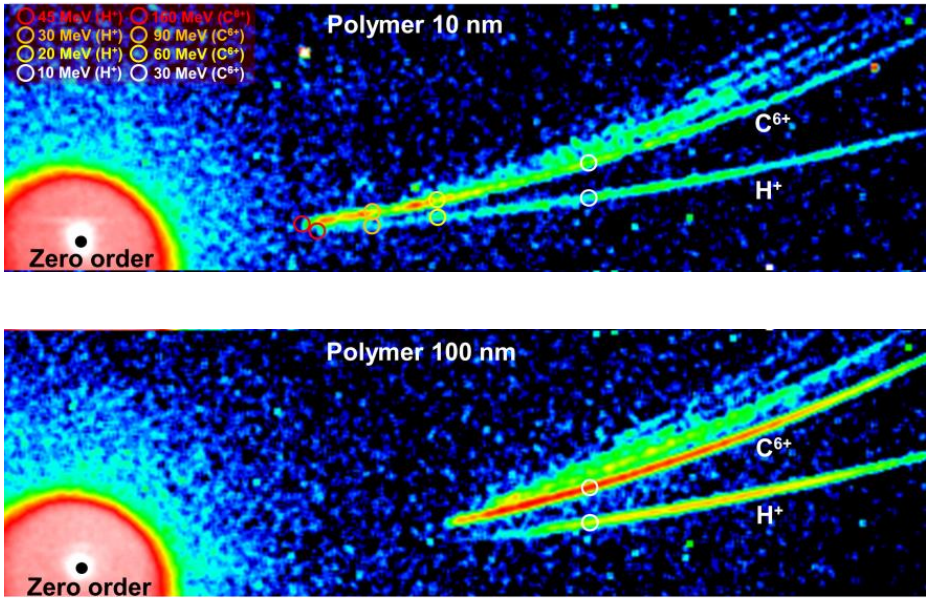

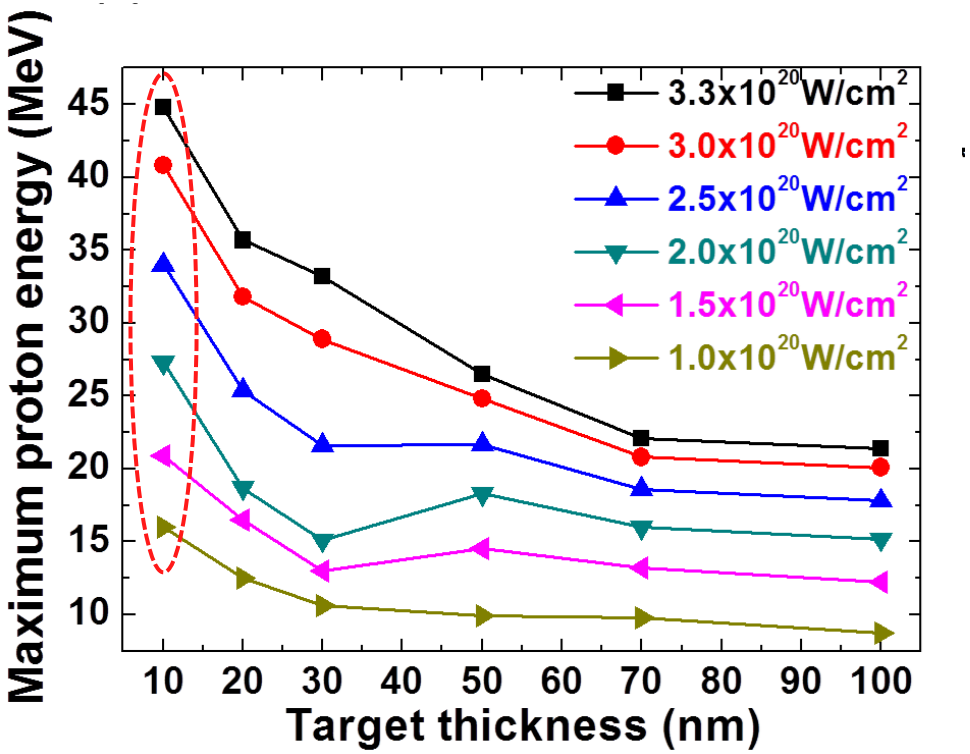

- ✓ Thomson parabola and ion energy spectra obtained with a 3.3×10^{20} W/cm^2 laser intensity and 10-nm thick polymer target
- ✓ Continuous energy increase until 10-nm target implies the high performance of double plasma mirror system, very high contrast up to several ps before main pulse arrival.

Conclusions

Several issues solved already or to be solved for real applications

Thank you for your attention

Laser beam

- ✓ Well-controlled temporal and spatial properties
- ✓ Low- or high- contrast, depending on target type
- ✓ Rough alignment for each shot and robust shooting
  - Reproduced focusing quality
  - Precise target positioning onto laser focus

Target

- ✓ Production of ultrathin targets with large area
- ✓ Cost effective, stable, and reproducible way
- ✓ New and exotic targets : foam, nano-structure

Diagnostics system

- ✓ Real-time and fast characterization
- ✓ Extending detection range to ~100 MeV and higher

Electron Spectrometer and Detection

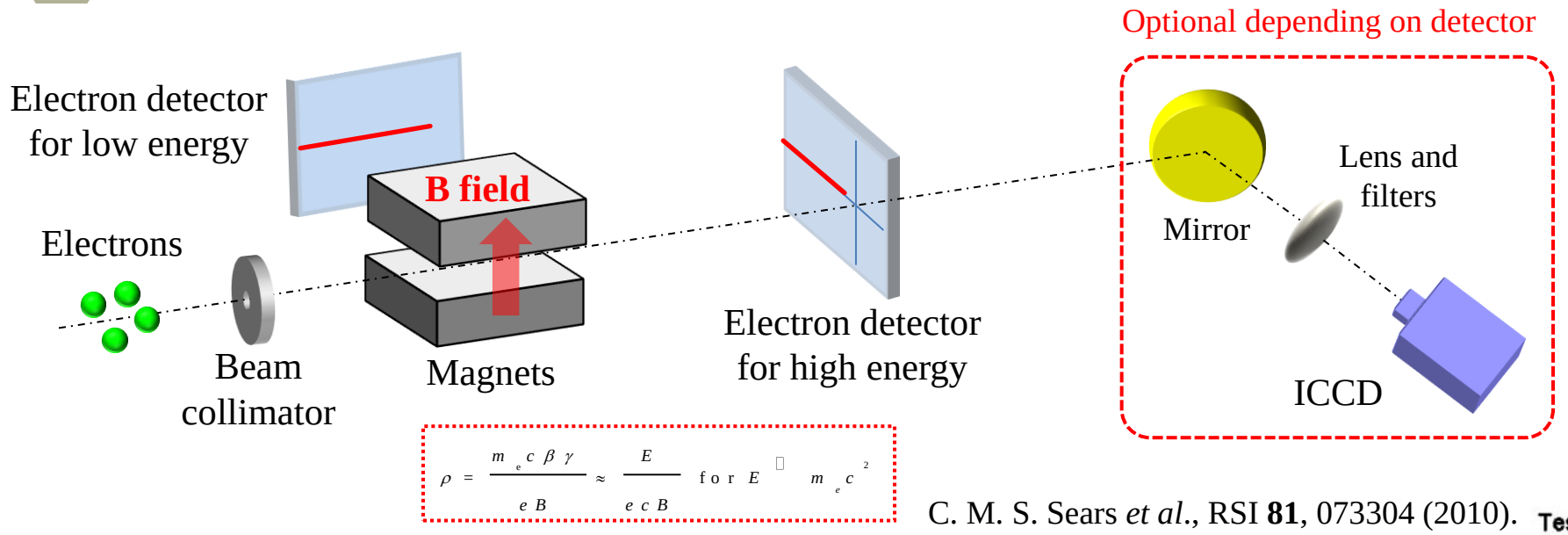

$$\rho = \frac{m_e c \beta \gamma}{e B} \approx \frac{E}{e c B} \quad \text{for } E \gg m_e c^2$$

C. M. S. Sears *et al.*, RSI **81**, 073304 (2010).

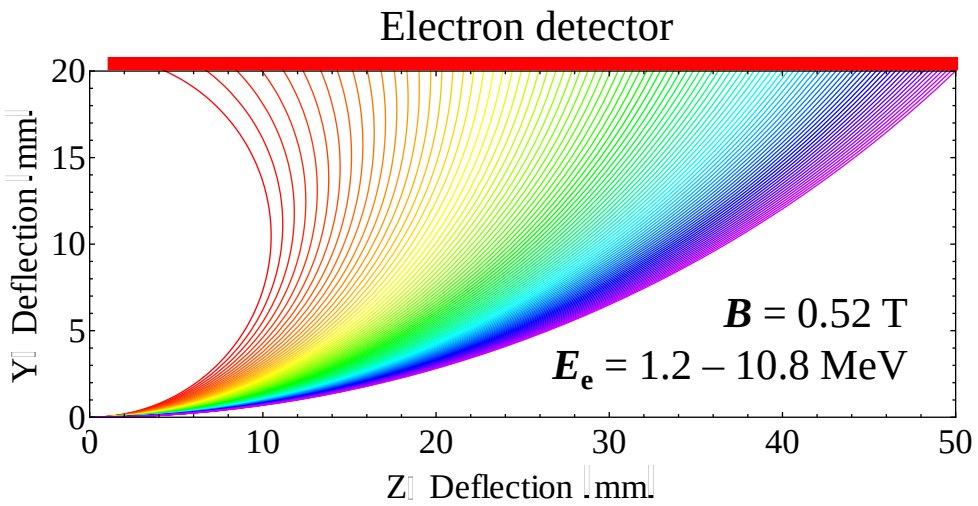

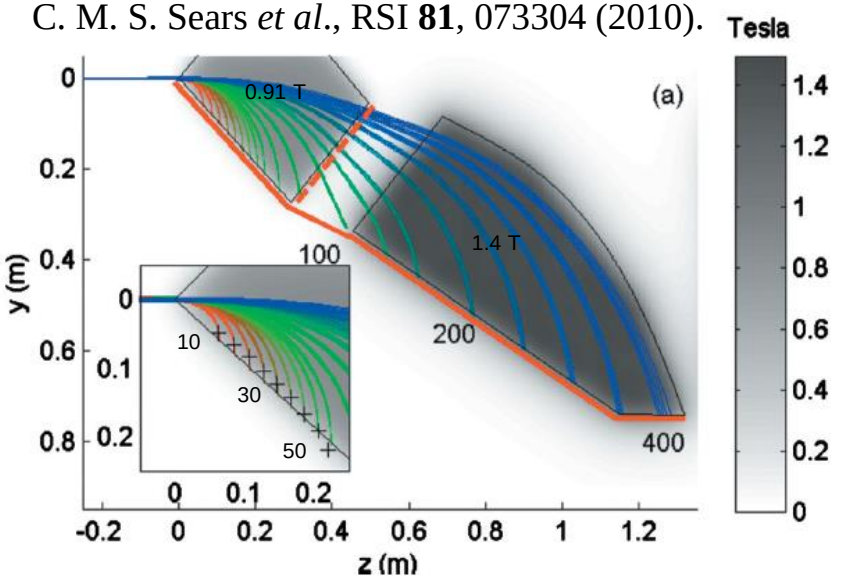

Electron Detectors : Imaging Pate, Lanex

Imaging plate : Fuji film

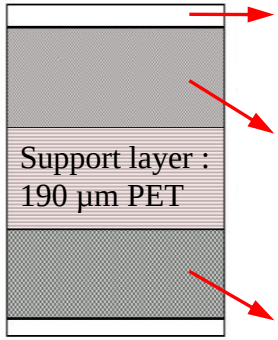

Protective layer
6 µm PEF

Photostimulable phosphor layer
thickness : 120 µm
Phosphor :
BaFBrI:Eu2+

160 µm ferrite layer

Structure of BAS-SR imaging plate

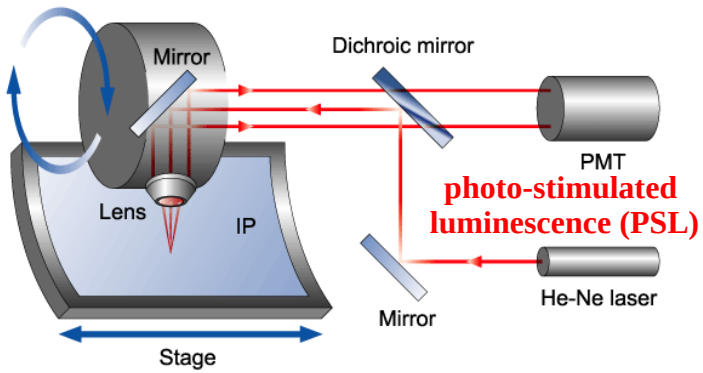

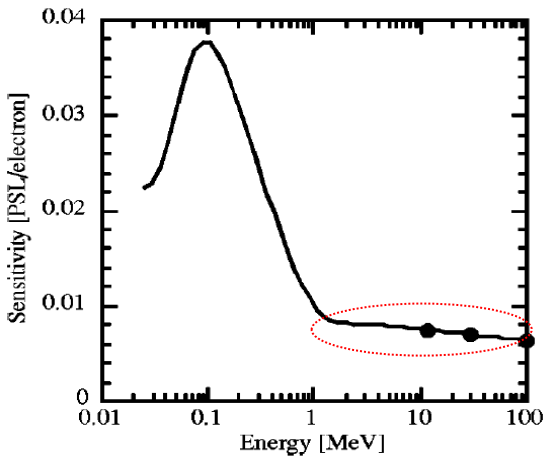

Response of BAS-SR to electrons

K. A. Tanaka, RSI **76**, 013507 (2005).

Lanex screen : Kodak

Y. Glinec, RSI **77**, 103301 (2006).

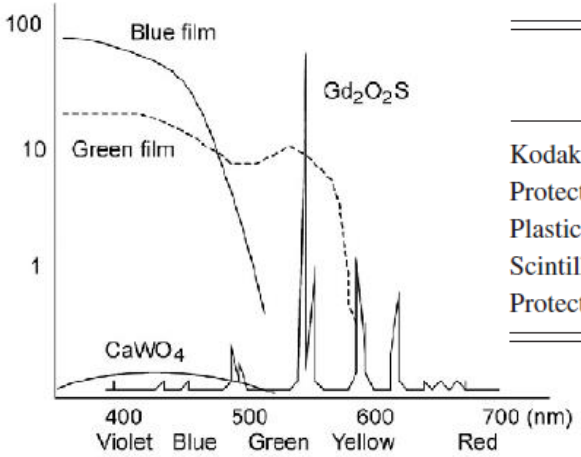

Emission spectra of Lanex screen

Item	Material	Density (g/cm^3)	Thickness (cm)
Kodak Lanex Fine screen			
Protective coating	Cellulose acetate1	1.32	0.0010
Plastic substrate	Poly(ethylene terephtalate)	1.38	0.0178
Scintillator	Gd_2O_2S+urethane binder	4.25	0.0084
Protective coating	Cellulose acetate	1.32	0.0005

Composition of Kodak Lanex Fine screen

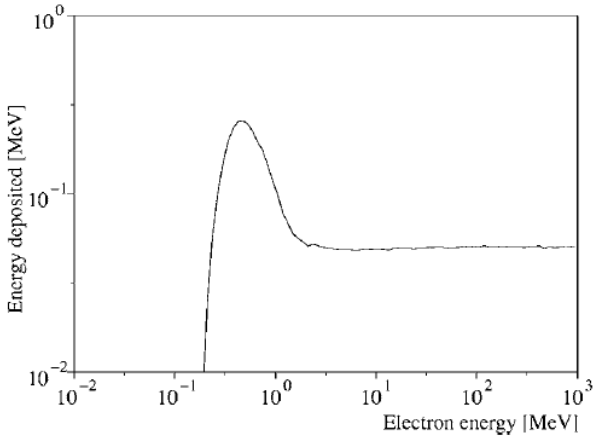

Energy deposited in the scintillator layer of Lanex Fine screen

Enhancement in Energy Resolution Adapting Focusing Geometry

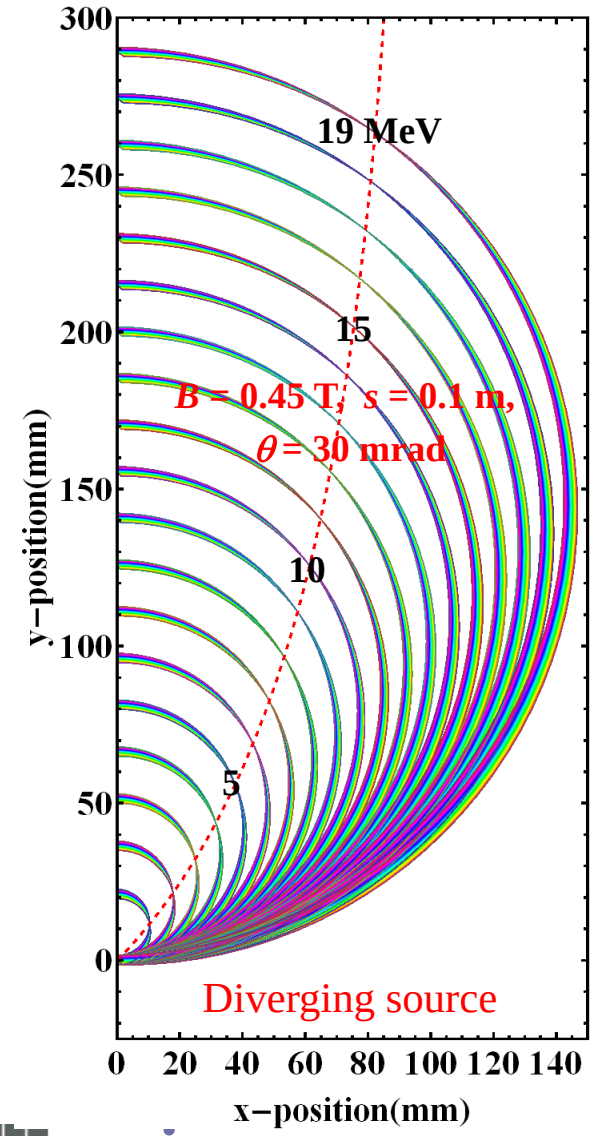

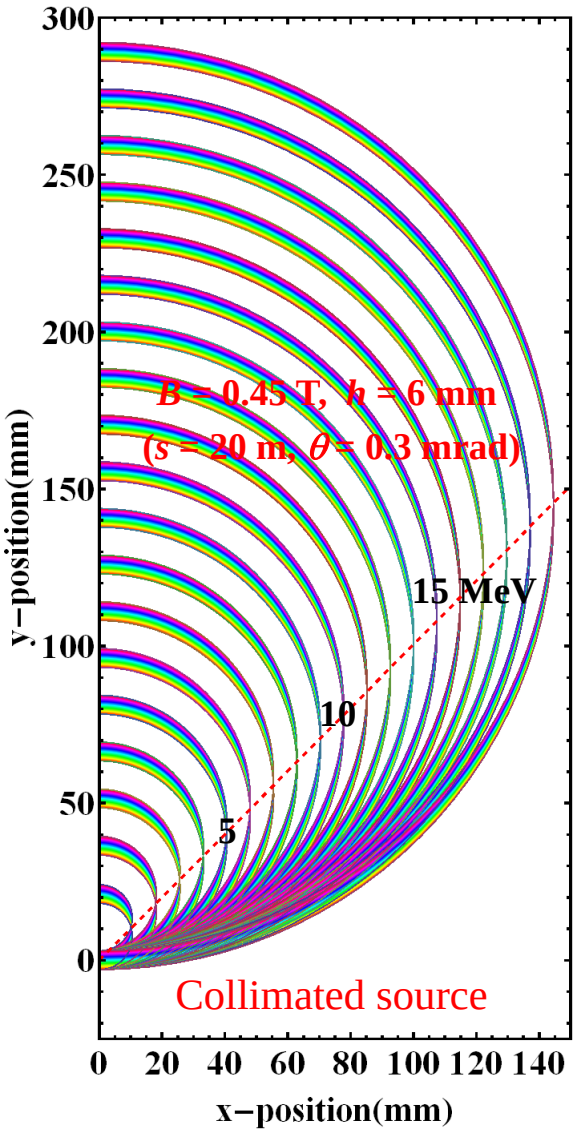

$$\Delta x = \frac{\partial x}{\partial \theta}\Delta\theta + \frac{\partial x}{\partial \rho}\Delta\rho$$

$$\approx \left[(a + d + f) + \left(\frac{d}{2} + \frac{3f}{2}\right)\left(\frac{d}{\rho}\right)^2\right]\Delta\theta$$

$$- \left[\left(\frac{d}{2} + f\right)\left(\frac{d}{\rho}\right) + (d + 3f)\left(\frac{d}{\rho}\right)^2\theta\right]\left(\frac{\Delta\rho}{\rho}\right)$$

for non-focusing geometry

$$\sigma_x^2 = \left(\frac{\partial x}{\partial \theta}\right)^2 \sigma_\theta^2 + \left(\frac{\partial x}{\partial \rho}\right)^2 \sigma_\rho^2$$

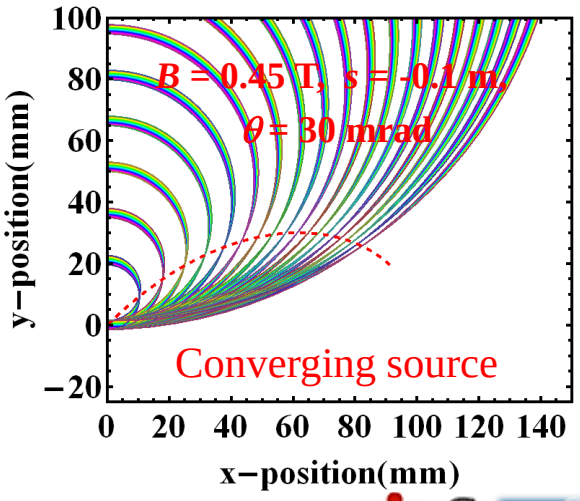

Proton Energy and Electron Spectra Dependent on Observation Angle

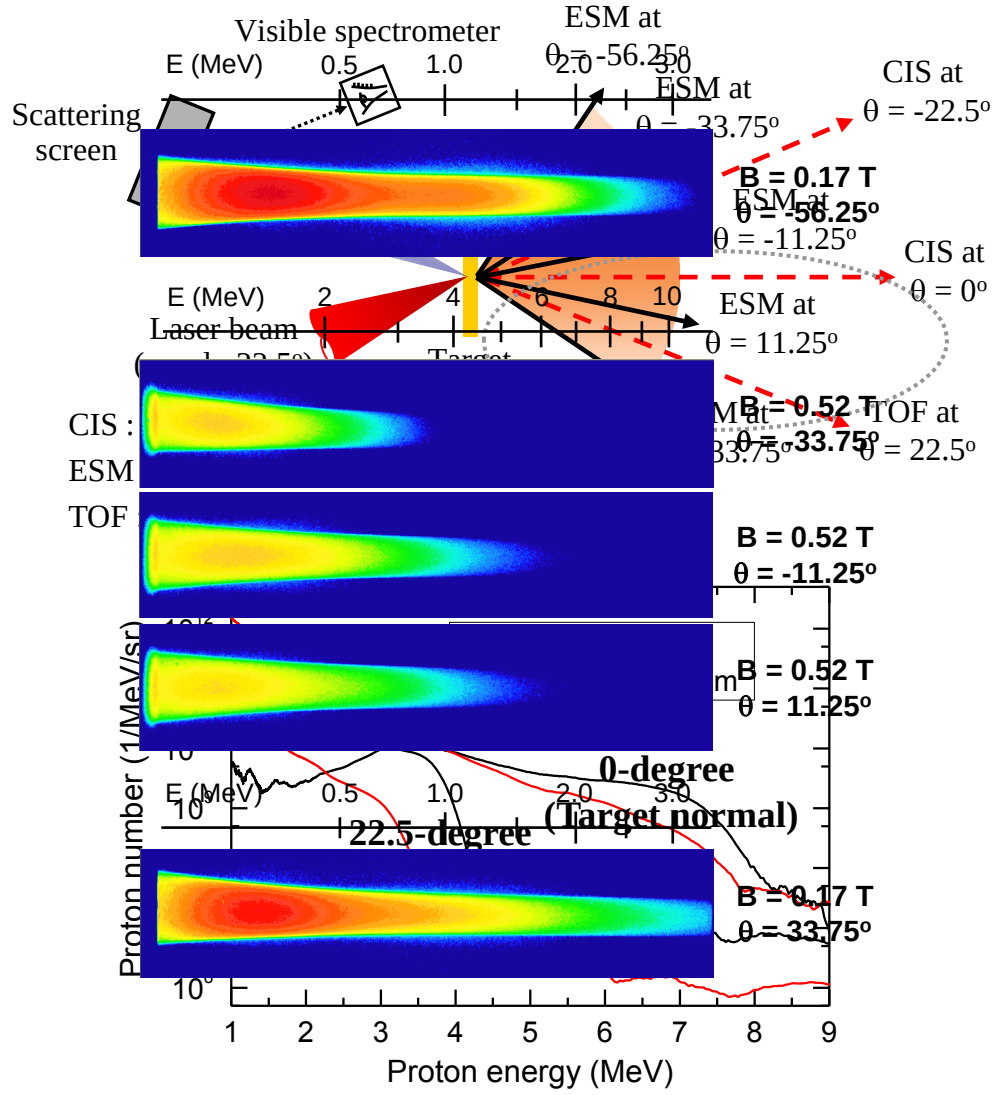

35 fs(FWHM) , 22.5° incidence angle
$I = 4\times10^{19}$ W/cm^2, $a_0 = 4.33$,

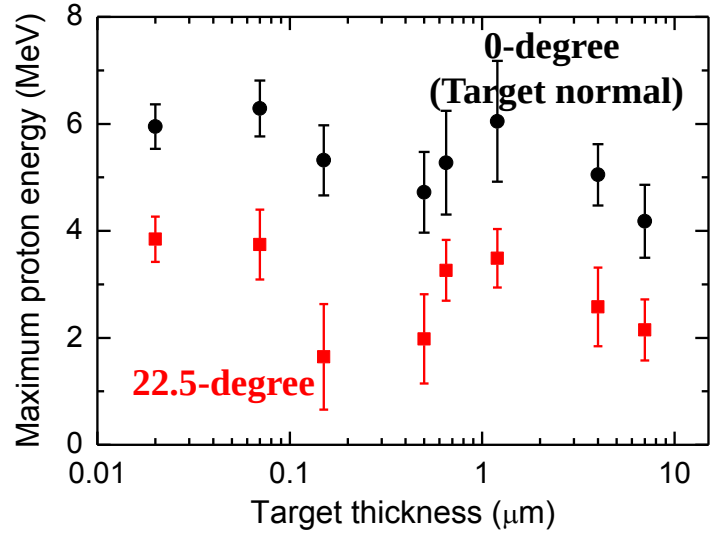

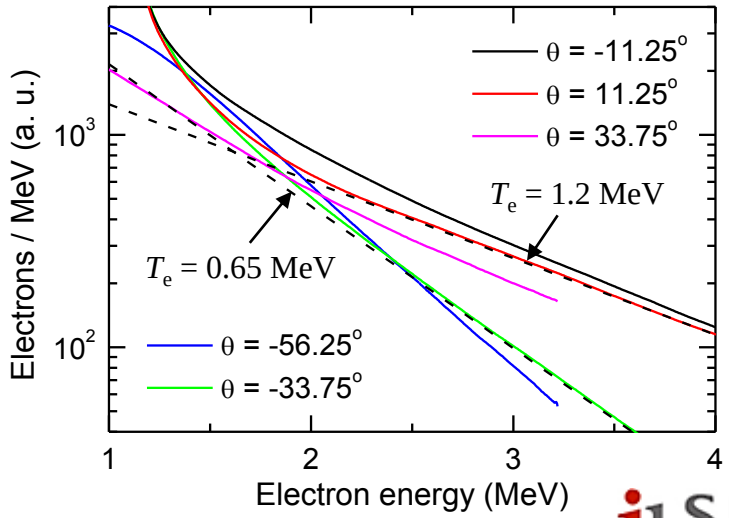

Proton Energy Increased Using PM and Ultrathin Targets

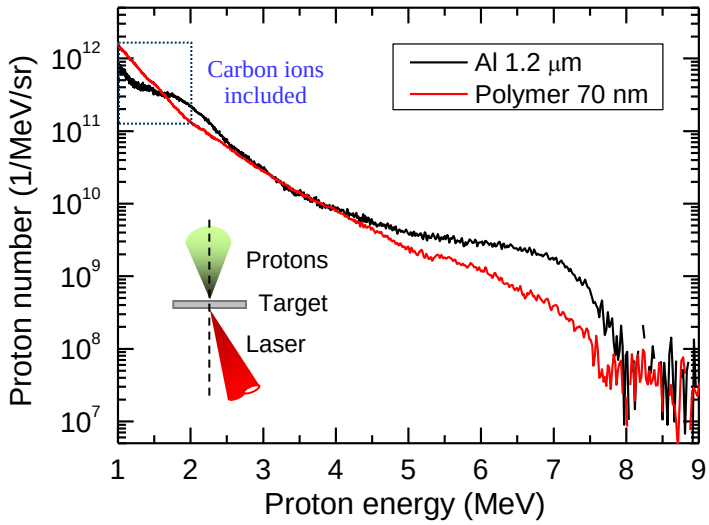

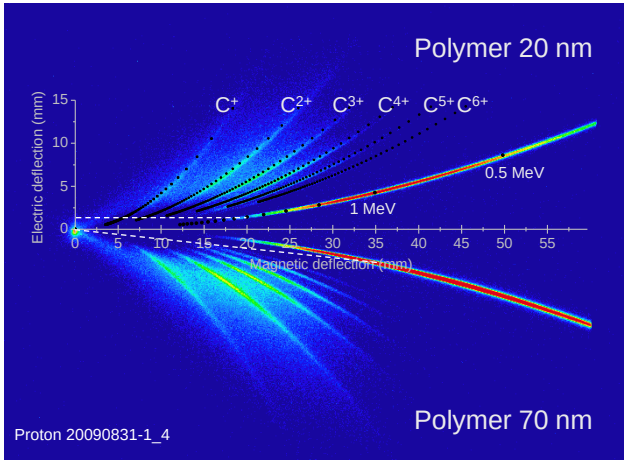

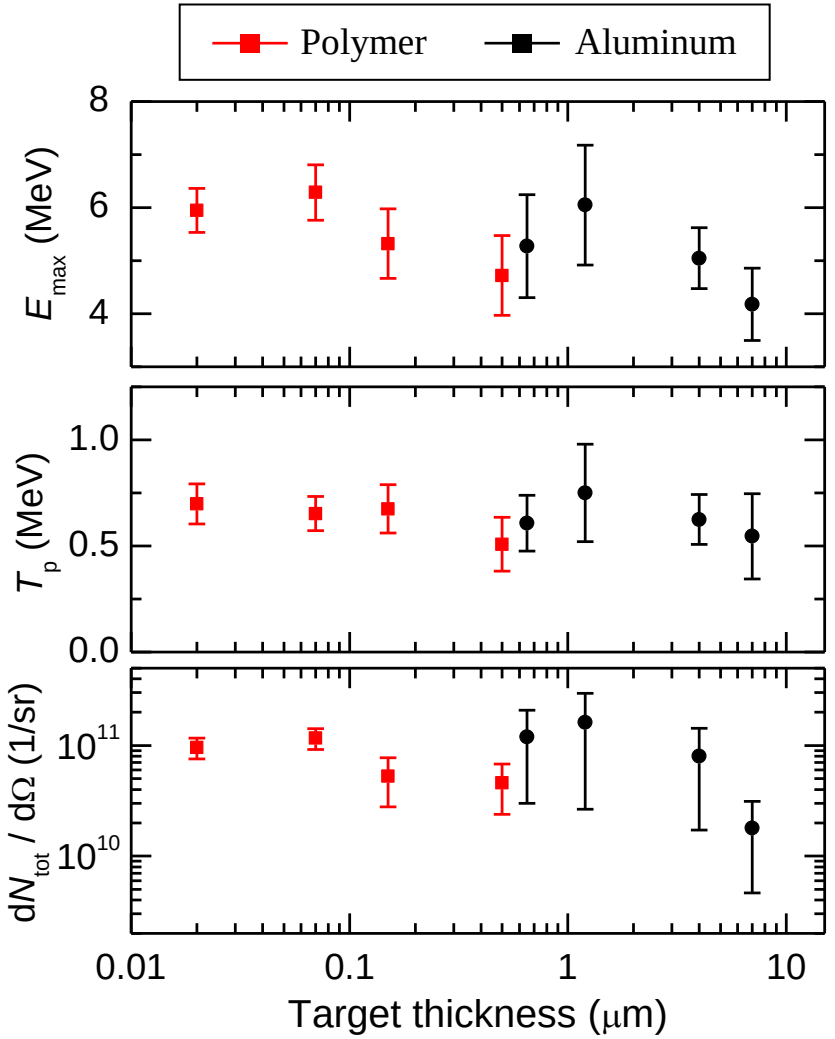

Maximum proton energy obtained : 8 MeV

I. W. Choi *et al.*, Appl. Phys. Lett. **99**, 181501 (2011).

Current Results Reproduced Well with PIC Simulation

- $I = 5\times10^{19}$ W/cm^2, $\omega = 5$ μm (FWHM), $\tau = 34$ fs,
- Linearly polarized pulse, 22.5-degree incident angle
- Assuming initial plasma density : $n = 250\ n_{cr}$

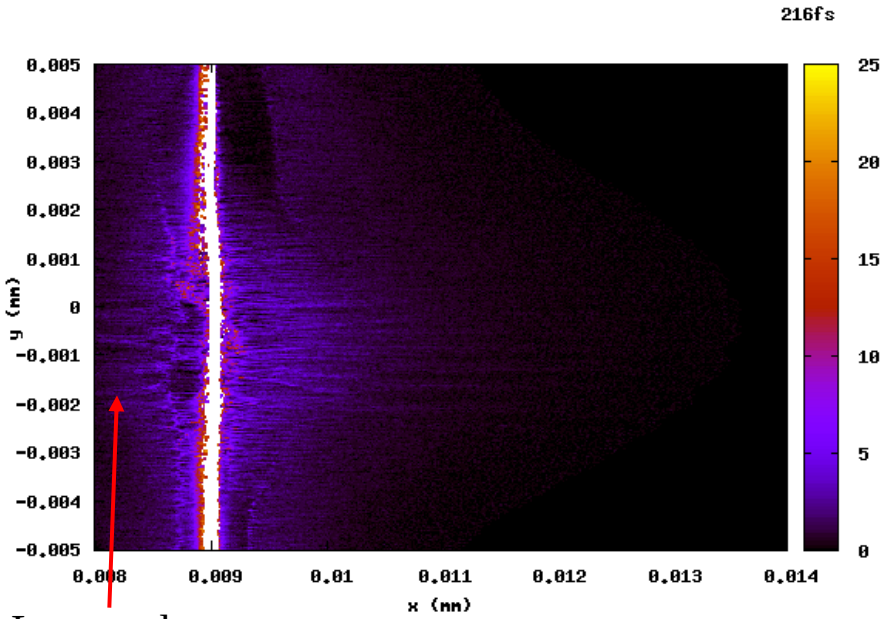

Laser pulse

Proton density map at 216 fs

70-nm thick polymer

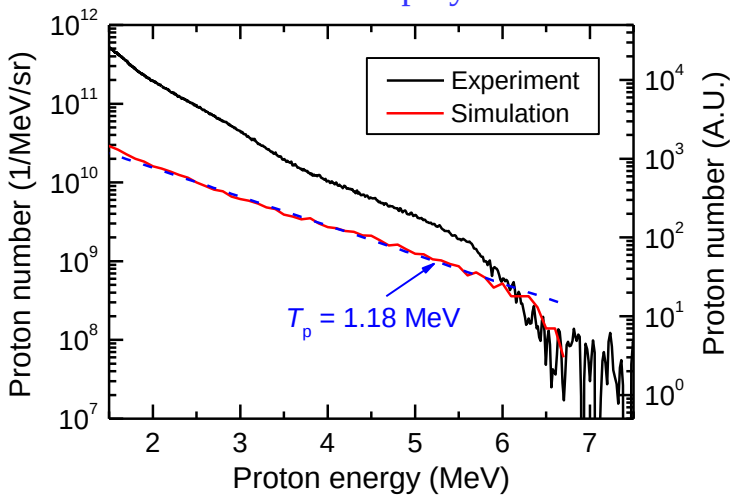

1.2-μm thick aluminum

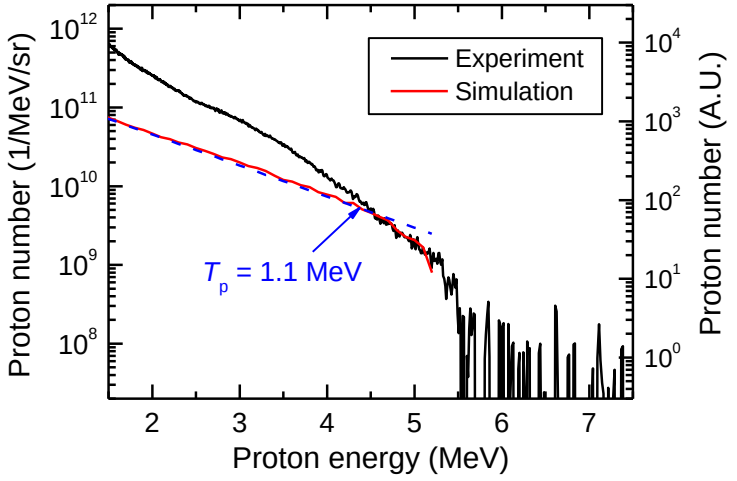

(Simulation with ALPS-2D code)

Optimal Target Thickness Well Agreed with PIC Simulation

PIC Simulation with ALPS-2D code

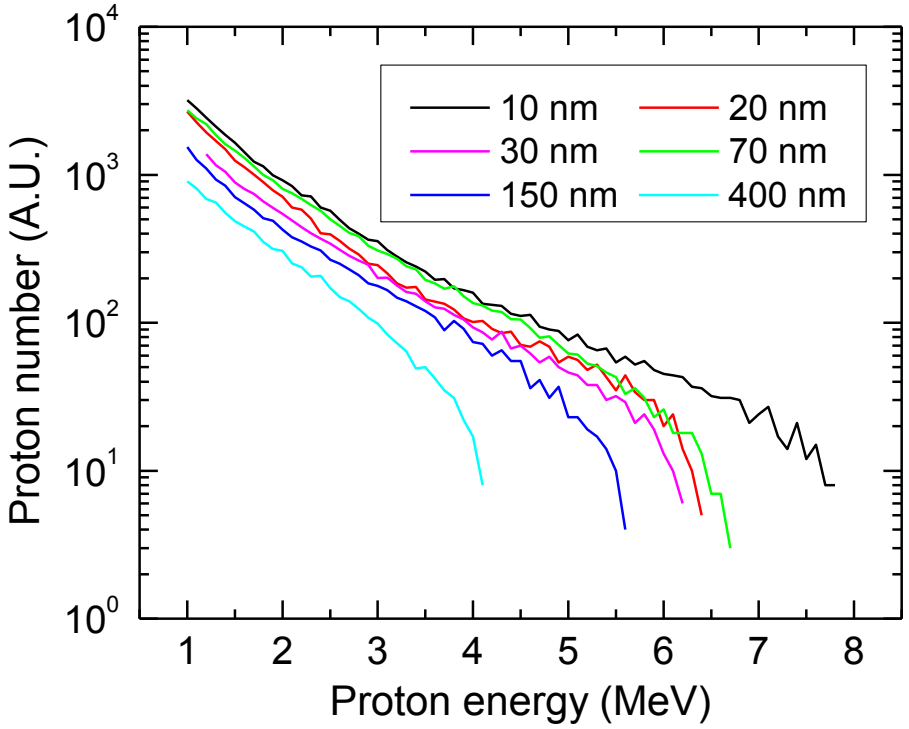

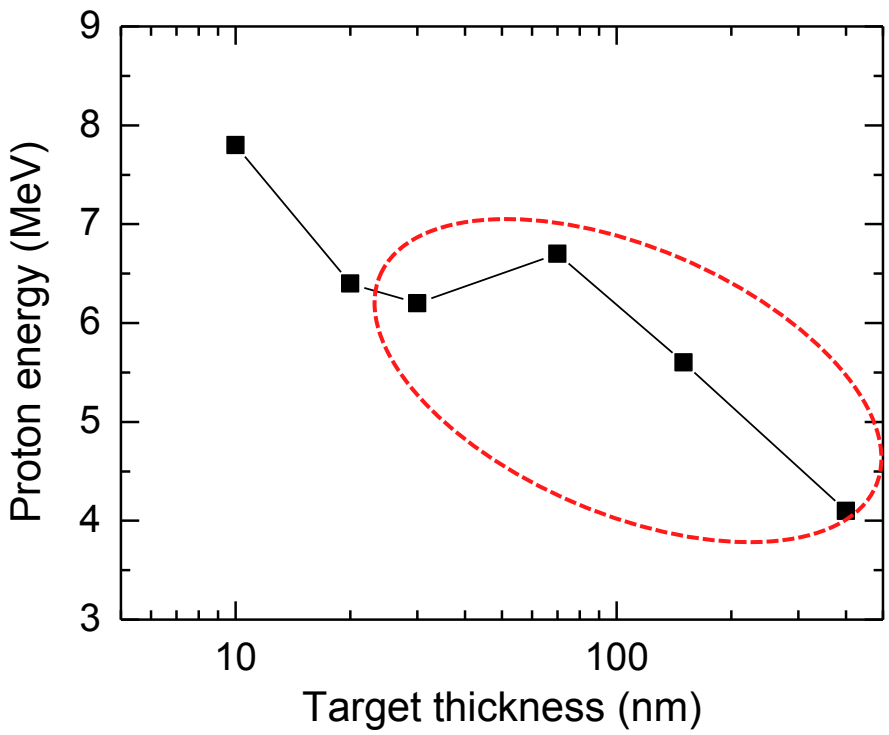

Accelerating sheath electric field in TNSA $E_{sheath} \approx \frac{k_B T_e}{e \lambda_D} = \sqrt{4 \pi n_e k_B T_e}$

Competition of two opposite tendencies :

- Large recirculation effect at thinner target : enhancing n_e
- Large laser absorption at thicker target : enhancing T_e

Relativistic Transparency Effect at the Thinnest Target : RPA

Dispersion relation : $\omega^2 = c^2 k^2 + \frac{\omega_{pe}^2}{\gamma}$, $n_c^{rel} = \gamma n_c$ Skin depth : $l_s = \frac{c}{\omega_{pe}^{rel}} = \frac{c}{\omega_{pe}}\sqrt{\gamma}$, where $\gamma = \sqrt{1 + a_0^2}$

$n_c^{rel} = 4.44 n_c$, $l_s = 19$ nm for $a_0 = 4.33$

10-nm target

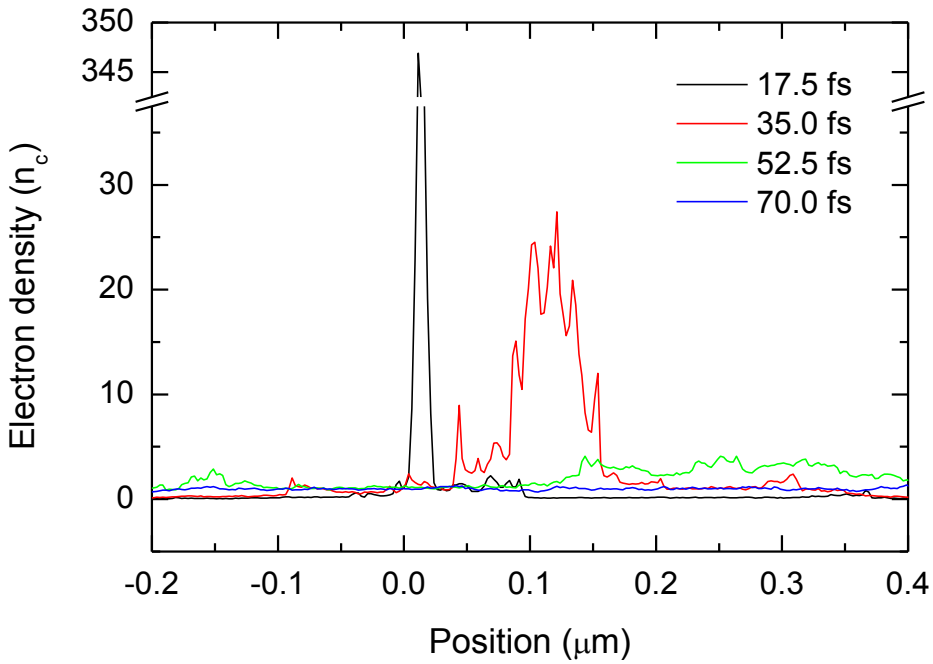

20-nm target

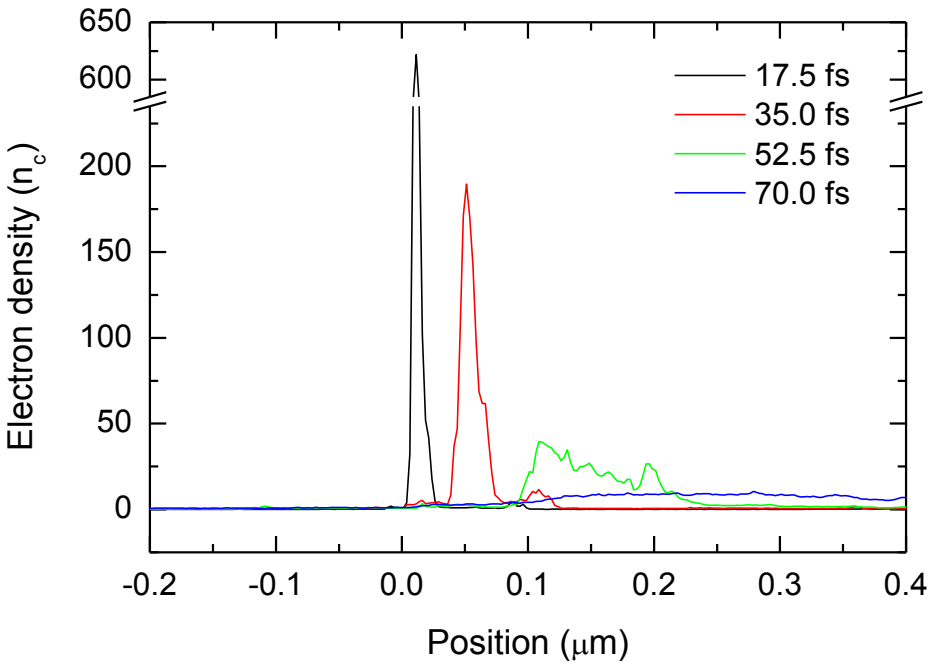

Relativistic transparency for an ultrathin target allows the additional heating.

Strong 2ω (in Experiment) and HOH (in PIC Simulation) Observed

- The 2ω spectra were not detected (or were nearly at the noise level) in the case of Al targets.
- The 2ω intensity shows similar dependence on the target position to proton energy.

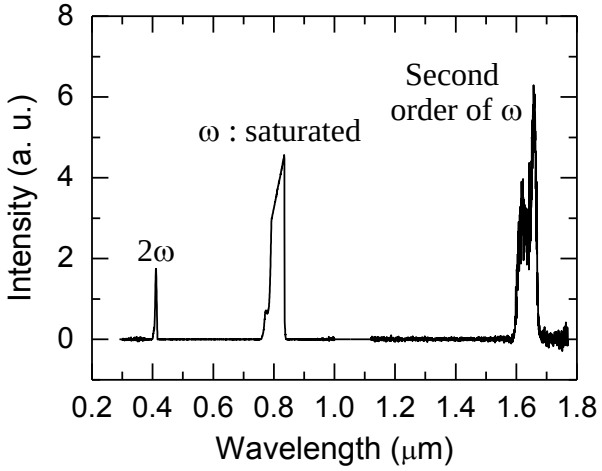

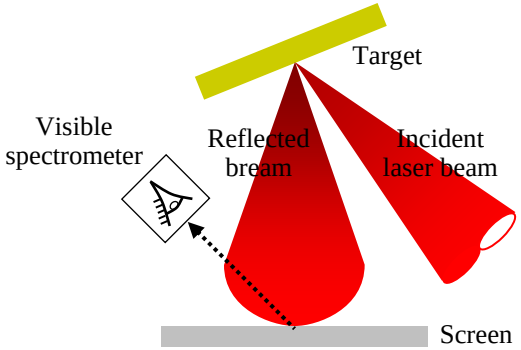

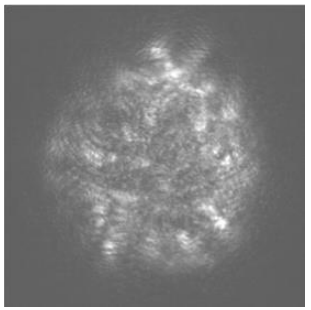

Incident laser beam profile on target

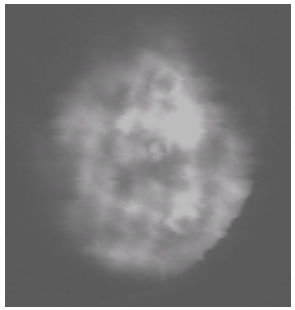

Reflected beam profile from target

PIC simulation on the harmonic generation with PIC simulation code

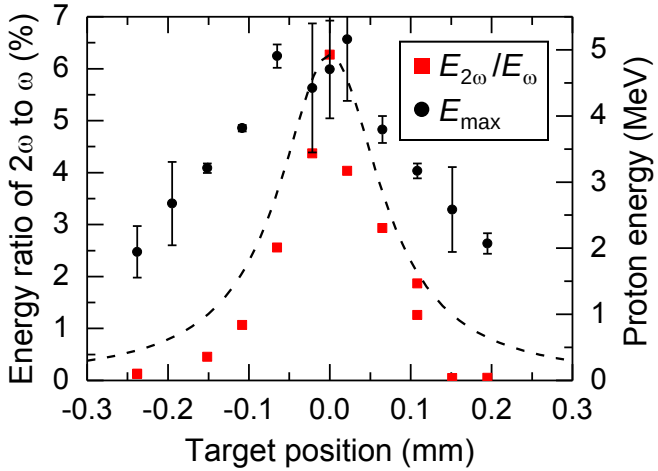

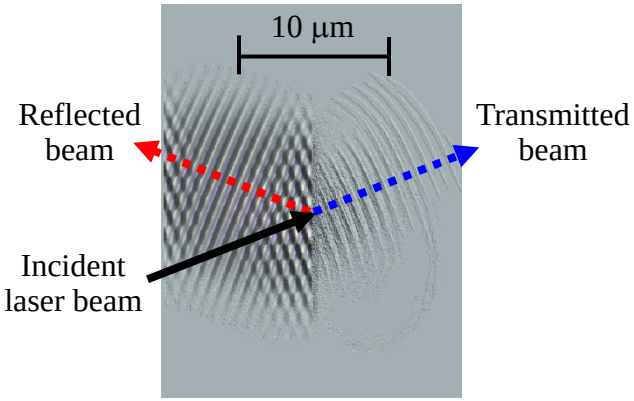

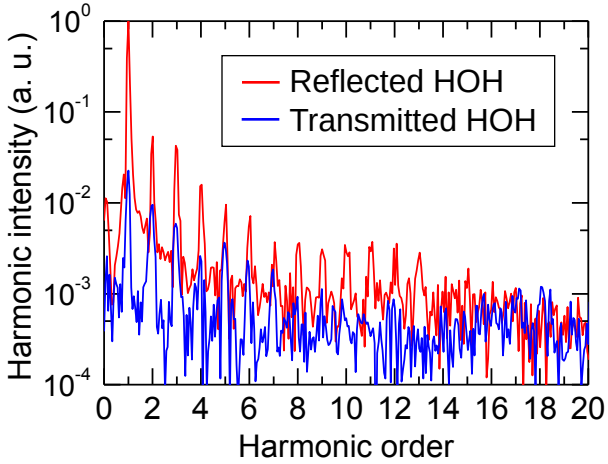

I. W. Choi *et al.*, Appl. Phys. Lett. **99**, 181501 (2011).

PW (PUSER) and 100 TW (LiFSA) Ti:Sapphire Laser System

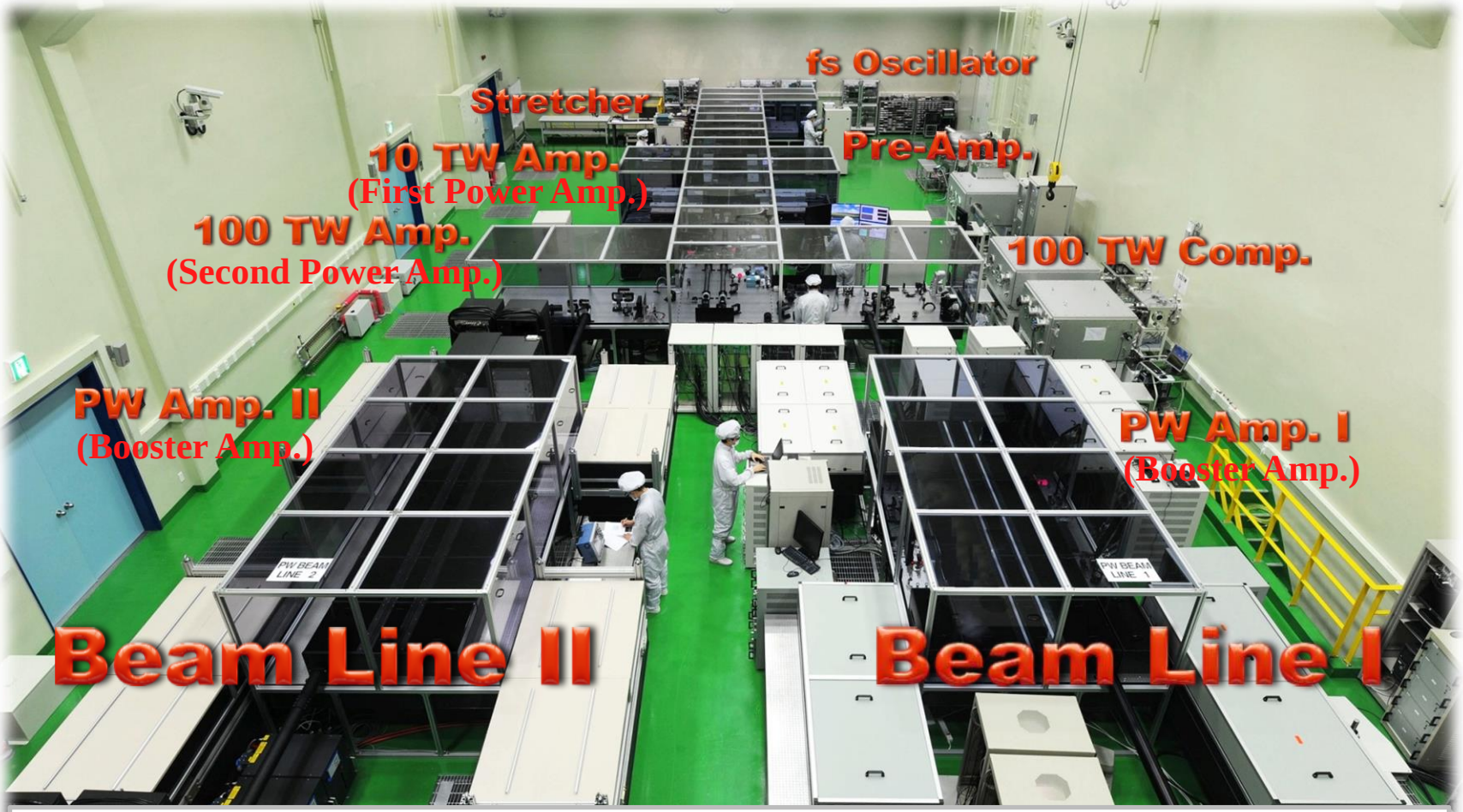

PULSER (1 PW : Petawatt Ultrashort Laser Source for Extreme science Research)

LiFSA (100 TW : Light source for Femto Science and Applications)

Space-Resolving Flat-Field Soft X-ray Spectrometer

❑ Flat-field soft x-ray spectrometer with varied line-spacing concave grating

- Components : Varied line-spacing concave grating (1200 or 2400 grooves/mm),

  Entrance slit, Toroidal mirror, Soft X-ray detector(e.g. CCD), Vacuum housing

❑ Space-resolving capability using pre-focusing optics

- Increasing light collection efficiency
- Source characterization vs position

$$* \text{ Tangential Focusing} \quad \frac{1}{r} + \frac{1}{r'_{m1}} = \frac{2}{R_1 \cos\alpha_1}$$

$$* \text{ Sagittal Focusing} \quad \frac{1}{r} + \frac{1}{r'_{s1}} = \frac{2\cos\alpha_1}{\rho_1}$$

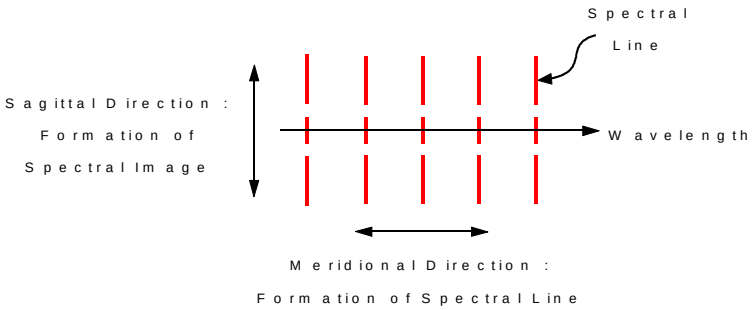

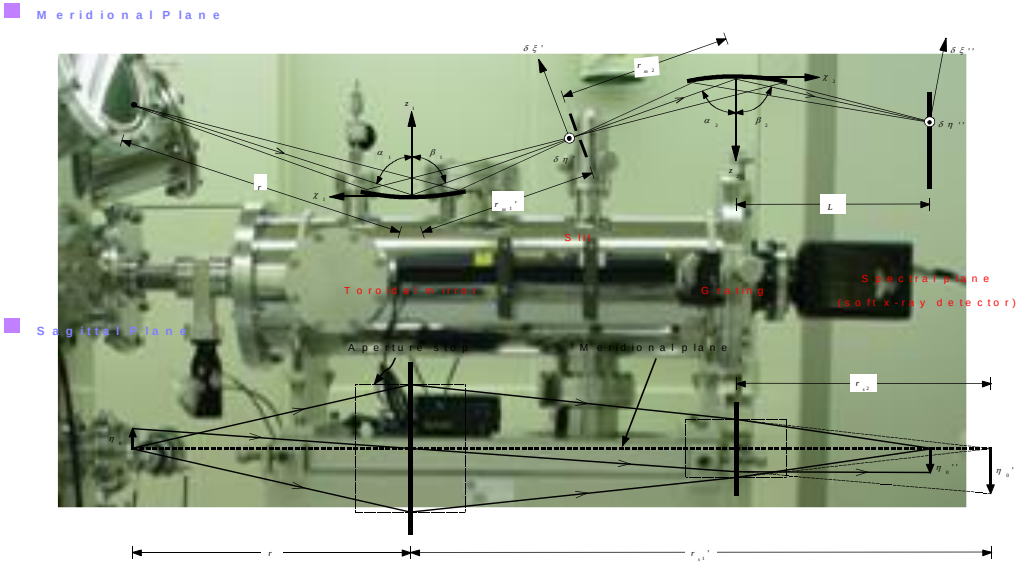

I. W. Choi *et al.*, Appl. Opt. **36**, 1457 (1996).

Diffraction Efficiency of VLS Grating

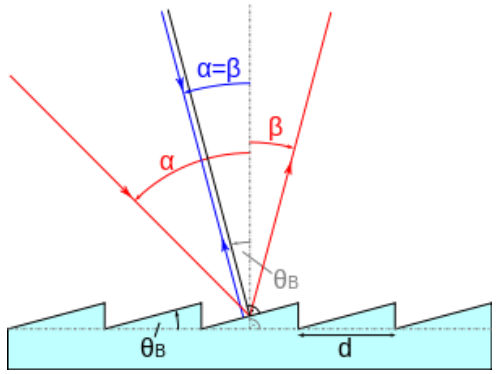

Blaze wavelengths

- $m\lambda_{b0}$ = 100.5 Å for 1200 grooves/mm grating
- $m\lambda_{b0}$ = 15.7 Å for 2400 grooves/mm grating

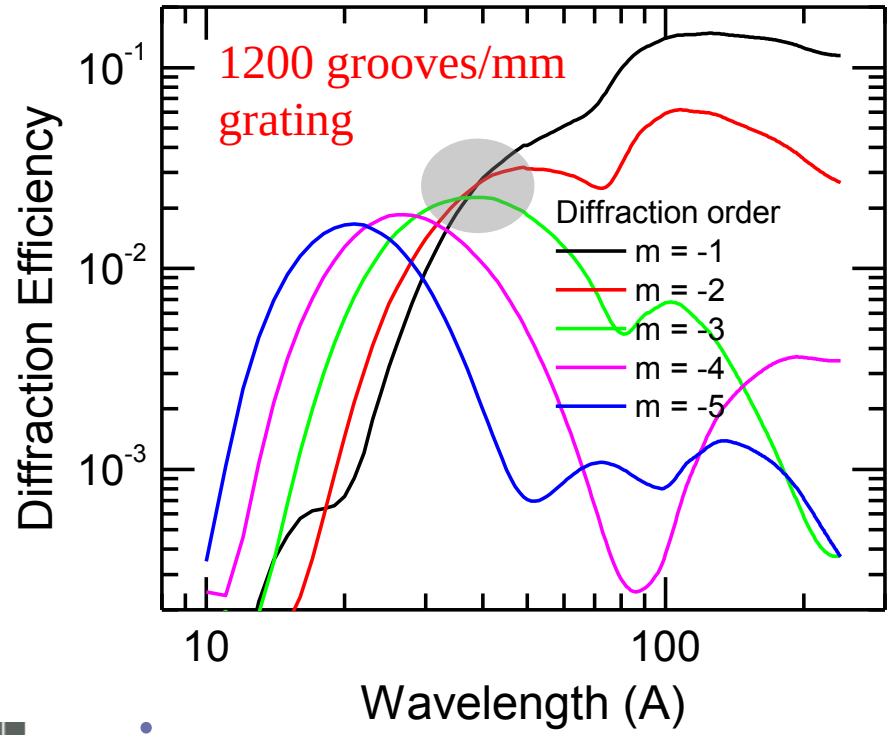

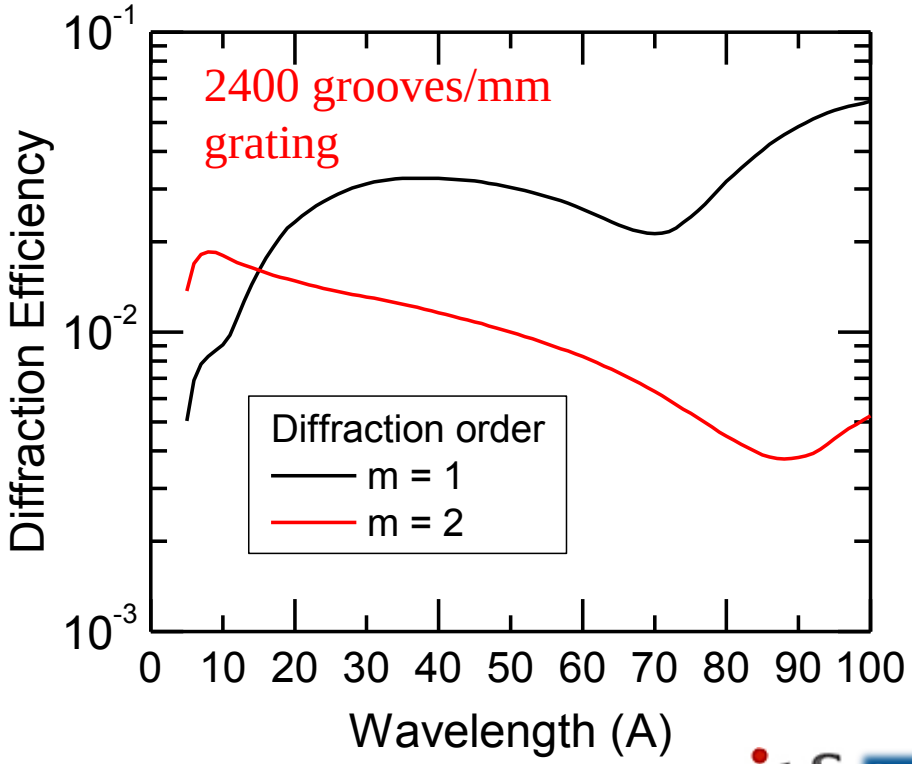

High Order Harmonics from Gas (He, Ar) Target

Continuously wavelength-tuned high-order harmonics from He atoms

Sagittal focusing
(Toroidal mirror)
→ Enhancing light collection

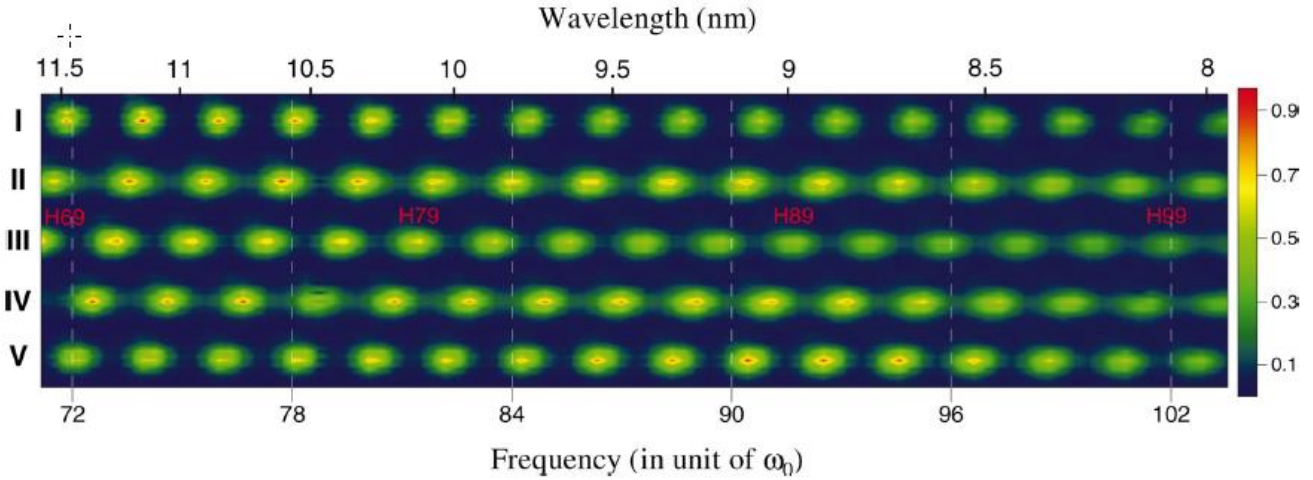

H. T. Kim *et al.*, Phys. Rev. A **67**, 051801(R) (2003).

Spectrally resolved divergence measurement of high-order harmonics

Sagittal diverging
(Cylindrical mirror)
→ beam profile measurement

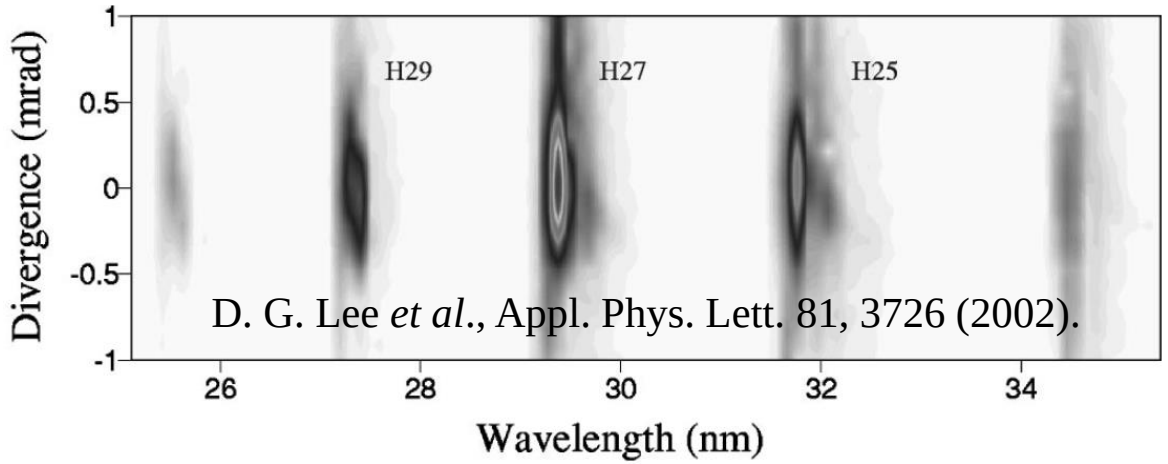

D. G. Lee *et al.*, Appl. Phys. Lett. 81, 3726 (2002).

RHHG with High and Low Contrast Laser Pulses

Highest Relativistic Harmonics with < 100 fs Laser Pulses

- High Contrast condition -

(1.4×10^{-12} with PM)

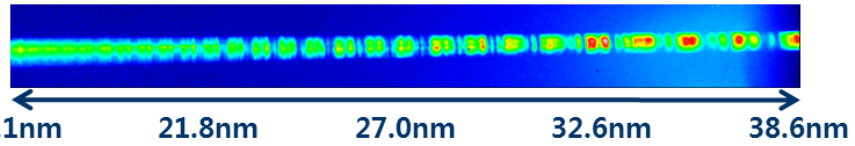

- Optimal Contrast condition -

(7×10^{-8} without PM)

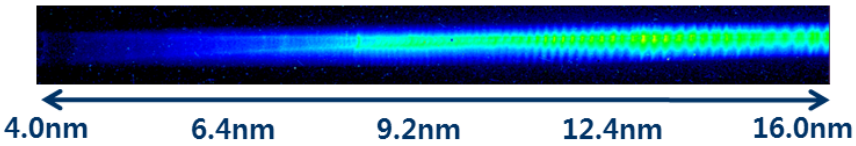

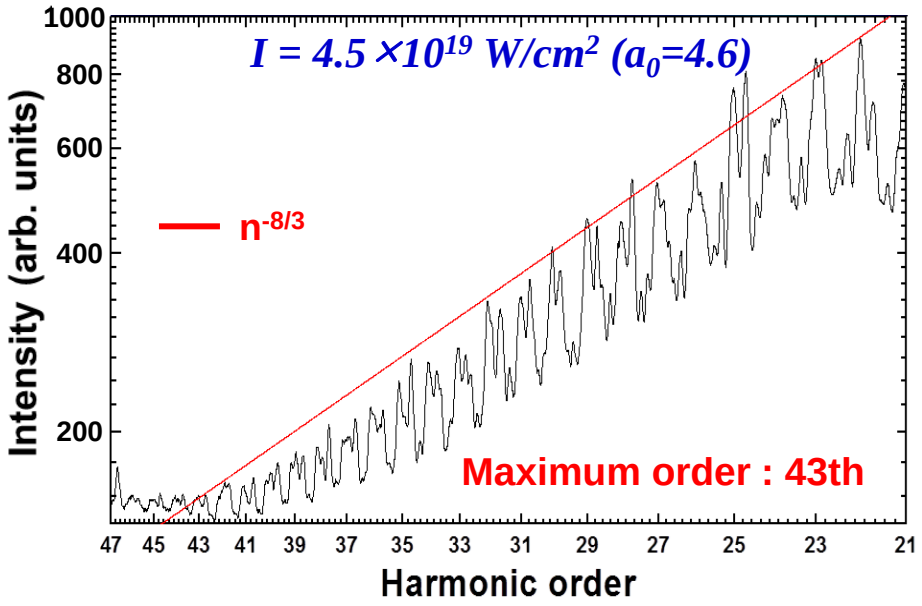

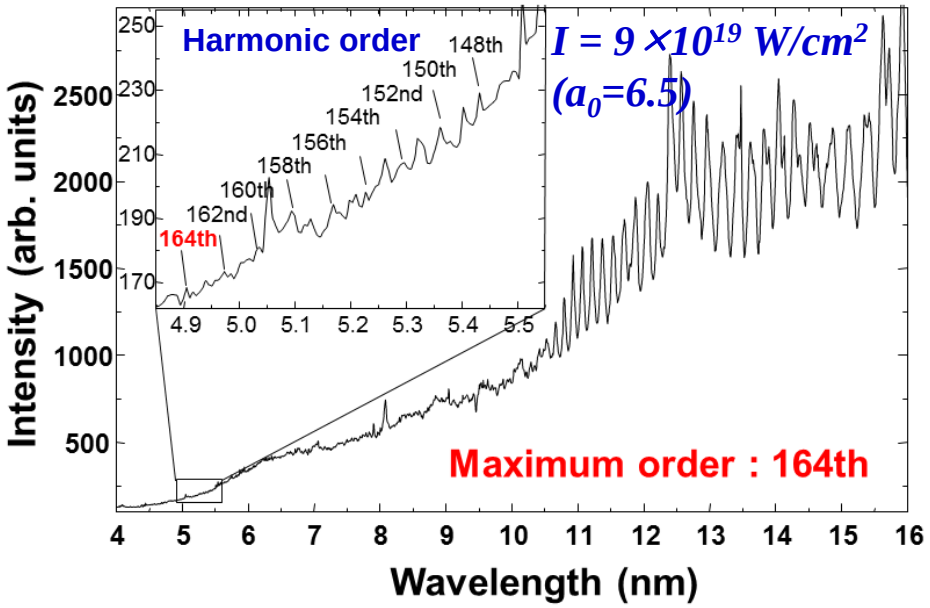

cf. When a_0=4.6, max order = 129 (6.4 nm)

I J. Kim, K.H. Pae, C.M. Kim, H.T. Kim, H. Yun, S.J. Yun, J.H. Sung, S.K. Lee, J.W. Yoon, T.J. Yu, T.M. Jeong, C.H. Nam, and J. Lee, "Relativistic frequency upshift to the XUV regime using self-induced oscillatory flying mirrors," Nat. Commun. (accepted).

Detectors Used for Laser-Driven Ion Diagnostics and Measurements

Table 1. Detectors commonly used for laser-driven ion diagnostics and measurements. Sensitivity: L: light, UV: ultraviolet, x: x-rays, e-: electrons; the notation '•' represents 'sensitive'.

	Spatial resolution	Time resolution	Treatment/ display time	Single-particle sensitivity	Dynamic range (DR)	Sensitivity			Features/refs
						L	UV, x	e-	
Solid-state nuclear track detectors, e.g. CR-39 (allyl diglycol carbonate), etc	~ a few to a few tens of μm (pit size, depends on the ion kind and energy and etching time)	No	A few hours (etching, scanning, pit counting)	Yes	~10^2–10^6 (background ~10^2–10^4 cm^{-2}, saturation ~10^6–10^8 cm^{-2})	—	—	—	(1) Sensitive to ions only[a], single particles
Radiochromic film (RCF)	~3–10 μm (film, scanner)	No	Several minutes (scanning)	No	~10^2–10^3 (e.g. 10–10^4 Gy)	—	•	•	(2) Self-developing
Imaging plate	Sub-100 μm (scanner)	No	Several minutes (scanning)	No	~10^5	—	•	•	(3) Reusable, high DR
Activation	Sub-mm (contact radiography)	No	Tens of minutes–a few hours (decay time)	No	Very high (>10^5)	—	—	—	(4) Very high DR
Micro-channel plate (MCP)+phosphor screen + CCD	~several 10 s of μm (imaging system)	~a few 100 ps (MCP gate time)	~a few seconds (CCD readout)	Yes	~10^3	—	•	•	(5) Online, single particles
Scintillator + gated I-CCD or EM-CCD	~several 100 μm (multiple scattering, imaging system)	~a few 100 ps (scintillation time)	~a few seconds (CCD readout)	No	~10^3	•	•	•	(6) Online, stackable in depth

H. Daido, M. Nishiuchi, and A. S. Pirozhkov, Rep. Prog. Phys. **75**, 056401 (2012).

Hard X-Ray Image Acquisition with X-Ray Pinhole Camera

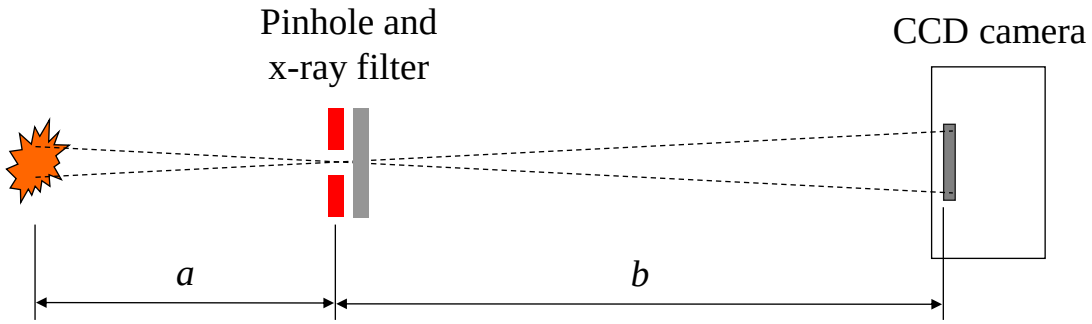

M = *b* / *a* = ~10, Resolution = d(1+1/M)

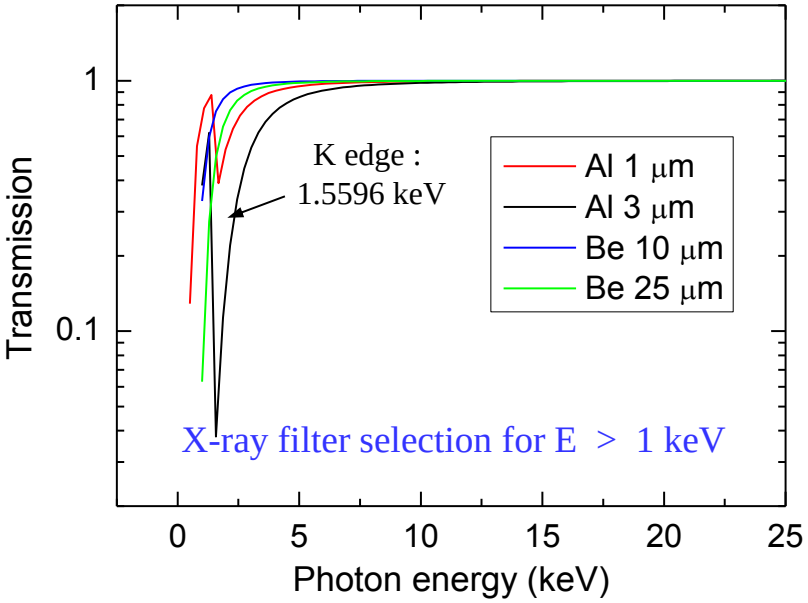

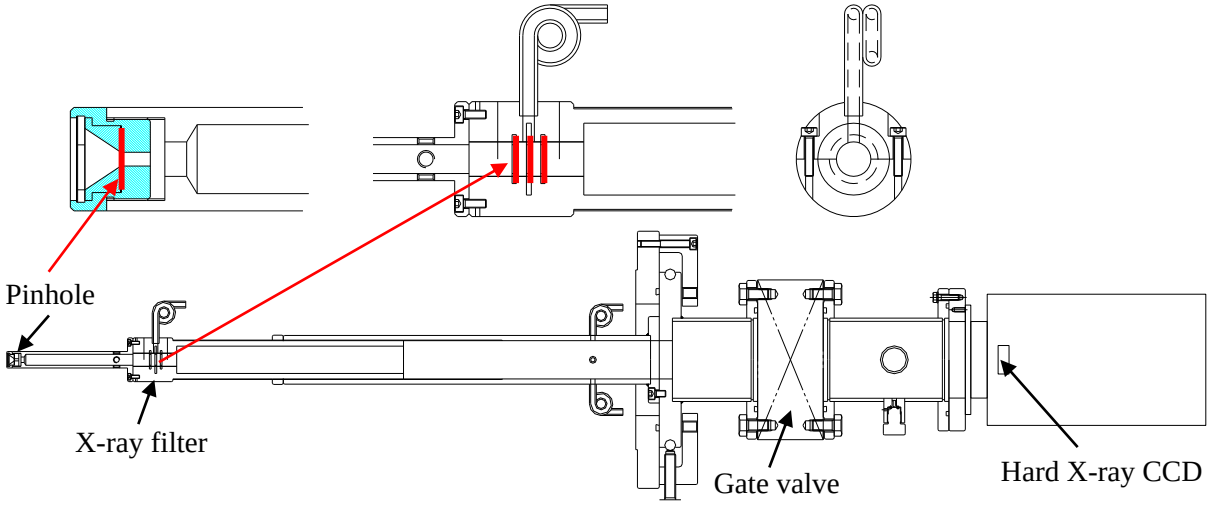

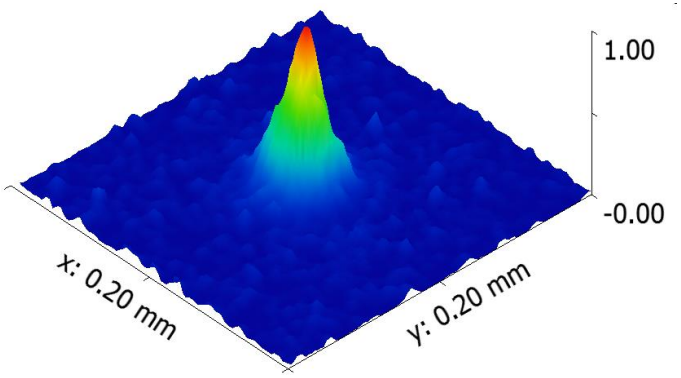

Correlation between Laser Focus Image, X-ray Image and Proton Energy

Hard X-ray image may give direct information on the hot electrons.

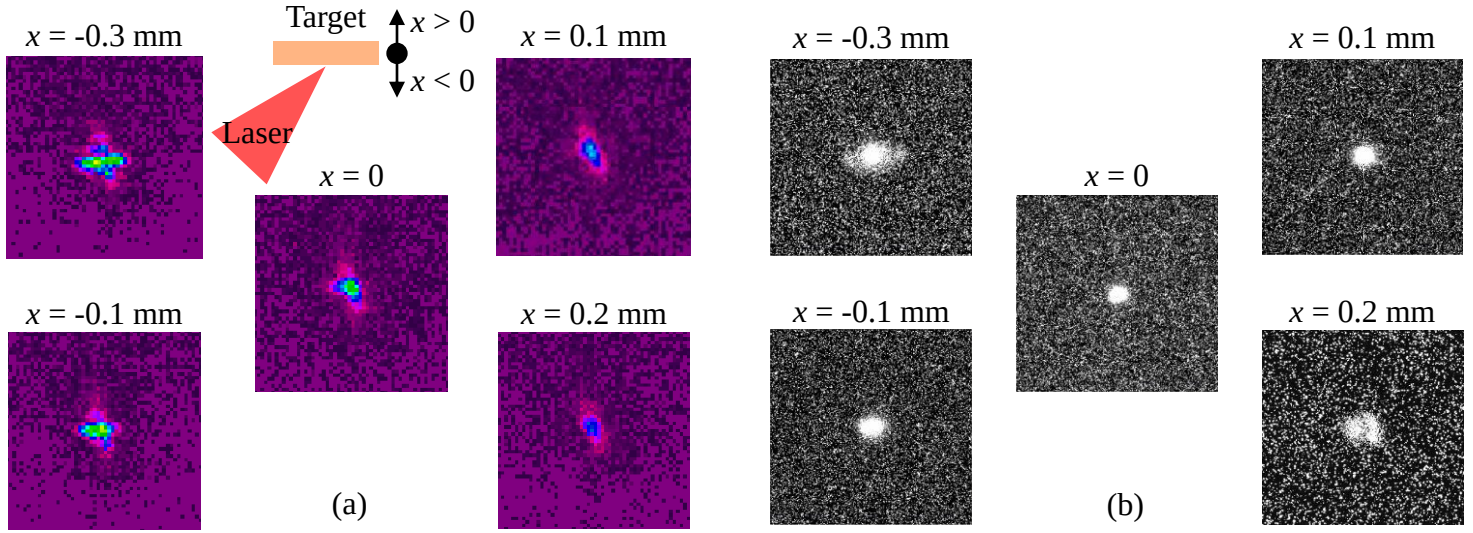

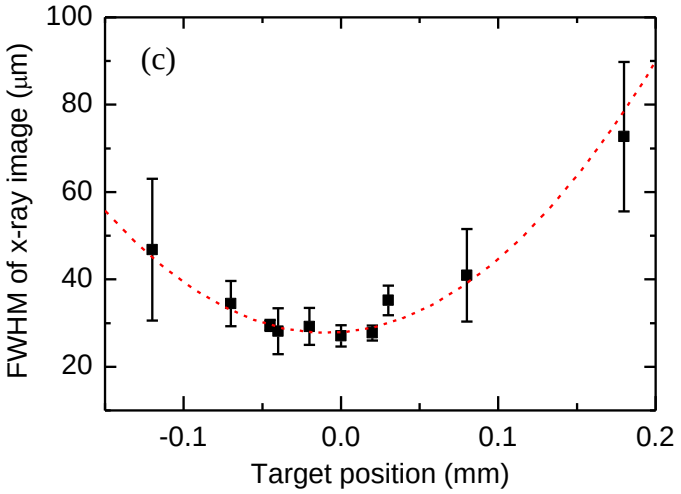

Self-similar, isothermal, fluid model

- P. Mora, PRL **90**, 185002 (2003).
- J. Fuchs, NP **2**, 48 (2006).

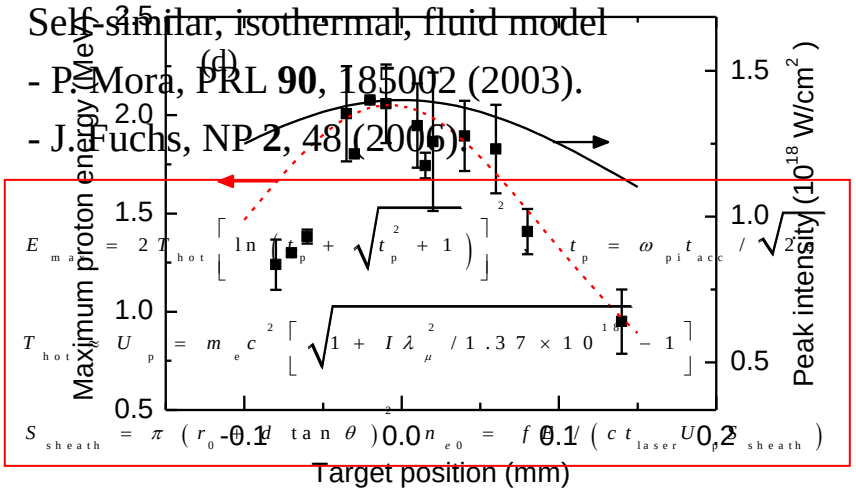

I. W. Choi *et al.*, J. Korean Phys. Soc. **55**, 517 (2009).

Contrast Ratio Enhancement Using Double Plasma Mirror System

Reflectivity of plasma mirror system : > 40% for laser energy fluences above 50 J/cm^2

Shock wave speed :
~10 mm/ns
~10 nm/ps

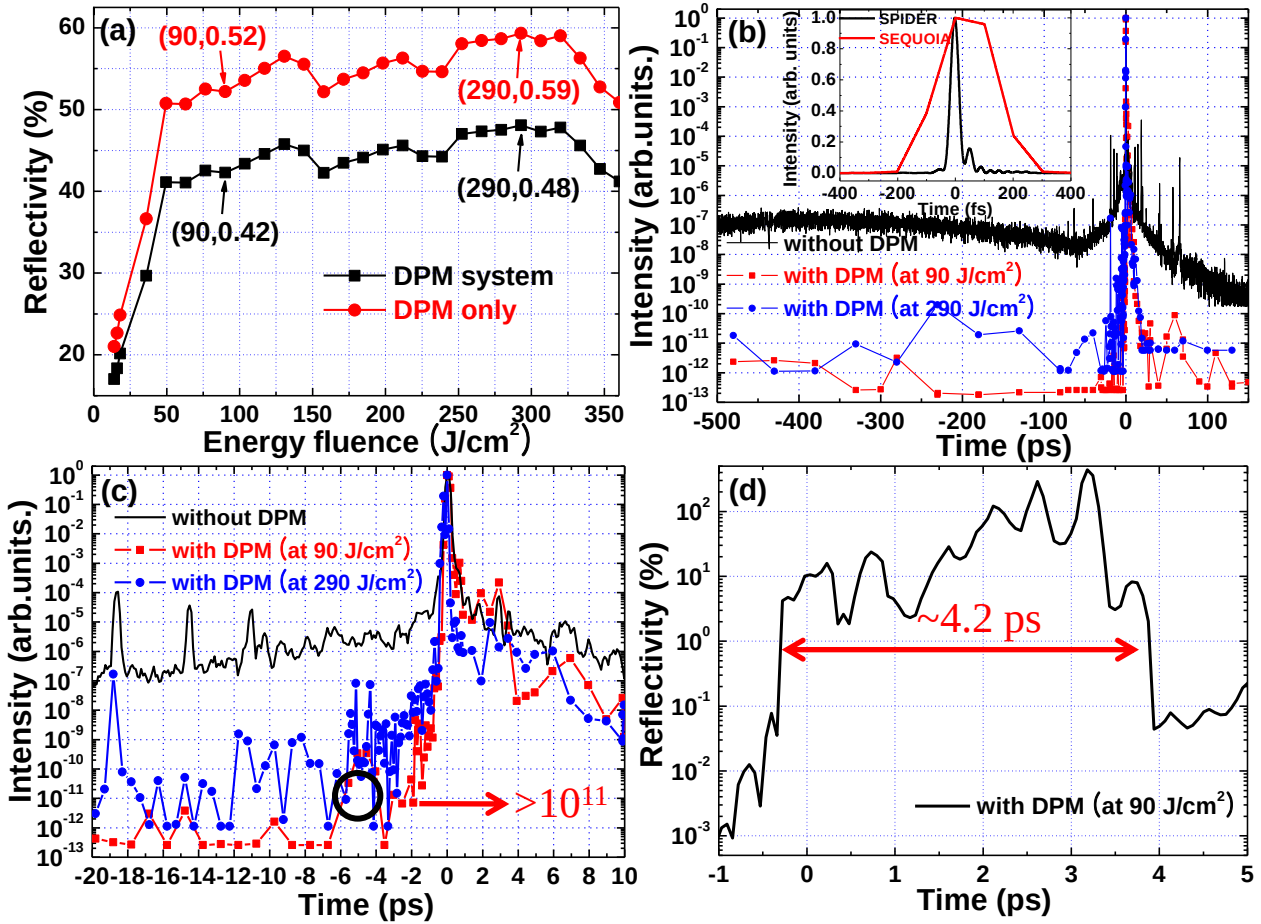

(a) Reflectivity as a function of the energy fluence incident on the first PM. (b) Temporal profiles of the laser beam between -500 ps and +150 ps, (c) between -20 ps and +10 ps and (d) Time-resolved reflectivity for the energy fluence of 90 J/cm^2 on DPM. The inset in Fig. (b) shows the temporal profiles of laser pulse measured with SPIDER and SEQUOIA respectively.